Transport phenomena and pharmacokinetics of anti-HIV microbicide drug delivery

by

Savas Tasoglu

A thesis submitted in partial satisfaction
of the requirements for the degree of

Doctor of Philosophy

in

Engineering − Mechanical Engineering

in the

GRADUATE DIVISION

of the

UNIVERSITY OF CALIFORNIA, BERKELEY

Committee in charge:

Professor Andrew J. Szeri, Chair
Professor Samuel S. Mao
Professor Mohammad R. K. Mofrad

Fall 2011

Transport phenomena and pharmacokinetics of anti-HIV microbicide drug delivery

Copyright © 2011

by

Savas Tasoglu

Abstract

Transport phenomena and pharmacokinetics of anti-HIV microbicide drug delivery

by

Savas Tasoglu

Doctor of Philosophy in Engineering − Mechanical Engineering

University of California, Berkeley

Professor Andrew J. Szeri, Chair

Microbicides are agents that can be applied to vaginal mucosal surfaces with the goal of blocking the transmission of sexually transmitted pathogens including HIV. They can be formulated in various delivery vehicles, including gels, creams, lotions, tablets or films. A recent study in South Africa has confirmed, for the first time, that a vaginal gel formulation of the antiretroviral drug Tenofovir, when topically applied, significantly inhibits sexual HIV transmission to women. However the gel for this drug, and anti-HIV microbicide vehicles in general, have not been designed using an understanding of how their spreading and retention in the vagina govern successful drug delivery.

Elastohydrodynamic lubrication theory can be applied to model spreading of microbicide gels and films. This should incorporate the full rheological behavior, including how rheological properties change due to contact with, and dilution by, ambient vaginal fluids. A Carreau-like non-Newtonian model is adopted as a rheological model. The effects of three important factors, i.e., dilution by vaginal fluid, a yield stress of the gel and swelling, are investigated. Dilution accelerates the coating flow by creating a slippery region near the vaginal wall akin to a dilution boundary layer. The concept of a yield stress fluid is attractive because such a material may tend to stay in place after coating vulnerable surfaces. We show that the lubrication approximation, which eases the efforts of design, may be applied to the elastic wall-squeezing problem for a prototype gel with yield stress. For the important presence of significant swelling of the gel by absorption of vaginal fluid, the model indicates more rapid coating. Then we study films that can be preferable over gels due to several reasons in many parts of the world. A model is developed for transient swelling and spreading of a film, and subsequent distribution of an active drug throughout the vaginal lumen. We investigate the effects of combination of many factors.

The theory developed here improves our understanding of the biophysics of microbicide gel and film flows in vivo. Ultimately, this dissertation contributes to a methodology that provides objective evaluations of microbicide gel and film performance and in the design of new, improved vehicles.

Annem Adalet Özdemir'e

ve babam Sait Taşoğlu'na

Contents

List of Figures

List of Tables

Previously Published Work

Chapter 2 appears in near entirety in

S. Tasoglu, J.J. Peters, S.C. Park, S. Verguet, D.F. Katz, A.J. Szeri, The effects of inhomogeneous boundary dilution on the coating flow of an anti-HIV microbicide vehicle, Phys. Fluids., 2011 (accepted).

Chapter 3 appears in near entirety in

S. Tasoglu, S.C. Park, J.J. Peters, D.F. Katz, A.J. Szeri, The consequences of yield stress on deployment of a non-Newtonian anti-HIV microbicide gel, J. Non-Newtonian Fluid Mechanics, 2011 (accepted).

Chapter 4 appears in near entirety in

S. Tasoglu, D.F. Katz, A.J. Szeri, Transient swelling behavior of a gel deploying an anti-HIV microbicide, J. R. Soc. Interface, 2011 (submitted).

Finally, other work that does not make an appearance in this dissertation, but that was a part of my graduate research experience includes

Peer-reviewed journals

- S. Tasoglu, U. Demirci, M. Muradoglu, The effect of soluble surfactant on the transient motion of a buoyancy-driven bubble, Physics of Fluids, 20, 040805 (2008). * Appears in near entirety in my M.Sc. thesis (2008), Koc University, Turkey. *Featured cover of Physics of Fluids (April 2008).
- M. Muradoglu, S. Tasoglu, A Front-Tracking Method for Computational Modeling of Impact and Spreading of Viscous Droplets on Solid Walls, Computers & Fluids, 39(4), 615-625 (2010).
- S. Tasoglu, G. Kaynak, A.J. Szeri, U. Demirci, M. Muradoglu, Impact and Spreading of a Compound Microdroplet on a Clean Substrate, Physics of Fluids, 22, 082103, (2010).
- B. Lopour, S. Tasoglu, H.E. Kirsch, J.W. Sleigh, A.J. Szeri, A continuous mapping of sleep states through association of EEG with a mesoscale cortical model, J. Computational Neuroscience, 30(2), 471 (2011).
- B.M. Ross, S. Tasoglu, L.P. Lee, Differences among near and far measures of localized surface plasmon resonance, Physical Review Letters, (in review).

Peer-reviewed Proceedings

- M. Muradoglu, S. Tasoglu, Impact and Spreading of a Microdroplet on a Solid Wall, Proceedings of the 7th ICNMM, Pohang, South Korea, June 22-24 2009.
- B.M. Ross, S. Tasoglu, L.P. Lee, Plasmon resonance differences between the near- and far-field and implications for molecular detection, Proceedings of the SPIE - The International Society for Optical Engineering, San Diego, CA, 739422 (9 pp.) 2009.

Acknowledgements

The past three years at Berkeley have been, in one word, amazing. I am heartily thankful to my supervisor, Andrew J. Szeri, whose encouragement, guidance and support from the initial to the final level enabled me to complete this dissertation. I consider myself very lucky to have been a part of Andrew's group and I'd like to thank him for his limitless enthusiasm in coaching that project to fruition.

I would like to thank David F. Katz for his steadfast encouragement to complete this study. His recommendations and suggestions have been invaluable for the project.

Over the years I had the great fortune of meeting with many people, and I am grateful. I owe special thanks to my first year roommates: Burhan and Sefa, for all fun chats, pc games, cooking. I'd like to thank I-House friends: Rada, Dogan, Merve, Mehmet, Gokcen, Ahmet, and Sarp, for their amusing company at meals and parties. I wish to recognize the crucial sustained support of my friend, Dogan, in the difficult times of qualifying exam. Special thanks to Ilgin, Fatos, and Aysin, and my summer roommates: Meredith and Kelly. I'd like to thank Onur and Guven for the great phone chats, and Ferda for the refreshing lunchs and joining me in skydiving.

I would like to mention fruitful discussions with coworkers: Benjamin M. Ross, Beth Lopour, Su Chan Park, Jennifer J. Peters and my labmates: Hope Weiss, Vera Dadok, Siew-Wan Ohl, and Prashanth Selvaraj.

For the past last semester and the summer, my girlfriend Gulsen had to put up with many conversations about "struggle and prize" and I'm grateful to her for her patience and support.

At last but most importantly, I would like to acknowledge the support of my dear family. I'd like to thank them for their endless love and care.

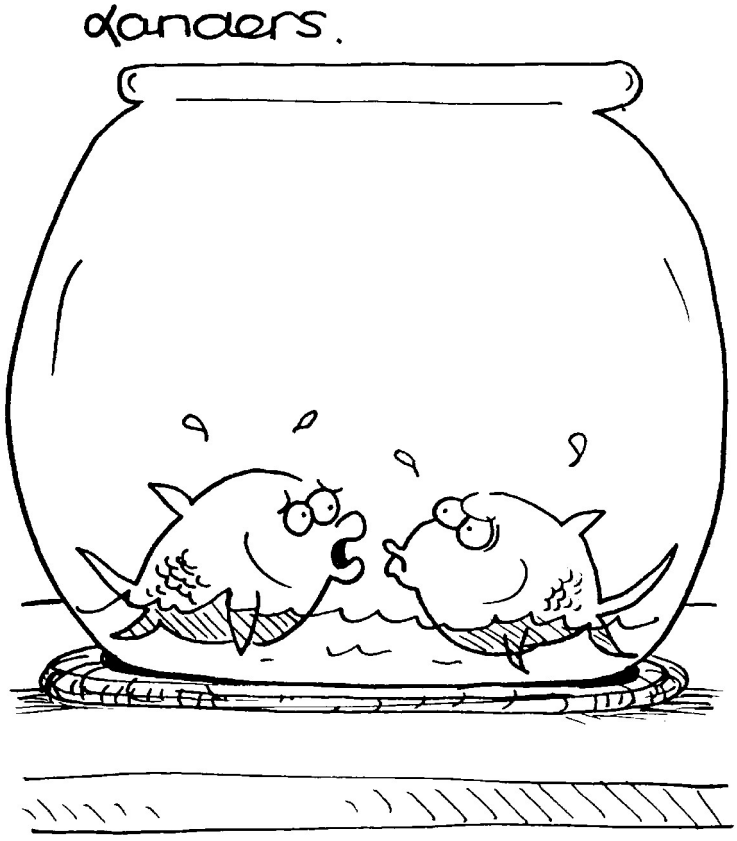

Cartoon by John Landers from CSL cartoonstock.
Reprinted with permission.
CSL Cartoons: www.cartoonstock.com

Chapter 1

Introduction

Growing industrialization, increase in per capita income, and advancements in human rights in the last century have motivated people to invest more resources in healthcare than ever before. Developing more sophisticated or alternative diagnoses, treatments, and prevention methods is a requirement for the continuation of civilization. This medical research has been naturally creating interfaces with other disciplines of the academy, including engineering and physics fields such as fluid mechanics, electromagnetism, optics, etc.

Fluid dynamics is one of the first collaborating disciplines, and the reason is simple. Water is vital for all known forms of life [2]. Up to 60% of the human body is water, the brain is composed of 70% water, and the lungs are nearly 90% water. About 83% of our blood is water, which helps digest our food, transport waste, and control body temperature. Owing to the nature of evolution, the majority of these fluids are dynamic. They diffuse through the porous membranes, carry ions, move within the elastic boundaries, mix with other fluids, and show the beauty of fluid dynamics.

The study of fluid mechanics originated at least as early as the days of ancient Greece, when Archimedes investigated fluid statics and buoyancy and formulated his famous law known now as Archimedes' Principle. In 1822, Claude-Louis Navier and George Gabriel Stokes established the mathematical framework, i.e. Navier-Stokes equations, that is central to fluid mechanics and since then it has evolved further. With new challenges discovered in the fields of health and medicine, the fluid mechanics of low Reynolds number flows has become of significant importance.

This dissertation offers a relatively recent and compelling application provided by the problem of the flow of a bolus of anti-HIV microbicide vehicle confined to the lower female reproductive tract. Microbicides are pharmacologic agents and chemical substances that can be applied to vaginal or rectal mucosal surfaces with the goal of blocking the transmission of sexually transmitted pathogens including HIV. They can be formulated in various delivery vehicles, including gels, creams, lotions, aerosol sprays, tablets or films. Effectiveness of a microbicide product such as a gel derives from completeness and durability of coating as well as potency of the active ingredients. A recent study in South Africa (CAPRISA 004, phase IIb trial) has confirmed, for the first time, that a vaginal gel formulation of the antiretroviral drug Tenofovir, when topically applied, significantly reduces sexual HIV transmission to women [3]. However, the gel in this trial and anti-HIV microbicide delivery vehicles in general, have not been designed using an understanding of how gel spreading and

retention in the lower female reproductive tract govern successful drug delivery. This dissertation aims to fill that gap by establishing the mathematical and the physical framework for a description of the relevant phenomena.

In the first subsection, HIV is briefly described and the most recent data about HIV are summarized. Then, the reasons why microbicide technology is a strong candidate to halt the spread of HIV are explained. Microbicides can be formulated in various delivery systems, and these are described in subsection 3. Finally, the physics of the delivery are discussed.

1.1 HIV

1.1.1 What is HIV?

The Human Immunodeficiency Virus (HIV) is the virus that leads to Acquired Immunodeficiency Syndrome (AIDS). AIDS is the final stage of HIV infection, which progressively reduces the effectiveness of the immune system and leaves individuals susceptible to opportunistic infections and tumors. HIV belongs to a subset of retroviruses called lentiviruses (or slow viruses), which means that there is an interval -sometimes years- between the initial infection and the onset of symptoms. HIV is transmitted through direct contact of a mucous membrane or the bloodstream with a bodily fluid containing HIV, such as blood, semen, vaginal fluid, preseminal fluid, and breast milk [4]. The four major routes of transmission are unsafe sex, contaminated needles, breast milk, and transmission from an infected mother to her baby at birth. Upon entering the bloodstream -through mucous membranes or blood-to-blood contact- HIV infects the CD4+T cells and begins to replicate rapidly. Without treatment, the net median survival time after infection with HIV is estimated to be 9 to 11 years, depending on the HIV subtype [5], and the median survival rate after diagnosis of AIDS in resource-limited settings where treatment is not available ranges between 6 and 19 months, depending on the study [6].

HIV is thought to have originated in non-human primates in sub-Saharan Africa and was transferred to humans late in the 19th or early in the 20th century [7], [8]. Clinically apparent HIV infection first was recognized in 1981 in San Francisco and New York City [9].

Although progress has been made in developing new tools to fight against HIV/AIDS, the prevention of this disease and other sexually transmitted pathogens is a global health priority. Here are the most recent facts about HIV/AIDS [10], [11]:

Global

- Since the beginning of the epidemic, almost 60 million people have been infected with HIV and 25 million people have died of HIV-related causes.
- In 2008, around 33.4 million people living with HIV, 2.7 million new infections and 2 million AIDS-related deaths.
- In 2008, around 430 000 children were born with HIV, bringing to 2.1 million the total number of children under 15 living with HIV.
- Young people account for around 40% of all new adult (15+) HIV infections worldwide.

- Sub-Saharan Africa is the region most affected and is home to 67% of all people living with HIV worldwide and 91% of all new infections among children.
- In sub-Saharan Africa the epidemic has orphaned more than 14 million children.

USA

- The U.S. HIV/AIDS epidemic began in 1981 and continues to disproportionately affect minorities, men who have sex with men of all races, women and youth.
- More than 1 million people in the U.S. currently are living with HIV/AIDS.
- 21 percent of those infected with HIV are unaware of their infection.
- Since the U.S. epidemic began, 565,927 people have died of AIDS.
- In 2006, there were approximately 53,600 new HIV infections, with the highest proportion among African Americans despite the fact that they make up only 12 percent of the U.S. population.

Eastern Europe and Central Asia

- In 2008, 1.5 million people living with HIV, 110 000 new infections and 87 000 AIDS-related deaths.

1.1.2 Prevention of transmission of HIV

The prevention of transmission of HIV and other sexually transmitted pathogens remains a top global health priority. There is currently no publicly available vaccine for HIV or AIDS. Efforts have not been conclusively successful so far, mainly because of the dynamic nature of the virus. Standard prevention methods such as the use of condoms and behavioral modifications (monogamy and sex abstinence) have also proven to be insufficient in halting the spread of STDs and AIDS.

Women face the greatest risk of acquiring HIV due to substantial mucosal exposure to seminal fluids, high prevalence of nonconsensual sex, sex without condom use, and unknown high-risk behaviors of their partners. A 1999 meta-analysis of condom use studies showed that the consistent use of latex condoms reduces the risk of sexual transmission of HIV by about 85% [12]. However, in many developing countries, women have little or no say in their sexual practices, and their partners are often not willing to use condoms [13]. According to a United Nations Population Division estimate [14], only 6.1% of married women of reproductive age globally use condoms regularly. While this percentage is 16.1% in more developed regions of the world, it is 4.4% for less developed regions. This ratio decreases to 1.7% in the continent of Africa. In addition, being faithful in a monogamous relationship will not protect women whose partners are unfaithful. The majority of women living with HIV/AIDS worldwide became infected through heterosexual intercourse, usually in settings where they could not refuse sex or negotiate condom use. These issues are the major motivations in order to develop HIV prevention tools that women can use in situations when negotiating with sexual partners is difficult or impossible.

Under these conditions, a new category of prophylactic agents and formulations known as "microbicides" present one of the most promising strategies to fight against the transmission of HIV/AIDS.

1.2 Anti-HIV microbicides

1.2.1 What is an anti-HIV microbicide?

Microbicides are pharmacologic agents and chemical substances that can be applied to vaginal or rectal mucosal surfaces with the goal of blocking the transmission of sexually transmitted pathogens including HIV. They can be classified as:

1. Membrane disruptive agents: detergent and surfactant microbicides, such as Nonoxynol-9 (N-9), sodium dodecyl sulfate and Savvy [15], act by disrupting the viral envelope, capsid or lipid membrane of microorganisms.

2. Entry inhibitors: polyanions such as Carraguard and PRO 2000 [16], [17], act by electrostatically binding the virus and preventing it from interacting with its target cells in the vagina. BufferGel is also a polyanion but is designed to maintain the low pH of the vagina [16].

3. Dendritic cell uptake inhibitors: dendrimers, such as VivaGel, are highly branched macromolecules that also prevent HIV from attaching to the target cells [18].

4. Antiretrovirals: a new generation of microbicides such as Tenofovir, in development, specifically target HIV, or the cells it infects.

The initial research into microbicides commenced in 1989. Joan Kreiss presented the findings of her study on the effectiveness of the Today sponge, containing N-9 versus a placebo suppository on HIV transmission among sex workers in Nairobi [19]. Their results suggested that N-9 actually increased HIV transmission, probably because of local genital toxicity. However, these findings cast a pall on microbicide research and sparked a decade-long debate about the safety and effectiveness of N-9 for STI protection. On the other hand, advocacy of microbicide technology began in 1990. South African epidemiologist and advocate Zena Stein published her seminal article [20]. For women from a variety of cultural backgrounds, concern has been raised about the difficulties associated with the lack of control over condom use [20]. In response to this concern, the Institute of Medicine committee and others recommended the development of female-controlled methods, particularly topical microbicides.

In the following years, 11 clinical trials with six candidate microbicides have all resulted in negative or inconclusive findings. The six candidate microbicides tested previously include N-9 [19], [21], [22], SAVVY (C31G; Cellegy Pharmaceuticals, USA) [23], [24], cellulose sulfate (CS; CONRAD Program, USA) [25], [26], Carraguard (PC-515; Population Council, New York) [27], PRO 2000 (Endo Pharmaceuticals, USA) [28], [29] and BufferGel (ReProtect LLC, USA) [29], [30].

Very recently, a research group from South Africa (CAPRISA, Centre for the AIDS Programme of Research in South Africa) has discovered that a microbicide gel formulation of the antiretroviral drug Tenofovir significantly inhibits sexual transmission of HIV to women [3]. This is the first time that a topical microbicide gel has shown statistically significant efficacy in a clinical trial.

Currently ongoing trials include the Vaginal and Oral Interventions to Control the Epidemic (VOICE) study (MTN-003), which is designed to investigate the safety and efficacy of both oral and topical ARV compounds. It also compares the safety and efficacy of single and dual drugs in oral form. This study started in September 2009, and will run for 4 years, enrolling approximately

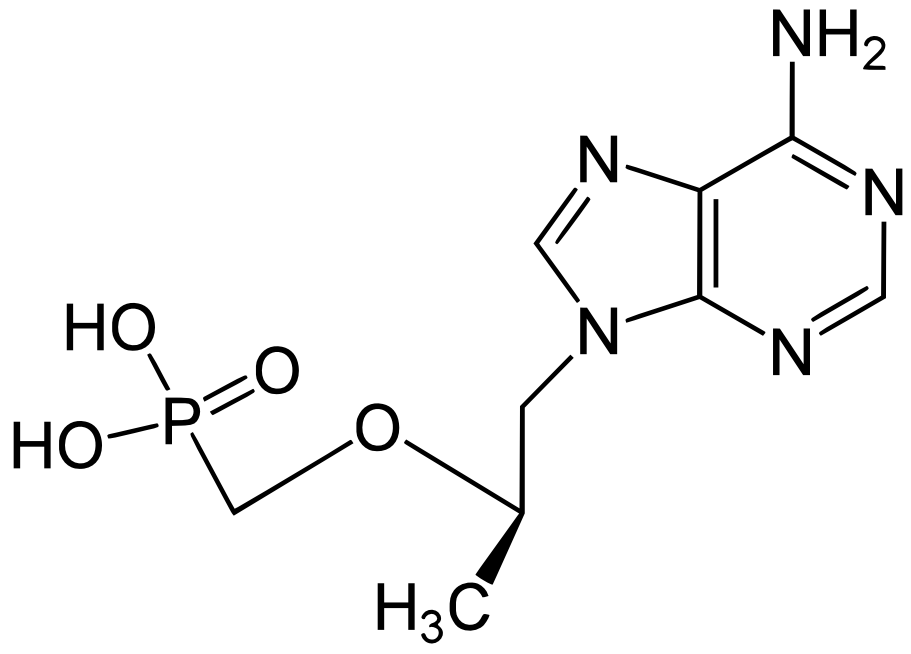

Figure 1.1. Chemical Structure of Tenofovir (molecular weight: 287.213 g/mol).

5000 women in Malawi, South Africa, Uganda, and Zimbabwe. Results from this study will provide the essential evidence that supports or challenges the findings from CAPRISA 004.

1.2.2 Tenofovir molecule

Prior to the CAPRISA 004 trial, none of the different products in other trials had had a protective effect against HIV in a clinical setting. Two products (N-9 and CS) even showed a trend towards increased risk of HIV infection. Most of these products have failed in clinical trials because they compromise genital epithelial integrity, increase the inflammatory response, and/or interfere with immune function [4], [9]. The field has switched to agents that act more specifically on viral receptors (using CCR5 inhibitors, for example) or viral enzymes (using reverse transriptase inhibitors, RTIs, for example).

Tenofovir disoproxil fumarate (TDF or PMPA) belongs to a class of antiretroviral drugs known as nucleotide analogue reverse transcriptase inhibitors (NRTIs), which block reverse transcriptase, an enzyme crucial to viral production in HIV-infected people. Tenofovir was discovered through a collaborative research effort between Academy of Sciences of the Czech Republic and Catholic University of Leuven, Belgium. The U.S. Food and Drug Administration (FDA) approved Tenofovir on October 26, 2001 for the therapeutic treatment of HIV infection, and on August 11, 2008 for the treatment of chronic hepatitis B [31]. The chemical Structure of Tenofovir is given in Fig. 1.1.

1.3 Microbicide drug delivery methods: gels, rings, and films

There is a widespread agreement that more effective drug delivery vehicles with more alternatives, as well as better active ingredients, must be developed to raise the efficacy of microbicide products. In this setting, there is now great interest in developing a range of delivery vehicles such as vaginal rings, gels, and films.

The most well-studied delivery method of anti-HIV microbicides is their deployment by gel vehicles that coat the vulnerable surfaces of the vaginal lumen prior to intercourse. For instance, the delivery vehicle employed in the very recent CAPRISA 004 study in South Africa [3] was a gel. However, this positive result does not mean that gels are the ideal vehicles for every region (in which sexual preferences and practices may vary), or for each person. There are alternative products that can be applied vaginally with the intent of reducing sexual transmission of HIV. These include a variety of formulations, such as creams, films, suppositories, sponges, and intravaginal rings.

In addition to biological functionality in impeding infection by HIV, behavioral acceptability is crucial to ensuring that a microbicide product will be successful. Data from safety and acceptability studies of microbicide gels in many developing countries point to the need for microbicides that do not interfere with sexual intercourse and that may be used discreetly [32]. Regional variations in cultural preferences and sexual practices suggest that no single product type is universally acceptable. Therefore, microbicide developers are investigating alternative delivery formulations including lotions, films, intravaginal devices, and solid dosage forms, such as foaming pills, and also novel polymers and biologically triggered drug-release approaches.

1.4 Physics of vaginal drug delivery via a gel

1.4.1 Rheology

A Newtonian fluid is a fluid whose stress versus rate of strain curve is linear and passes through the origin. The constant of proportionality is defined as the viscosity of the fluid. Water is an example of a Newtonian fluid. However, most biological fluids are non-Newtonian. A fluid whose flow properties are not described by a single constant value of viscosity is defined as a non-Newtonian fluid. There are many constitutive equations, for non-Newtonian fluids, that relate the stress and the rate of strain [33]. The viscosity may be independent of time, and with increasing shear rate it may increase (shear-thickening) or may decrease (shear-thinning); the apparent viscosity may increase with duration of stress (Rheopectic) or not (Thixotropic); there may be a minimum stress for the existence of flow (e.g. Bingham or Herschel Bulkley) [33]. Many polymer solutions and molten polymers are non-Newtonian fluids, for example ketchup, starch suspensions, paint, blood and shampoo. The most well-studied delivery systems of anti-HIV microbicides are gels. Such gels inherently do not have a simple rheology. For example, in chapters 2 and 4, we consider an aqueous gel with 3% hydroxyethylcellulose that is similar to the placebo gel used in the successful microbicide gel trial [3]. From the results of viscometric measurements of this gel, the Carreau model [34] is adopted as a constitutive model for it. The Carreau model was chosen because microbicide gels (which are highly hydrated) are shear thinning and typically exhibit a plateau at low shear strain rates in a log-log plot of shear stress vs. shear strain rate. Because vaginal coating flows are slow flows in which much of the flow field experiences low shear strain rates, it is important to employ a

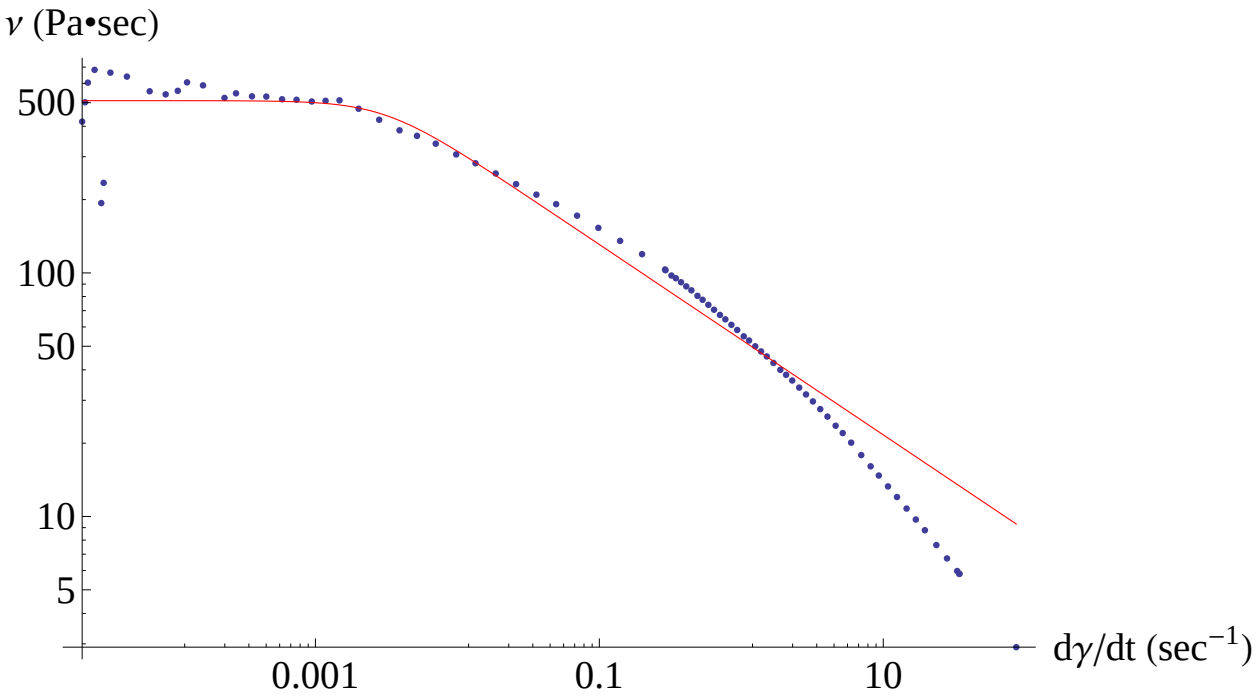

Figure 1.2. Viscosity (Pa.sec) versus rate of strain (sec^{-1}) for 10% diluted prototype gel. Dots are experimental data, and the solid (red) line is the fitted Carreau model.

constitutive equation that embodies such plateau behavior. Viscosity (Pa.sec) versus rate of strain (sec^{-1}) for this prototype gel, diluted by 10% with vaginal fluid simulant (see below) is plotted in Fig. 1.2 In Chapter 3, another significant property of gel rheology is taken into account: a yield stress. In a limiting case, a yield stress fluid is a material that behaves as a rigid body at low applied stress but flows as a viscous fluid at higher applied stress. The physical reason for such behavior is that the liquid contains particles, (e.g., clay), or large molecules, (e.g., polymers), which can interact to create a weak solid structure. A threshold amount of stress is required to break this structure. A microbicide gel can be designed to have a yield stress, e.g. by including derivatives of polyacrylicacid such as Carbopol and/or polycarbophil in its composition. The measurement of yield stress has been historically problematical [35]–[38]. The yield stress can be determined as the point where the slope of elastic modulus vs. oscillatory stress or displacement vs. shear stress curve abruptly changes. The yield stress can also be determined as the shear value at which the gel rested to after being sheared and relaxed. To illustrate, gamma (total strain) versus stress of a different prototype gel, containing Carbopol is plotted in Fig. 1.3. The curve breaks are at about the same stress value as the residual stresses. In Fig. 1.4, all of the curves for dilution rates from 0 to 75% are superposed. At higher dilutions, e.g. 75% the break is gone; the material is no longer well characterized by a yield stress. Higher dilution is shown tending up and to the left in Fig. 1.4. As an alternative microbicide class of delivery vehicles, dissolving films, also show non-Newtonian effects, and for small dilutions they have a yield stress (please see Chapter 5).

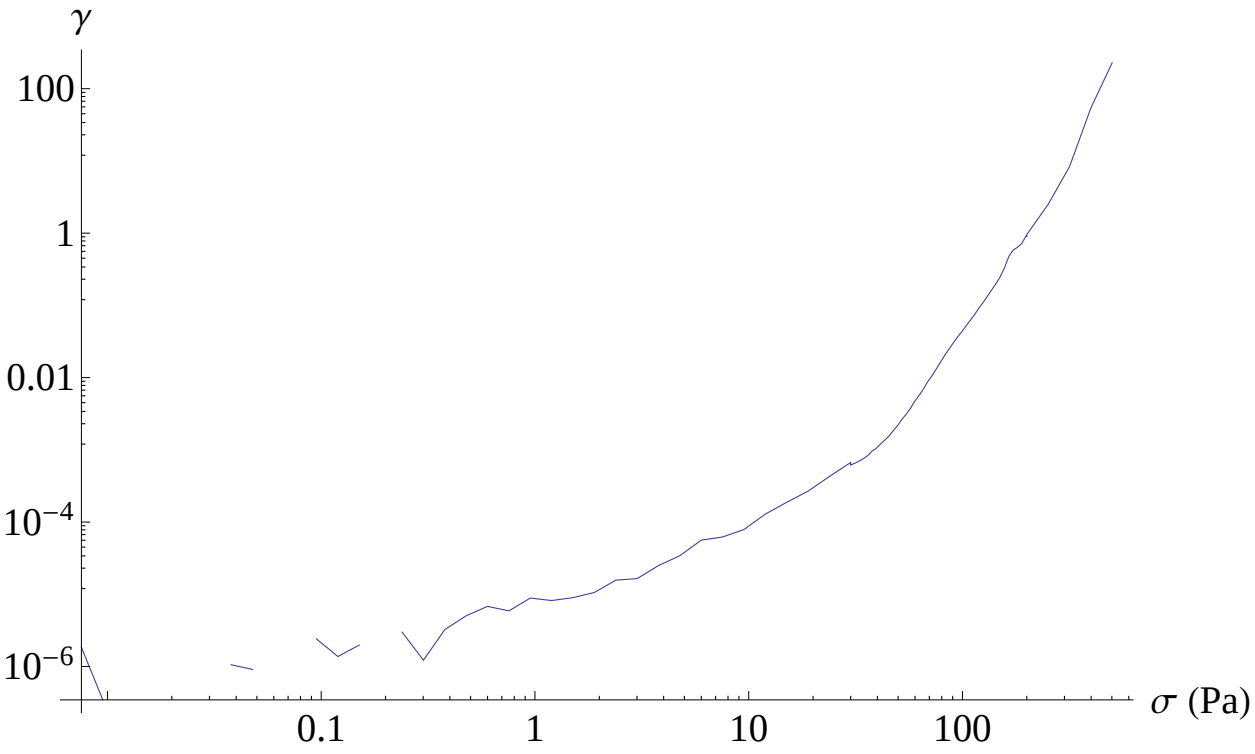

Figure 1.3. Strain (radian) versus stress (Pa) for 10% diluted prototype gel.

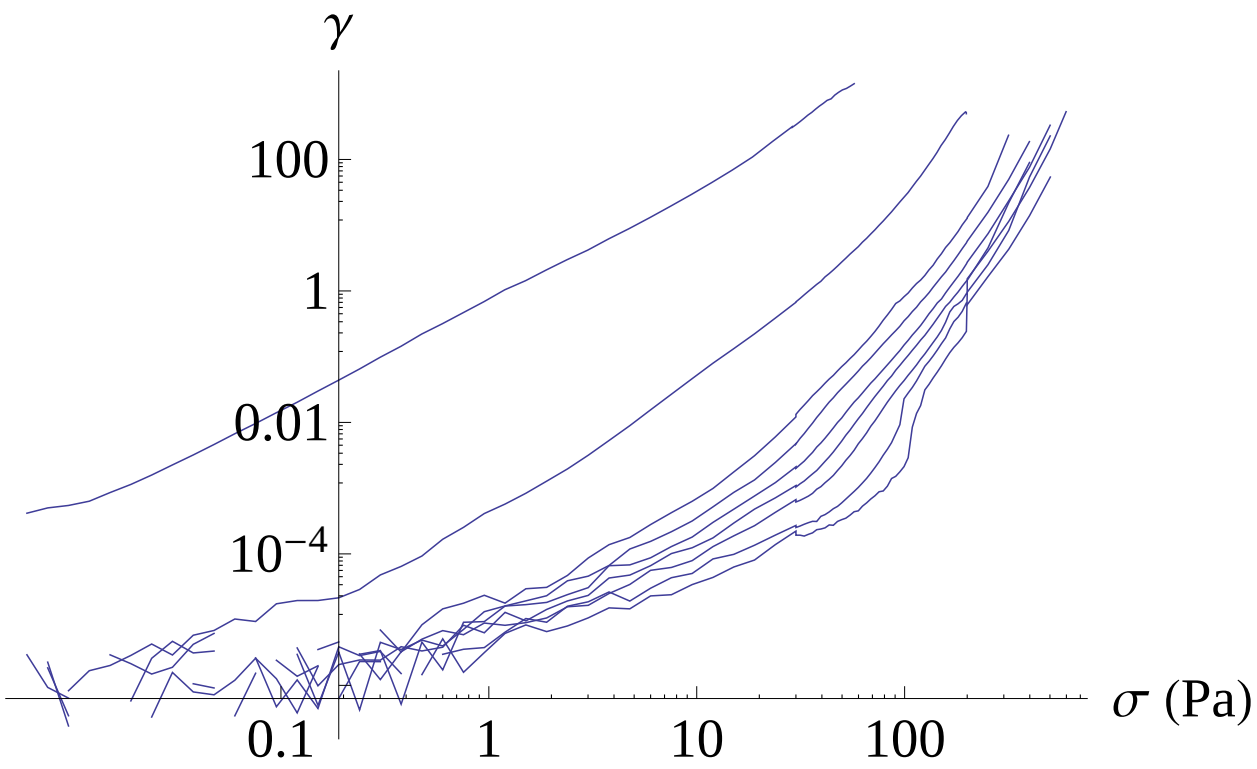

Figure 1.4. Strain (radian) versus stress (Pa) for dilution rates from 0 to 75%. Higher dilution is tending up and to the left.

1.4.2 Elastohydrodynamic lubrication flows

In many real world situations, e.g. when applying eye drops or spreading marmalade onto freshly toasted bread, lubrication flows occur. Lubrication theory is often employed as a one dimensional flow for example, in a two-dimensional system, when the longitudinal dimension is much longer than the transversal dimension. This theory also generally requires that inertial forces are comparable with or smaller than viscous forces.

In this thesis, we shall introduce the main elements of the mathematical framework for lubrication theory, which will be used extensively. We refer the reader to the textbooks by Leal [39] and Deen [40] for a further detailed description of the theory.

Consider a steady ($\frac{\partial}{\partial \tilde{t}} = 0$) two-dimensional flow and define $\tilde{x}$ and $\tilde{y}$ as the longitudinal and transverse coordinates, the scales $\tilde{L}$, $\tilde{H}$, $\tilde{U}$ and $\tilde{V}$ and then perform the following non-dimensionalization: $\tilde{x} = \tilde{L}x$, $\tilde{y} = \tilde{H}y$, $\tilde{u} = \tilde{U}u$, and $\tilde{v} = \tilde{V}v$. By rescaling the continuity equation:

$$(\frac{\tilde{U}}{\tilde{V}}\frac{\tilde{H}}{\tilde{L}})\frac{\partial u}{\partial x} + \frac{\partial v}{\partial y} = 0 \tag{1.1}$$

This suggests the following relationship for the velocity scales:

$$\tilde{V} = \frac{\tilde{H}}{\tilde{L}}\tilde{U} = \epsilon\tilde{U} \tag{1.2}$$

where $\epsilon = \tilde{H}/\tilde{L}$. Now non-dimensionalize the Navier-Stokes equations:

$$(\frac{\tilde{\rho}\tilde{U}\tilde{H}}{\tilde{\eta}})(\frac{\tilde{H}}{\tilde{L}})\left[u\frac{\partial u}{\partial x} + v\frac{\partial u}{\partial y}\right] = -\frac{\partial p}{\partial x} + (\frac{\tilde{H}}{\tilde{L}})^2\frac{\partial^2 u}{\partial x^2} + \frac{\partial^2 u}{\partial y^2} \tag{1.3}$$

where we choose to scale the pressure by $\Pi = \frac{\tilde{\eta}\tilde{U}\tilde{L}}{\tilde{H}^2} = \frac{\tilde{\eta}\tilde{U}}{\tilde{H}\epsilon}$ so that the pressure gradient terms can subsequently be retained in the limit $\epsilon \to 0$ (the system of equations would otherwise be overdetermined) and:

$$(\frac{\tilde{\rho}\tilde{U}\tilde{H}}{\tilde{\eta}})(\frac{\tilde{H}}{\tilde{L}})\left[u\frac{\partial v}{\partial x} + v\frac{\partial v}{\partial y}\right] = -(\frac{\tilde{L}}{\tilde{H}})^2\frac{\partial p}{\partial y} + (\frac{\tilde{H}}{\tilde{L}})^2\frac{\partial^2 v}{\partial x^2} + \frac{\partial^2 v}{\partial y^2} \tag{1.4}$$

Define $Re = \frac{\tilde{\rho}\tilde{U}\tilde{H}}{\tilde{\eta}}$ and $\epsilon = \frac{\tilde{H}}{\tilde{L}}$ we have

$$\begin{aligned}(\epsilon Re)\left[u\frac{\partial u}{\partial x} + v\frac{\partial u}{\partial y}\right] &= -\frac{\partial p}{\partial x} + \epsilon^2\frac{\partial^2 u}{\partial x^2} + \frac{\partial^2 u}{\partial y^2} \\ (\epsilon Re)\left[u\frac{\partial v}{\partial x} + v\frac{\partial v}{\partial y}\right] &= -\frac{1}{\epsilon^2}\frac{\partial p}{\partial y} + \epsilon^2\frac{\partial^2 v}{\partial x^2} + \frac{\partial^2 v}{\partial y^2}\end{aligned} \tag{1.5}$$

Then take the limit $\epsilon Re \to 0$ and $\epsilon \to 0$, we obtain the so-called lubrication equations:

$$\begin{aligned}0 &= -\frac{\partial p}{\partial x} + \frac{\partial^2 u}{\partial y^2} \\ 0 &= -\frac{\partial p}{\partial y} \to p = p(x)\end{aligned} \tag{1.6}$$

The lubrication approximation intrinsically contains two requirements:

1. a geometric requirement e.g. $\epsilon \ll 1$,

2. a dynamical requirement e.g. $\epsilon Re \ll 1$,

The general lubrication theory (also known as Reynolds lubrication theory) is constructed on the assumption of constant viscosity, in particular, that the viscosity is independent of pressure. This assumption is valid at low pressures and isothermal flows. On the other hand, elastohydrodynamic lubrication theory with a solid boundary normally implies enormous pressures; there is considerable local heating, and the assumption of constant viscosity may no longer be valid. In this dissertation, we consider elastohydrodynamic lubrication theory with an elastic tissue boundary. Neither pressure dependence of viscosity, nor viscous heating are likely to occur. However, large distention of the elastic tissue boundaries is important.

1.4.3 Multi-component flow and mass transport

Mass transfer is the net movement of mass from one location, usually meaning a stream, phase, fraction or component, to another. Mass transfer occurs in many processes, such as absorption, evaporation, adsorption and drying.

In Chapter 4, mass transfer is one of the critical components in the analysis. In the problems considered in this dissertaion, mass transport occurs due to inhomogeneous dilution of gel by vaginal fluid contacting it along a moving boundary (the locally deforming vaginal epithelial surface). In this complex process, we assume that gel and vaginal fluid (exuded from the boundary) are miscible. Miscibility is defined as capable of mixing in any ratio without separation of two phases. For instance, oil and water do not mix. Pouring half glass of oil into another half glass of water results in two distinct layers, clearly separated by a curved meniscus. Each layer has the same volume and essentially the same composition as in the original liquids. Because very little mixing has apparently occured, the liquids are called "immisicible" or unmixable. On the other hand, in our problem, vaginal fluid dilutes the gel and we assume that no meniscus forms between the gel and the vaginal fluid. Here, the two liquids are considered "miscible".

For a multicomponent fluid containing n chemical species, an equation of continuity for each species present in the fluid reads as,

$$\frac{D}{Dt}\rho_i = -\rho_i(\bar{\nabla}\cdot\bar{u}) - (\bar{\nabla}\cdot\bar{j}_i) + r_i \quad \text{i = 1,2,...,n} \tag{1.7}$$

where r_i is the rate of production of the ith component by chemical reaction, $\bar{u}$ and is the mass-average velocity vector. Here, ρ_i and $\bar{j}_i$ are the density of the ith component and mass fluxes of species i relative to mass-average velocity. Combination of all n equations of this kind gives the equations of continuity for the mixture. Any one of the n equations above may be replaced by the equation of continuity for the mixture in a fully determined –but not redundant– system.

The equation of motion for the mixture read as,

$$\rho\frac{D\bar{u}}{Dt} = \left[\bar{\nabla}\cdot\bar{\bar{\pi}}\right] + \sum_{i=1}^{n}\rho_i\bar{g}_i \quad \text{i = 1,2,...,n} \tag{1.8}$$

Here we have introduced the stress tensor $\bar{\bar{\pi}} = \bar{\bar{\tau}} + p\bar{\bar{\delta}}$, in which $\bar{\bar{\tau}}$ is the viscous part of the momentum flux (or shear stress tensor), p is the static pressure, and $\bar{\bar{\delta}}$ is the unit tensor. Note that Eq. 8

differs from the equation of motion for a pure fluid only in the last term, where $\rho\bar{g}$ is replaced by $\sum \rho_i \bar{g}_i$. In that term account is taken of the fact that each chemical species present may be acted on by a different external force per unit mass $\bar{g}_i$.

Here, the equation of energy for the mixture is not included. For a bi-component mixture, such as a gel-vaginal fluid mixture, the mass conservation equation must be defined either for each component or for the mixture and one of the components, in order to close the problem. The mass conservation equation for the mixture and first component can be written as,

$$\begin{aligned} \frac{\partial \rho}{\partial t} + \bar{\nabla} \cdot (\rho \bar{u}) &= -\bar{\nabla} \cdot \bar{\gamma} \\ \frac{\partial \rho_1}{\partial t} + \bar{\nabla} \cdot (\rho_1 \bar{u}) &= \bar{\nabla} \cdot \rho D_{12} \bar{w}_1 \end{aligned} \tag{1.9}$$

where, ρ and ρ_1 are the densities of the mixture and the first component, respectively, and $D_{12}(= D_{21})$ is the mutual diffusion coefficient. Here, $\bar{\gamma}$ is a source term, e.g. boundary dilution, and w_1 is the density ratio of the first component to the mixture ρ_g/ρ.

The placement of a bolus of fluid of finite volume, here the gel delivery vehicle, within the vaginal canal results in an initial elastic deformation of the originally flat upper and lower epithelial surfaces. Gel flow immediately ensues. Simultaneously, the gel dilution process begins, and vaginal fluid concentration within the gel, in total, increases. However, vaginal fluid concentration is initially expected to be higher near the locally deforming vaginal epithelial surface rather than the regions near the centerline (along the vaginal canal). Given the length scales, diffusion occurs faster across the thickness of the gel than longitudinally along it. However, diffusion is not the only mechanism of mass transport. Neglecting gravity, flow is driven by the squeezing forces due to elastic boundaries. As time passes, the squeezing forces are expected to decline owing to the more uniform profile of the bolus and smaller wall distention. Eventually, diffusion becomes the dominant process. Depending on the timescales, we can determine the relative importance of the initial non-uniform concentration interval within the entire spreading period. The time scale for diffusion across the thickness of the gel, $t_D = H^2/D$, should be much smaller than that for flow, $t_{flow} = L/U$ to neglect the former time interval. This plausible assumption enables us to make simplifications to the mass conservation equations. Further discussions can be found in Chapter 4.

1.4.4 Fluid transport across epithelia

The mechanism of epithelial fluid transport relevant to our problem remains incompletely understood. This is partly due to inherent experimental difficulties. Physiologists have long been impressed by the large volumes of fluid absorbed across gastrointestinal and renal epithelia. Surprisingly, nearly one hundred years of investigation has not resulted in a consensus about the mechanism of this transport. Major routes for epithelial fluid transport are accepted as cellular and paracellular pathways. Paracellular transport refers to the transfer of substances between cells of an epithelium. The standing-osmotic gradient model for isosmotic fluid transport proposed by Diamond & Bossert [41] is still widely accepted. Considerable progress has been made on the identification of proteins in the tight junction complex. An electroosmotic model for transport across tight junctions (TJs) has been recently reviewed [42].

A large number of the sophisticated experimental studies of this problem have been performed on corneal endothelium. This can be partly attributed to the relatively simpler structure of that

epithelium. However, with the topical application of anti-HIV microbicides into the lower female reproductive tract, and owing to the compelling importance of that application, transport across vaginal epithelium has become an issue to be resolved. In Chapter 4, we explore the potential physiological mechanisms of this. We consider three separate putative driving forces across the epithelium: (1) hydrodynamic pressure difference, (2) osmotic gradient, and (3) electroosmotic forces.

Transport across epithelium is also important for drug absorption. Drug molecules may diffuse within and/or be carried by these fluids (mostly water, and the components of gel or dissolved film) across the epithelium. Drug molecules may move within the paracellular pathways depending on the size of the molecule and the gap between cells, or they may diffuse into the cells depending on permeability of the membrane, hydrodynamic pressure difference, osmotic gradients, and physicochemical affinity of the drug for the lipids in cell membranes, etc. Chemical activity of these drug molecules is another story, which will not be studied in this dissertation. The field of pharmacokinetics includes some of the phenomena studied in Chapter 4.

Pharmacokinetics is divided into several areas including the extent and rate of absorption, distribution, metabolism and excretion. This is commonly referred to as the ADME scheme. However recent understanding about the drug-body interactions brought about the inclusion of new term Liberation. Now Pharmacokinetics can be better described as LADME.

1. Liberation - the process of release of drug from the formulation.
2. Absorption - the process of a substance entering the blood circulation.
3. Distribution - the dispersion or dissemination of substances throughout the fluids and tissues of the body.
4. Metabolism - the irreversible transformation of parent compounds into daughter metabolites.
5. Excretion - the elimination of the substances from the body. In rare cases, some drugs irreversibly accumulate in body tissue.

Here this scheme is ordered according to a typical oral drug mechanism. However, for the topical microbicide problem, distribution takes place before absorption. Here, motion of drug molecules released from the gel or film through the epithelium and the subsequent movement via multi-channel and cellular motion is referred to as absorption. In this dissertation, the metabolism (4) and excretion (5) components of LADME are not studied.

Chapter 2

The effects of inhomogeneous boundary dilution on the coating flow of an anti-HIV microbicide vehicle

2.1 Introduction

Elastohydrodynamic flows occur in many biomedical phenomena [43]–[47]. A recent example involves application of a bolus of a semi-solid microbicide vehicle to the lower female reproductive tract, to inhibit infection by sexually transmitted pathogens such as HIV [43], [48]–[52]. Very recently, a vaginal gel has shown promising effectiveness in blocking HIV transmission in women [3]. Women who used a formulation of the antiretroviral drug Tenofovir were 39 percent less likely overall to contract HIV than those who used a placebo. However, the gel in this trial was not designed using knowledge of the mechanisms of its vaginal spreading and consequent drug release. Moreover, there is widespread agreement that more effective microbicide vehicles should be developed, to improve behavioral acceptability, i.e. willingness of patients to choose to use the product [53], as well as biological functioning against HIV.

There are several active factors that govern the distribution, or coating process of semi-solid or fluid microbicide vehicles [54]–[58]. Among these are gravity, transvaginal pressure gradients due to contractility of the supporting viscera, and transverse squeezing forces from the distended epithelium. Salient gel rheological properties are related to its shear thinning and the possible existence of a yield stress, both of which can be altered by dilution. There have been initial fluid mechanical studies of intravaginal vehicle flows; these focused on the individual effects of gravity or epithelial squeezing [55]–[57]. Those initial studies are instructive in developing a physical understanding of the mechanisms of intravaginal vehicle deployment flows. The second generation model developed by us [34] involves simultaneous effects of a longitudinally directed force along

the vaginal canal, e.g., gravity, and transversely directed elastic epithelial squeezing, in a lubrication flow analysis. Both Newtonian and non-Newtonian fluids (Carreau constitutive model) were considered. A single dimensionless number, independent of viscosity, was derived to characterize the relative influences of squeezing and gravitational acceleration on the shape of spreading in the Newtonian case. A second scale, involving viscosity, was used to determine the spreading rate. In the case of a non-Newtonian shear-thinning fluid, the Carreau number also played a role.

This second generation analysis did not, however, take into account the dilution of gel due to contact with ambient vaginal fluids. Such dilution begins immediately after gel insertion, prior to the deposition of semen. It can alter gel rheological properties and, consequently, the flow process itself. In general, effects of dilution on the rheology of a fluid have been investigated in terms of molecular structure [59], [60]. Effects of dilution on vaginal gel rheology have specifically been investigated [61]. Initial work on how vaginal gel flows are influenced by dilution involved comparing models outputs when input with rheological properties for diluted, fully mixed gels vs. undiluted gels [58]. However, gel dilution *in vivo* involves contact of the bolus with fluid at the gel-tissue interface, not homogeneous mixing. The result is a time and space-dependent distribution of local gel dilution, as fluid from the boundary permeates the gel and alters its local properties. The goal of the present chapter is to address this inhomogeneous gel dilution problem, focusing upon effects of vaginal fluid present on the surface of the epithelium.

In the method introduced here we supplement our elastohydrodynamic lubrication model [34] with a convective-diffusive transport equation to account for boundary dilution that is inhomogeneous throughout the diluted, non-Newtonian fluid. In this process flow of the fluid −in our focus, a gel− is driven by a transversal force (e.g., wall compliance). This flow influences transport of the fluid from the boundary, that is permeating the gel. Consequently, gel dilution by boundary fluid can be interpreted as a convective-diffusive phenomenon. The present chapter begins by applying our initial results to spreading of a homogenously diluted microbicide gel, over a range of dilutions. Then, an associated convection-diffusion equation for boundary fluid dilution is formulated. This is suitable for inhomogeneous dilution along the boundary, but we illustrate its application by considering a fluid flux at the boundary that is constant in time and space; values of this flux derive from data on production of human vaginal fluid. The governing Reynolds lubrication equation and convective-diffusive transport equation are solved simultaneously using an implicit multi-step scheme in a moving domain.

2.2 Problem formulation

We first present the Reynolds lubrication equation as an evolution equation for the shape of a bolus of non-Newtonian fluid, and then derive a governing equation for the distribution of vaginal fluid exuded from epithelial surfaces. The equations are developed in the symmetric domain $-h(x,t) \leq y \leq h(x,t)$. The physical problem and computational domain are sketched in Fig. 2.1. The model is formulated in a 2D Cartesian domain. The simplification of two dimensional flow is quite relevant anatomically; the cross section of the undistended human vaginal canal is "H" shaped, with the transverse dimension large compared to the vertical openings on its two sides [62], [63]. For the constitutive model we take the form,

$$\dot{\gamma}_{xy} = \tau_{xy} F(\tau_{xy}) \tag{2.1}$$

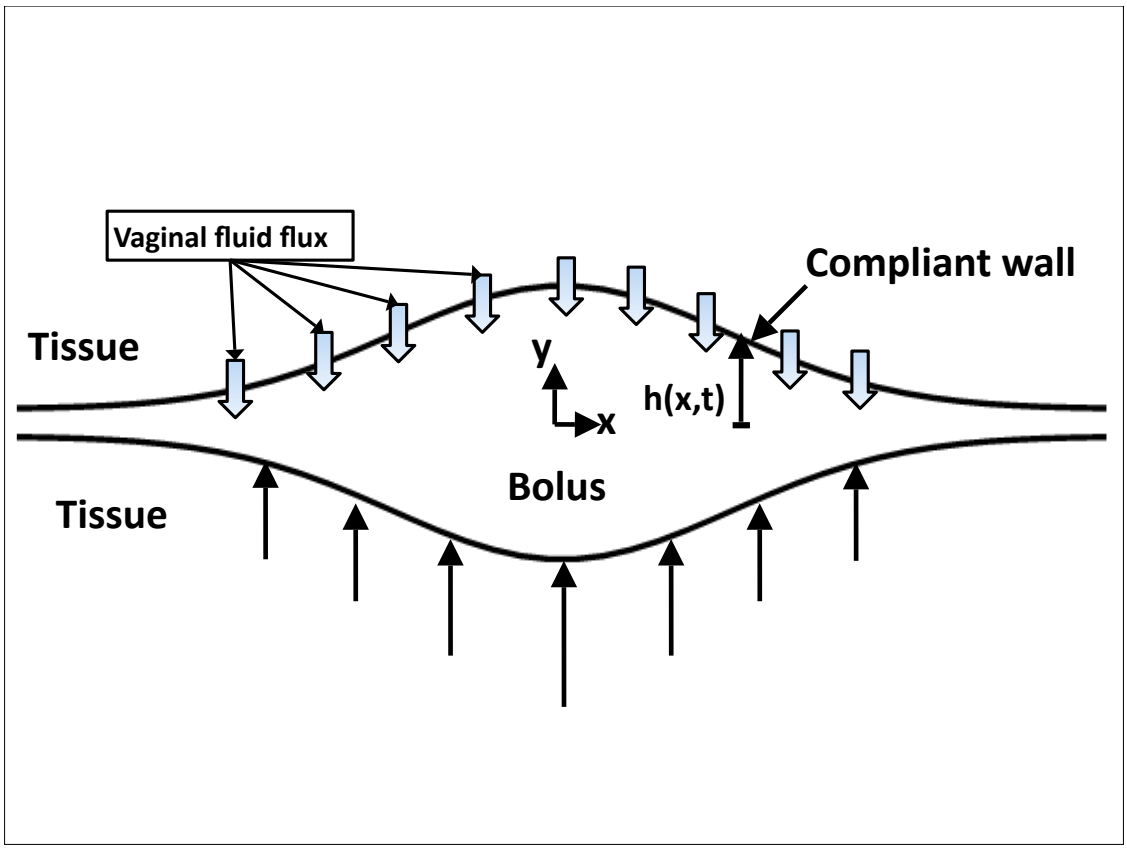

Figure 2.1. Definition sketch of the vaginal canal. The introitus is to the right. Vaginal fluid fluxes and squeezing forces are effective for both of the vaginal surfaces.

Here, $\dot{\gamma}_{xy}$ is the shear rate and τ_{xy} is the shear stress. One can choose $F(\tau) = 1/m_0$ for a Newtonian fluid or, as we do below,

$$F(\tau) = \frac{1}{m_0} + \frac{1}{m}\left(\frac{|\tau|}{m}\right)^{(1-n)/n} \tag{2.2}$$

for a Carreau-like fluid which exhibits shear thinning and a finite viscosity at zero-shear rate, m_0. m is the viscosity of the Carreau-like model and n is the power index. The original Carreau model can be written as $\eta/\eta_0 = (1+(\lambda\dot{\gamma})^2)^{(n-1)/2}$. Here, η is the viscosity of the Carreau model, η_0 is the zero shear viscosity, and λ is the relaxation time of the fluid. The parameters of the Carreau model can be converted into those of Carreau-like model asymptotically [34] in the relationship $m_0 = \eta_0$ and $m = \eta_0/\lambda^{1-n}$. The two models may be matched at small and large strain rates although they are not precisely equivalent.

Next, we present Reynolds lubrication equation into which our constitutive model is substituted,

$$\frac{\partial h}{\partial t} + \frac{1}{2}\frac{\partial}{\partial x}\left(M\frac{\partial h}{\partial x}m_2\right) = 0 \tag{2.3}$$

where,

$$m_2 = \int_{-h}^{h}\left[\int_{-h}^{y} F(\tau_{xy})y dy\right]dy \tag{2.4}$$

Here, we made use of the one dimensional constrained continuum model [64] approximation. The idea is to relate the fluid pressure near a compliant wall to the local deformation of that wall. In general, for a deformation h, the fluid pressure is given by $p = (E/T)\,h \equiv Mh$. Here, E is the elastic (Young) modulus of the compliant layer, T is its thickness, and M is the compliance of the elastic wall.

In our problem, inhomogeneous dilution by vaginal fluids being exuded from the boundaries changes the rheological properties of the overlying microbicide gel. Therefore, rheological parameters −zero-shear viscosity, power-law exponent, and relaxation time scale− must be updated at each time step and at each location in the fluid. The relationship between the rheological properties and the volume fraction is estimated experimentally. That is, we use data for rheometry of gels that have been serially diluted by our collaborators, and thoroughly mixed with a test fluid, here, vaginal fluid simulant [65]. The assumption is that local rheological properties of a spreading, diluting gel are well approximated by those properties of homogeneously diluted gel, in equilibrium at each degree of dilution. Now, we introduce two-dimensional convection-diffusion equation for coating flow of a microbicide gel,

$$\frac{\partial \nu}{\partial t} = \left(\frac{\partial}{\partial x}\hat{\imath} + \frac{\partial}{\partial y}\hat{\jmath}\right)\cdot\left[D\left(\frac{\partial \nu}{\partial x}\hat{\imath} + \frac{\partial \nu}{\partial y}\hat{\jmath}\right)\right] - \left(u_1\frac{\partial \nu}{\partial x} + u_2\frac{\partial \nu}{\partial y}\right) \tag{2.5}$$

Here, u_1 and u_2 are the velocities of the gel in the x- and the y-direction. $\hat{\imath}$ and $\hat{\jmath}$ are unit vectors in the x- and the y-direction. ν is the concentration of absorbed water. Generally, the diffusion coefficient, D, varies with concentration [66]. In this study, we utilized a dilution dependent diffusion coefficient D, which has the form,

$$D \equiv D_0 exp(a_d\nu) \tag{2.6}$$

Here, D_0 is the diffusion coefficient in the dry state, i.e., ν is equal to zero. The parameter, a_d, defines the interaction of the network with water [67].

A boundary condition for the transient dilution of a microbicide gel is given in terms of the fluid flux at the wall,

$$q = -D\frac{\partial \nu}{\partial y} \tag{2.7}$$

Boundary flux may alter based on the time of day, or the phase of the ovulation cycle. It may be affected by osmotic effects, or by hydrodynamic pressure in the vaginal lumen. Here, we assume that this flux is constant. Clearly, experimental work is a necessary prerequisite to a more sophisticated theoretical treatment. Usually, the direction of the flux is normal to the wall. Strictly, the flux direction must be updated for each time step because the shape of the bolus is varying through time. Here, we assume that the flux direction is normal to the x-axis. The assumption is reasonable when the gradient of the height profile in the x-direction, $\partial h/\partial x$, has a small value, i.e., $\partial h/\partial x \ll 1$. During spreading of a microbicide gel, the physical domain changes shape. The computational domain in the x-direction must be chosen to be of sufficient length. The upper and lower limits in the y-direction are taken as $\pm h(x,t)$. Hence, special attention should be paid to redefining the grid points in the y-direction at each time step. Although the grid points in the y-direction are changing, the Reynolds lubrication equation, Eq. (2.3) is solvable because only the integrated value over the grid points in the y-direction, not the individual value, is involved in the equation. On the other hand, in the case of the convection-diffusion equation, Eq. (2.5), the grid points in the y-direction should be fixed in order to solve the equation. This is because the dependent variable must be found at individual values of the grid points in the y-direction.

In order to make progress on this problem, the straightforward domain mapping $(x,y) \longrightarrow (x,\zeta)$ is applied. Here, $y = h(x,t)\zeta$. The domain (x,ζ) has the shape of a rectangle instead of the shape of the bolus and the grid points in the ζ-direction are fixed for every time step. The shape of each domain is shown in Fig. 2.2. With this domain mapping, Eq. (2.5) takes the form:

$$\begin{aligned}
\frac{\partial V}{\partial t} &= -u_1\frac{\partial V}{\partial x} - \frac{1}{h}\frac{\partial V}{\partial \zeta}\left[u_2 - \zeta\left(\frac{\partial h}{\partial t} + u_1\frac{\partial h}{\partial x}\right)\right] + \frac{D_0 exp(a_d V)}{h^2} \\
&\times\left\{-\zeta h(1+a_d V)\frac{\partial^2 h}{\partial x^2}\frac{\partial V}{\partial \zeta} + (2a_d + a_d^2 V)\left(\frac{\partial V}{\partial \zeta}\right)^2 + (1+a_d V)\frac{\partial^2 V}{\partial \zeta^2}\right. \\
&+\zeta\left(\frac{\partial h}{\partial x}\right)^2\left[2(1+a_d V)\frac{\partial V}{\partial \zeta} + (1+a_d V)\frac{\partial^2 V}{\partial \zeta^2} + a_d\zeta(2+a_d V)\right. \\
&\times\left.\left(\frac{\partial V}{\partial \zeta}\right)^2\right] - 2\zeta h\frac{\partial h}{\partial x}\left[a_d(2+a_d V)\frac{\partial V}{\partial \zeta}\frac{\partial V}{\partial x} + (1+a_d V)\frac{\partial^2 V}{\partial \zeta \partial x}\right] \\
&\left.+h^2\left[a_d(2+a_d V)\left(\frac{\partial V}{\partial x}\right)^2 + (1+a_d V)\frac{\partial^2 V}{\partial x^2}\right]\right\}
\end{aligned} \tag{2.8}$$

Here, $h = h(x,t)$, $u_1 = u_1(x,y,t)$, $u_2 = u_2(x,y,t)$, and $V = V(x,\zeta,t) = \nu(x,y,t)$. The boundary condition has the form $q = D_0 exp(a_d V)\frac{1}{h(x,t)}\frac{\partial V}{\partial \zeta}$ in the (x,ζ) domain.

The initial condition for the shape of the bolus is taken as,

$$h(x, t=0) = h_\infty + b\ exp\left[-(x/a)^2\right] \tag{2.9}$$

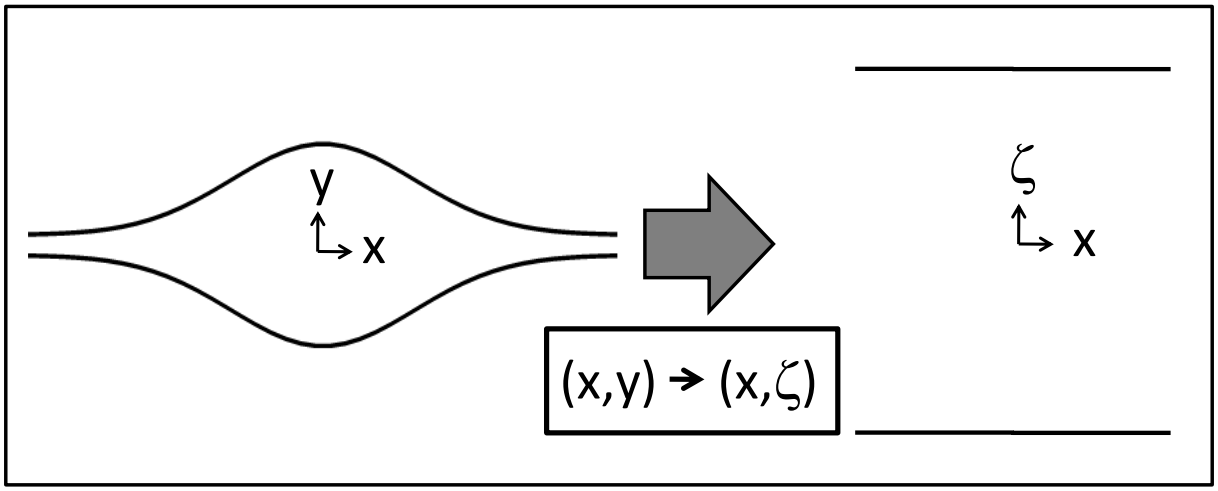

Figure 2.2. Shape of domains. Left domain represents the physical domain. Right domain represents mapped domain by $y = h(x,t)\zeta$.

The volume contained in such a bolus (above h_∞) is $V_b = 2abc\sqrt{\pi}$, where c is the vaginal width, i.e. 2 cm. The volume of the bolus, V_b, is 3 mL. As a scale for the height H, we choose 0.5 cm; this scale is of the order of magnitude of the maximum height of the bolus at time zero. Here we choose $h_\infty = 0.05H$ and $b = 0.45H$, and one obtains $a = V_b/2bc\sqrt{\pi}$.

Basically, two governing transport equations and one constitutive equation, which vary through time and space, are required to define transient inhomogeneous boundary dilution of a flowing microbicide gel. Here, elastohydrodynamic flow is driven by initial distention of elastic surfaces, and the resultant squeezing of the fluid bolus, which is initially at rest. This distention leads to pressure gradients and flow, eventually. For the convective-diffusive transport equation of vaginal fluid, the concentration of added vaginal fluid is initially zero everywhere. We first integrate the x-momentum equation in the y-direction to obtain the shear stresses. The x-momentum equation is the x component of Navier-Stokes equation with the lubrication approximation ($\partial p/\partial x = \partial \tau/\partial y$) with gravity neglected. Here, shear stress can be obtained as, $\tau = y\partial p/\partial x = yM\partial h/\partial x$. Note that at $y = 0, \tau = 0$ due to symmetry. Then by substituting shear stresses into Eq.(2.2) and integrating the x-momentum equation in the y-direction twice, u_1 values are calculated. Velocities in the y-direction (u_2) are easily extracted from the incompressibility condition. Thus far, equations are solved in (x, y) domain. We then solve the convection-diffusion equation (2.8) in (x, ζ) domain, by substituting velocities. After finding the local volume fraction distribution of vaginal fluid, the constitutive equation (2.2), which is a function of ν, is updated at each point. Iteration now proceeds and the Reynolds lubrication equation is solved with the updated parameters. We have developed the governing equations accounting for the gravitational forces. However, there is not a standard way of placing these microbicide vehicles. Gravitational effects can be in any direction of the spreading, as determined by the patients posture during and after insertion of the microbicide. In the present manuscript, gravity is set to zero for simplicity.

We solved the Reynolds lubrication equation explicitly. On the other hand, the convection-diffusion equation for the exuded vaginal fluid was solved implicitly. We split the convective-diffusive transport finite difference equation into two, one with the x-derivative taken implicitly and the next with the y-derivative taken implicitly, following Alternating Direction Implicit (ADI) method. The resulting tri-diagonal matrices were solved by the Thomas algorithm. Central differences were used for the first and second order spatial derivatives.

2.3 Results

2.3.1 Preliminary results for spread of a homogeneously diluted microbicide gel

The volume of native vaginal fluid present in the vagina is estimated at approximately $0.5-0.75$ mL [65]. The production of fluid is measured as $1 - 10$ cm^3/day, depending on the phase of the menstrual cycle [68]. Taking the vaginal surface area as about 100 cm^2, this corresponds to a flux of $q \approx 10^{-9} - 10^{-8}$ m/s. Hence, for a typical gel volume of 3 mL the range of dilution by vaginal secretions is 10% to 30% [58]. As a preliminary analysis, the effect of dilution by vaginal secretions on a prototype gel will be considered. This is an aqueous gel with 3% hydroxyethylcellulose (known as Azopharma Orange) that is similar to the placebo gel used in the successful microbicide gel trial [3]. As an initial approach to effects of gel dilution on flow, we assume that the mixing ratio of gel and vaginal secretions is constant and that dilution is homogeneous during the spreading

Case	Dilution	n	$m_0(Pa.s)$	$m(Pa.s^n)$
1	0%	0.640693	738.965	78.5395
2	10%	0.609243	509.617	53.2084
3	20%	0.58495	229.597	27.7059
4	30%	0.474114	146.972	16.4701

Table 2.1. Parameters of Carreau-like model for homogeneously diluted AO gel by viscometric experiments.

process, as in the initial studies of dilution [58]. Gel rheological properties at body temperature (37^oC) were obtained for serial dilutions of the gel with vaginal fluid simulant [65], using a constant stress protocol on a TA Instruments model AR 1500ex rheometer, with a 4^o cone and 20 cm plate configuration. Shear rates ranged from $\sim 10^{-4} - 42\ sec^{-1}$ and data were fitted to the Carreau-like model, cf. Table 2.1.

Results are illustrated in Fig. 2.3 for the profile of the bolus at 30 minutes after the onset of flow. The height profiles are shown for 0%, 10%, 20%, and 30% dilutions. Plots show only the upper half of the bolus because flow is symmetrical about the x-axis. The spreading length of the bolus increases with the extent of gel dilution. This effect was also observed in [58]. Table 2.1 shows that the zero shear viscosity m_0 decreases by about 80% and the shear thinning exponent n decreases by about 25% as dilution increases to 30%. Qualitatively, dilution enhances the spread of the gel. In order to quantify the effect of dilution clearly, the coated area is shown in Fig. 2.4. The length of spreading of the bolus, which is proportional to the effective surface area coated, we define as four standard deviations of the bolus height profile. Then, this is multiplied with the physical width of the vagina, i.e. 2 cm. The effect is clearly significant; for example, a 30% diluted gel coats in 2 minutes the same area coated in 10 minutes by an undiluted gel.

In order to understand the basis for increased spreading with dilution an effective viscosity of the gel is estimated, in relation to the shear stress on the wall. The shear stress can be written as,

$$\tau_{wall} = \left(M \frac{\partial h}{\partial x} - \rho g \right) h \tag{2.10}$$

We show the shear stress on the wall, or $y = h(x,t)$, for each case at 30 minutes in Fig. 2.5. Effective viscosity can be defined as inverse of $F(\tau_{xy})$. Fig. 2.6 shows the effective viscosity on the wall at 30 minutes. The larger effective viscosity leads to less coated area. Therefore, the coated area of more diluted gel is increasing because of the smaller effective viscosity.

2.3.2 Boundary dilution of a microbicide gel by vaginal fluid

In order to conduct analysis of the consequences of inhomogeneous boundary dilution, the parameters of the constitutive equation and the volume fraction of vaginal fluid are linked to data from experiments, as described above. From curve fitting of experimental data obtained for the AO gel diluted in 5% increments from 0% to 75%, the parameters of the Carreau-like constitutive model take the form,

$$m_0 \quad = \quad -2274.02\nu^3 + 4922.72\nu^2 - 3437.98\nu + 786.04$$

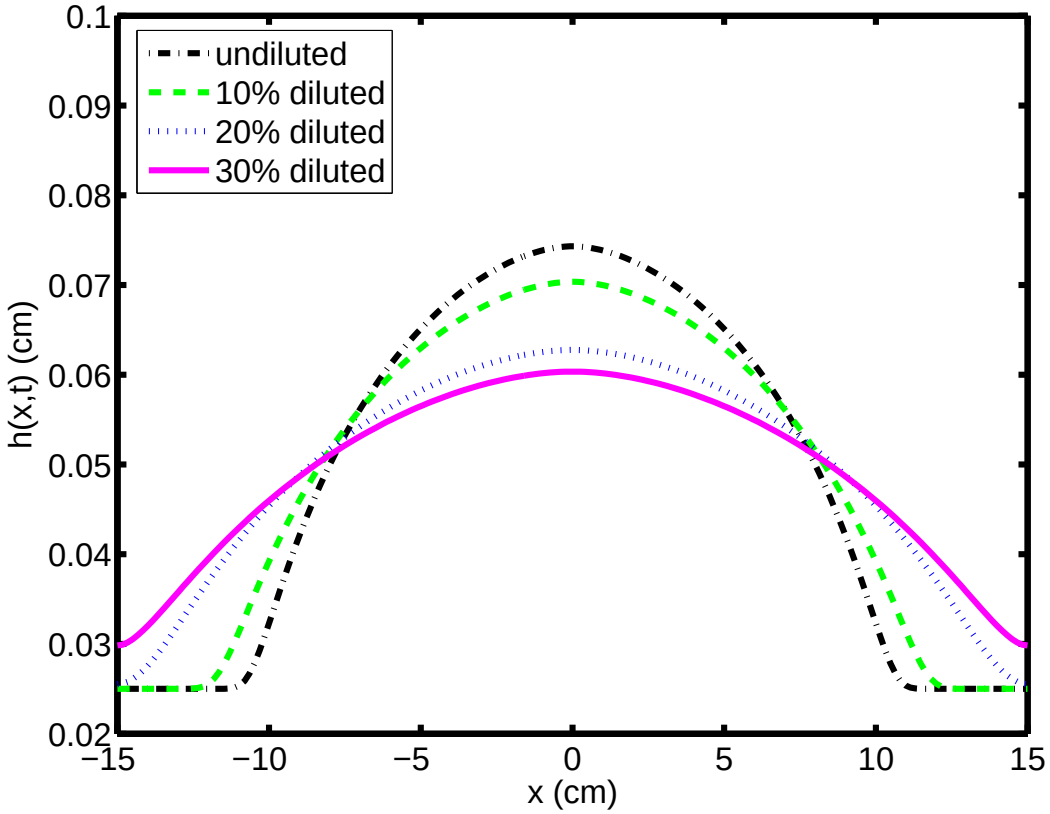

Figure 2.3. Height profile of boluses of homogenously diluted at 30 minutes.

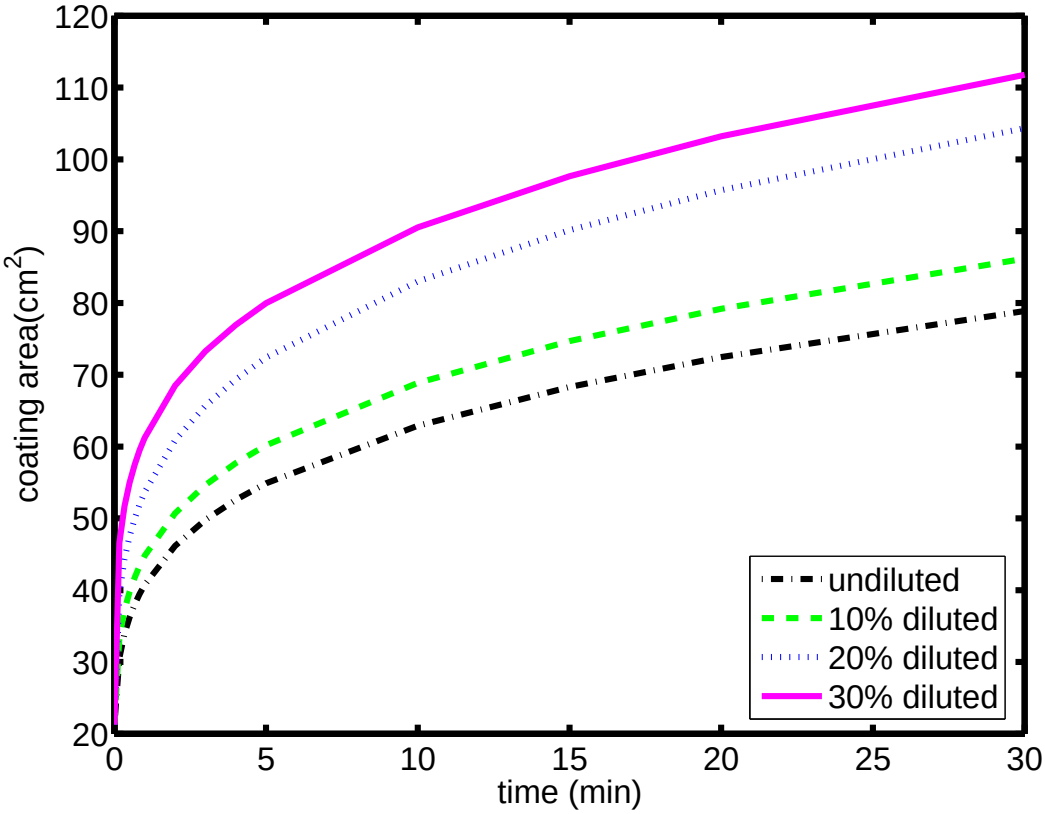

Figure 2.4. Coated area of homogenously diluted gel vs. time.

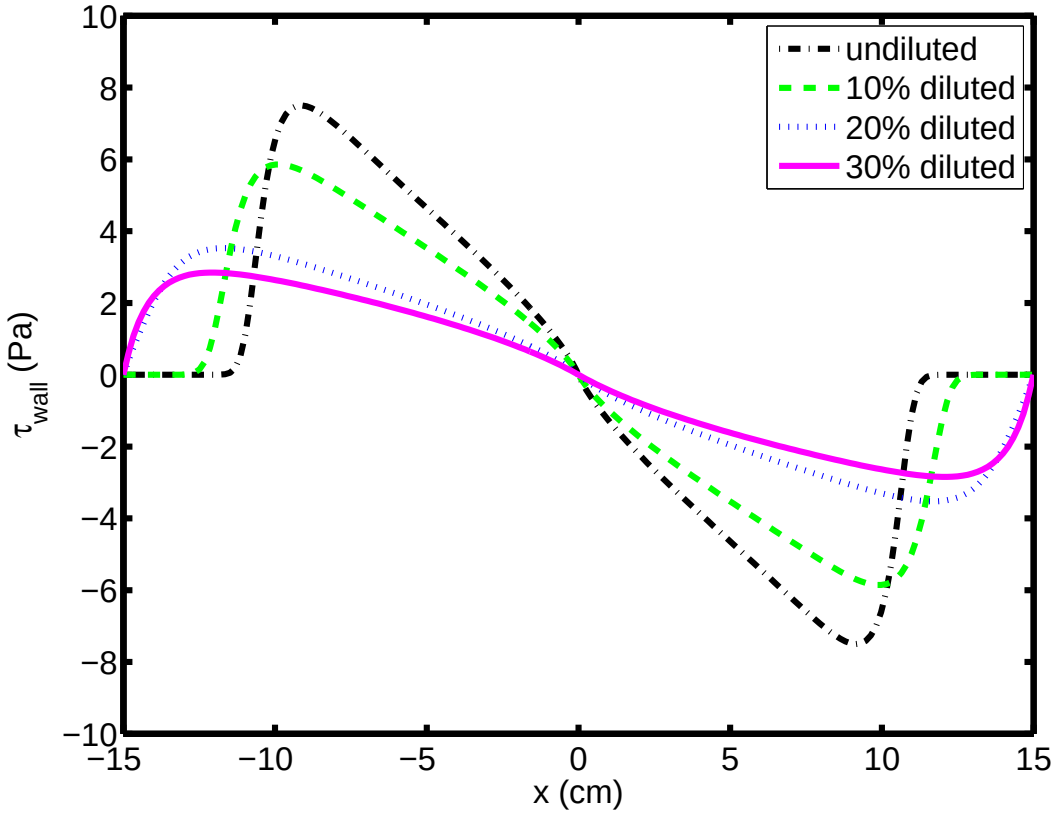

Figure 2.5. Shear stress on the wall for homogenously diluted gel at 30 minutes.

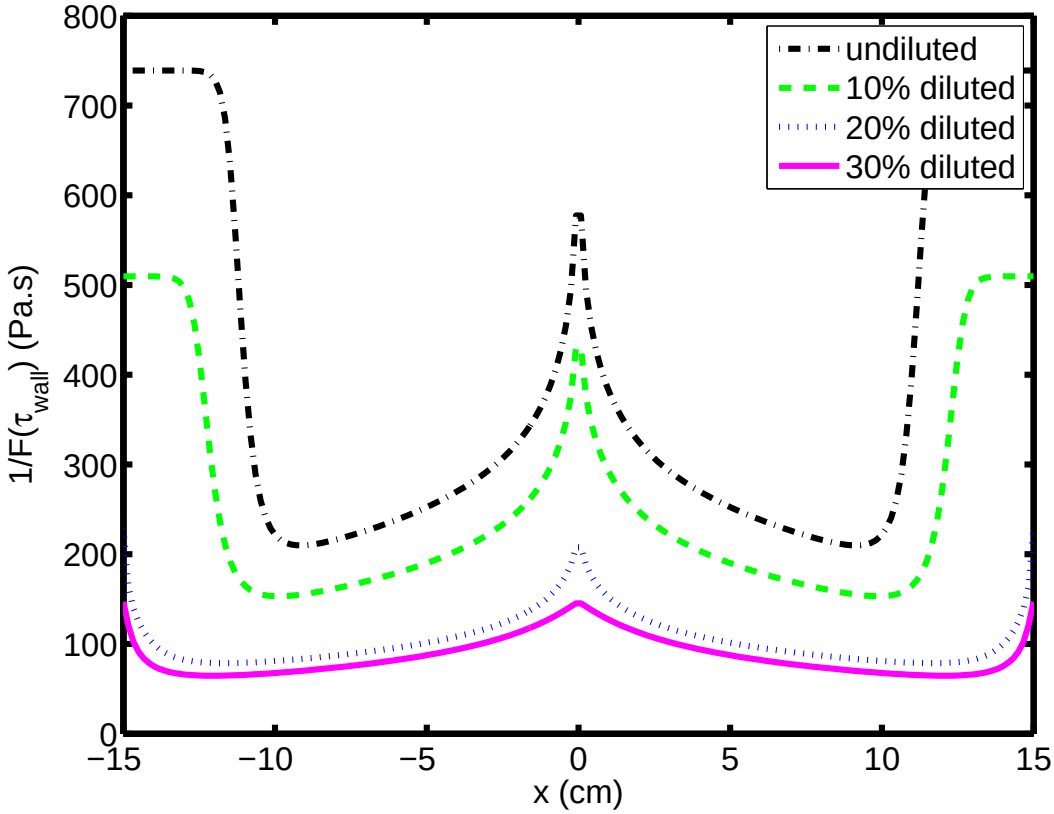

Figure 2.6. Effective viscosity of homogenously diluted gel on the wall at 30 minutes.

Case	$q(m/s)$	MVF1	MVF2
1	0	0	0
5	1×10^{-9}	0.000140	0.000137
6	5×10^{-9}	0.000698	0.000686
7	1×10^{-8}	0.001424	0.001371

Table 2.2. ($D_0 = 10^{-6} cm^2/s$) The constant wall flux of vaginal fluid. Mean volume fractions are obtained at 1 minute. MVF1 is obtained from numerical solution of Eq. (2.8). MVF2 is calculated by Eq. (2.12).

$$\begin{aligned} n &= -0.6905\nu^3 + 1.9704\nu^2 - 0.9217\nu + 0.6601 \\ \lambda &= 27936.58\nu^3 - 18847.95\nu^2 + 1847.44\nu + 382.10 \end{aligned} \tag{2.11}$$

Here, ν is the volume fraction of vaginal fluid, and the parameter, m, can be obtained from the relationship, $m = m_0\lambda^{n-1}$. The volume of the bolus is 3 mL, the compliance of the wall is $10^4/0.5$ Pa/cm [34]. The factor D_0 in the diffusion coefficient is set to either 10^{-6} cm^2/s or 10^{-5} cm^2/s. These values were chosen in relation to the diffusivity of water molecules in water (2×10^{-5} cm^2/s [69]). Because the gel is initially quite hydrated ($> 90\%$), we expect relatively little restriction in diffusion of water molecules into and within it.

For simplicity, a constant flux of vaginal fluid exuded from the walls is assumed here. Although this assumption may not correspond exactly to *in vivo* conditions, the results provide conceptual insight for the transient dilution phenomenon. Volume fraction at the boundary is found iteratively because both ν and time-derivative of ν at the boundary are used in the boundary condition, $q = D_0 exp(a_d V) \frac{1}{h(x,t)} \frac{\partial V}{\partial \zeta}$. Additionally, the physical properties of the vaginal fluid are equal to those of water [65].

Coated area is plotted for different a_d values in Fig. 2.7. Here, q is kept constant at 1×10^{-8} m/s (~ 8 cm^3/day): if effects of non-zero a_d are not manifest at this value, then for lower values of flux we can simply equate a_d to zero. As seen in Fig. 2.7, coated area is insensitive to the value of a_d. This can be partly explained, as noted above, by the relatively low rate of dilution and the fact that the gels, as prepared, are generally already quite dilute. In the analyses that follow, a_d will be set equal to 0.

We now present results for different q values, cf. Table 2.2. The height profile of the bolus for each case is shown in Fig. 2.8. In Fig. 2.9, the coated area is plotted. As can be seen from the figure, coated area increases as the flux of the exuded vaginal fluid increases. In Figures 2.10 and 2.11, the diffusion coefficient is increased from 10^{-6} cm^2/s to 10^{-5} cm^2/s. In Fig. 2.10, the height profiles of the bolus for $D_0 = 10^{-5}$ cm^2/s are shown. Coated area for each case is given in Fig. 2.11. Here, coated area again increases as the flux of the exuded vaginal fluid increases.

Table 2.2 gives the mean volume fraction of the vaginal fluid for each case. In addition, the value of the volume fraction, as calculated based on the volume of a microbicide gel and the exuded vaginal fluid, MVF2, is shown to help verify the accuracy of the numerical analysis. This latter volume fraction can be obtained from

$$MVF2 = [q \times (\text{area of vaginal wall}) \times (\text{time})] / [\text{total volume}] \tag{2.12}$$

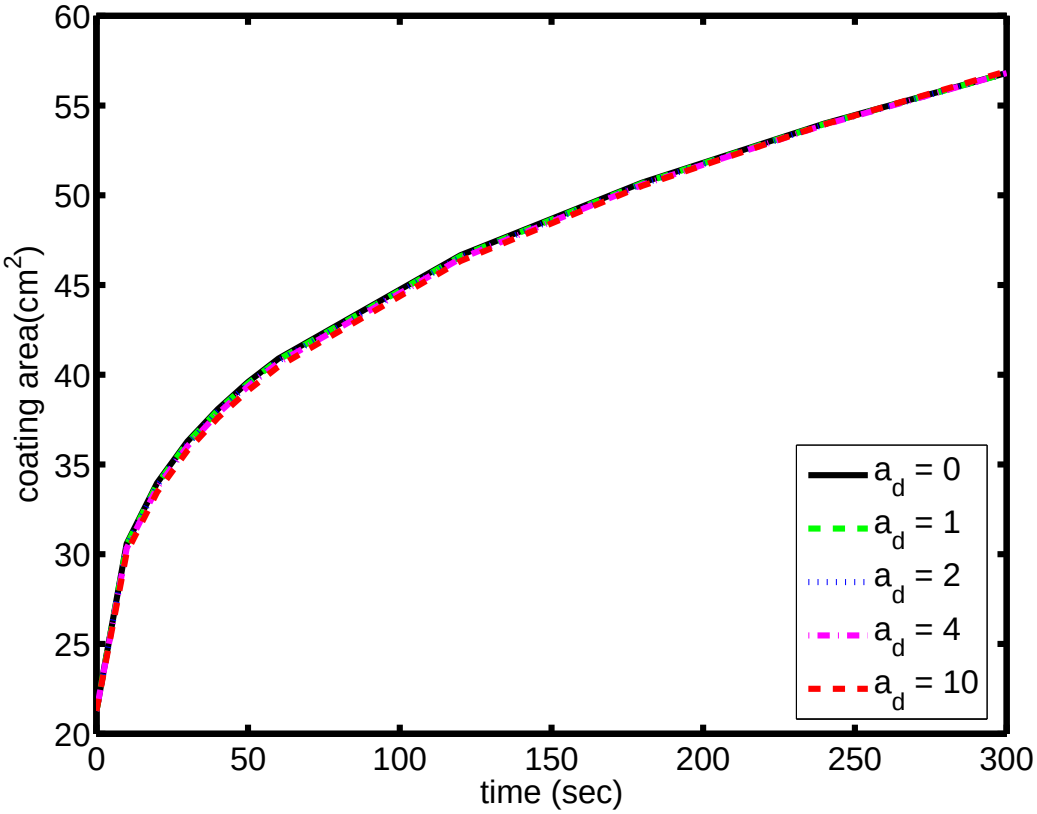

Figure 2.7. Coating area of the gel on the surface for $a_d = 0$, 1, 2, 4, and 10 ($q = 1 \times 10^{-8}$ m/s, $D = 10^{-6}$ cm^2/s).

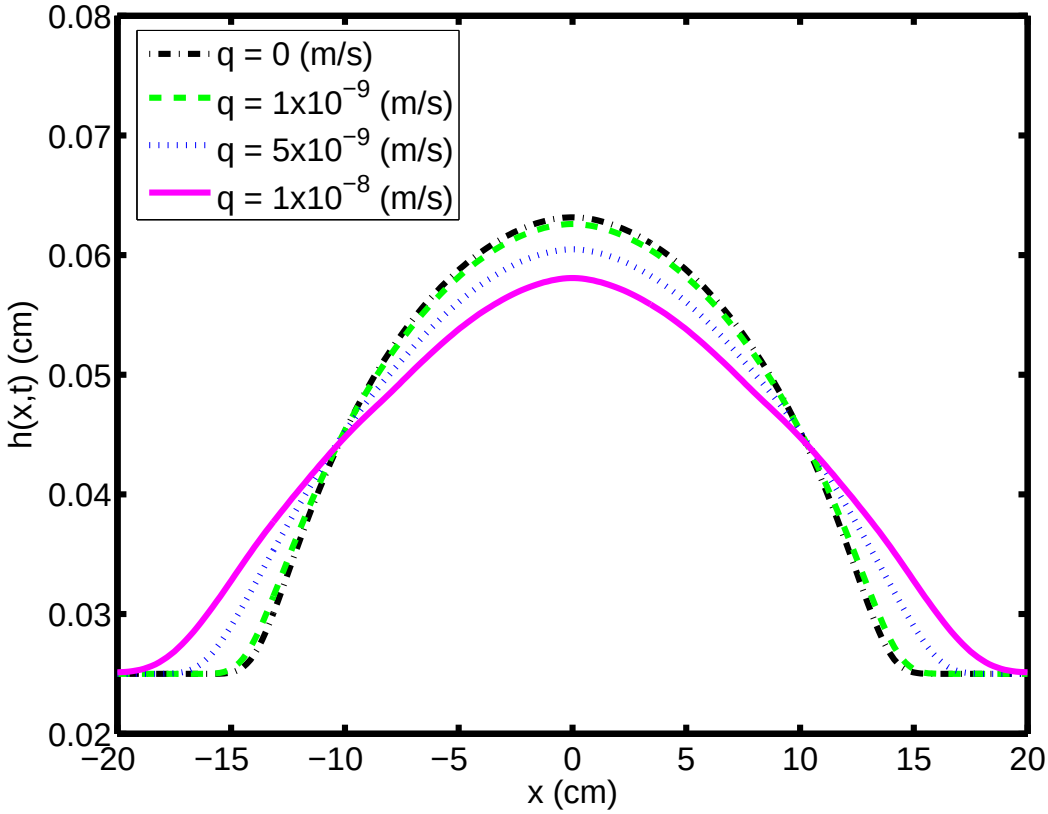

Figure 2.8. Height profile of bolus at 2 hours for $q = 0\ m/s$, $1 \times 10^{-9}\ m/s$, $5 \times 10^{-9}\ m/s$, $1 \times 10^{-8}\ m/s$ ($D = 10^{-6}\ cm^2/s$).

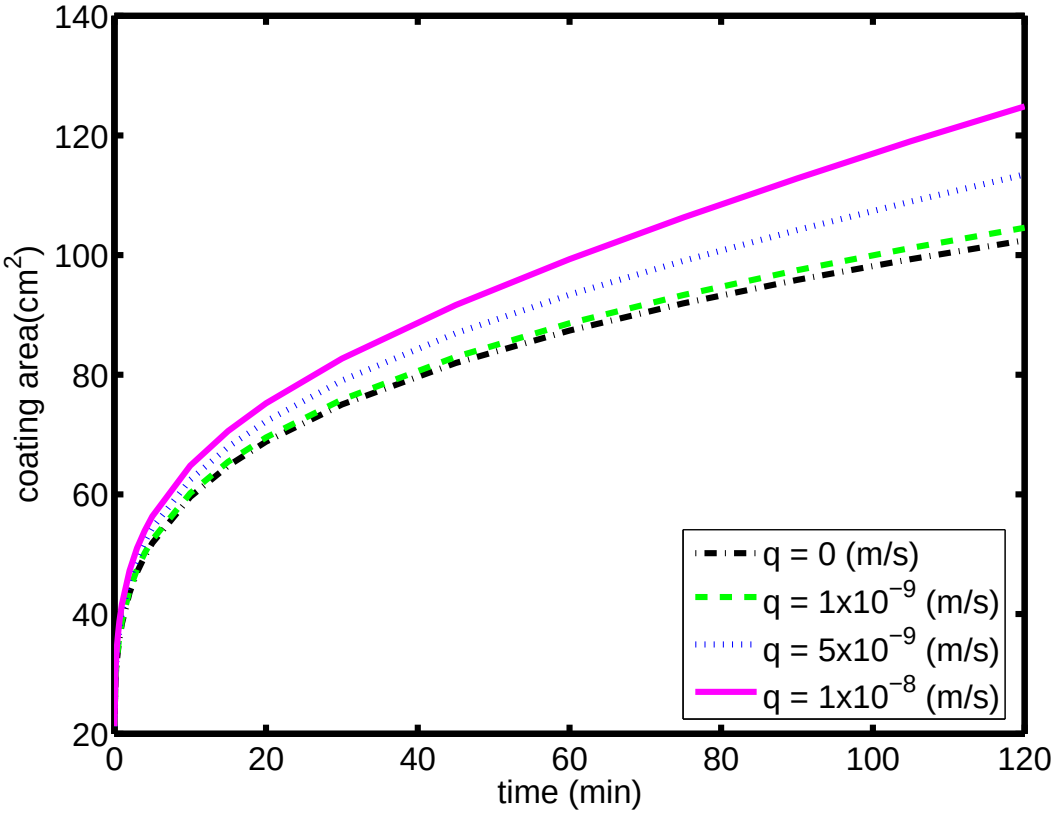

Figure 2.9. Coating area of the gel on the surface for $q = 0\ m/s$, $1 \times 10^{-9}\ m/s$, $5 \times 10^{-9}\ m/s$, $1 \times 10^{-8}\ m/s$ ($D = 10^{-6}\ cm^2/s$).

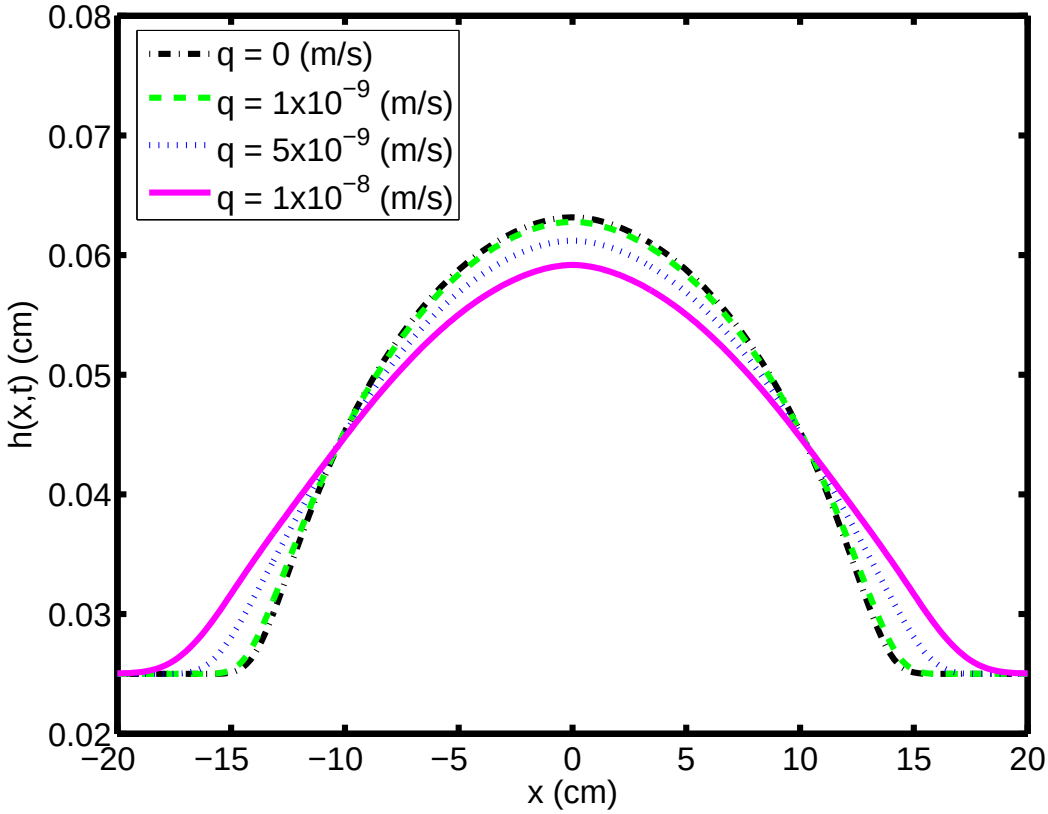

Figure 2.10. Height profile of bolus at 2 hours for $q = 0\ m/s$, $1 \times 10^{-9}\ m/s$, $5 \times 10^{-9}\ m/s$, $1 \times 10^{-8}\ m/s$ ($D = 10^{-5}\ cm^2/s$).

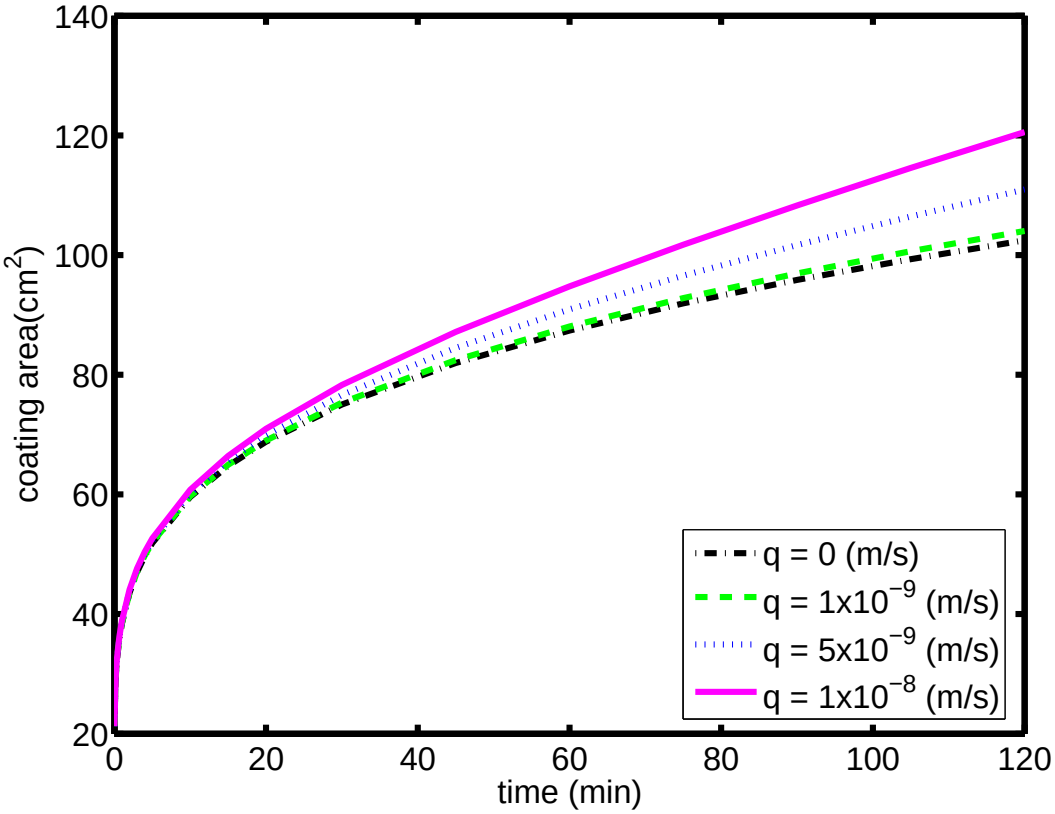

Figure 2.11. Coating area of the gel on the surface for $q = 0\ m/s$, $1 \times 10^{-9}\ m/s$, $5 \times 10^{-9}\ m/s$, $1 \times 10^{-8}\ m/s$ ($D = 10^{-5}\ cm^2/s$).

2.4 Discussion

Dilution of a fluid from its boundary during the course of flow within an enclosed channel is a time and space dependent process. At each instant, the spatial distribution of local rheological properties −which depend upon the local dilution− has a profound effect upon the velocity profile. This effect is exacerbated for a non-Newtonian, shear thinning gel, as was considered here. Analyses of the vaginal coating flows of microbicide drug delivery gels, the application of primary interest here, should therefore account for the boundary dilution process. There are many factors, (e.g., the diluent fluid flux at the boundary, and the diffusion coefficient of diluent within the gel), which influence the coupled dilution-gel flow processes −in this model and, presumably, *in vivo*. More accurate results can be obtained when all of these factors are considered, as discussed in the following paragraphs.

2.4.1 Distribution of volume fraction and the diffusion coefficient

The coating area of the gel increases due to dilution by fluid from the boundary. In this model and presumably for microbicide gel flow *in vivo*, the local distribution of gel dilution (expressible as the volume fraction of fluid penetrant added to the gel) is not uniform. In Fig. 2.12 and 2.13, we show the volume fraction of diluent fluid for $D = 10^{-6}\ cm^2/s$ and $D = 10^{-5}\ cm^2/s$, respectively. Results are plotted for case 7 in Table 2.2 at 1 minute, 5 minutes, 30 minutes and 2 hours. Here we note the high volume fraction in the vicinity of the wall, giving rise to what we term a slippery region. In addition, at the leading edge the volume fraction of diluent fluid is also increased. This can be interpreted as due to the gel flow from the center to the leading edge. The presence of such a slippery region near the vaginal wall increases the flow rate and coating area even though the size of the slippery region is relatively small, appearing as a dilution boundary layer. For the case of the higher diffusion coefficient, the contours of increased dilution near the boundaries extend further into the gel, cf. Fig. 2.13. That is, the diluent fluid is diffusing more easily from the slippery regions to inner regions of the gel bolus, thereby decreasing the spreading rate. This is illustrated in Figure 2.14.

In the context of intravaginal flow of a microbicide gel, we have very little information about variability, spatial and temporal, of vaginal fluid flux at the wall. This flux is due to a transudation process rather than active secretion [65]. Such transudation is influenced by vaginal wall fluid permeability which has been shown to vary [70], [71]. The current model, by assuming a temporally and spatially constant wall flux, is an approximation, strictly speaking. Still, results in this study provide insight about the importance of transient dilution for the coating flow of the gel.

2.4.2 Coating area and velocity profile

Obviously, the coating area increases when the magnitudes across the velocity profile increase. The mean values of the magnitude of the velocity are shown in Tables 2.3 and 2.4. As expected, for larger coating areas (e.g., case 7 in Fig. 2.9), the velocity reaches higher values.

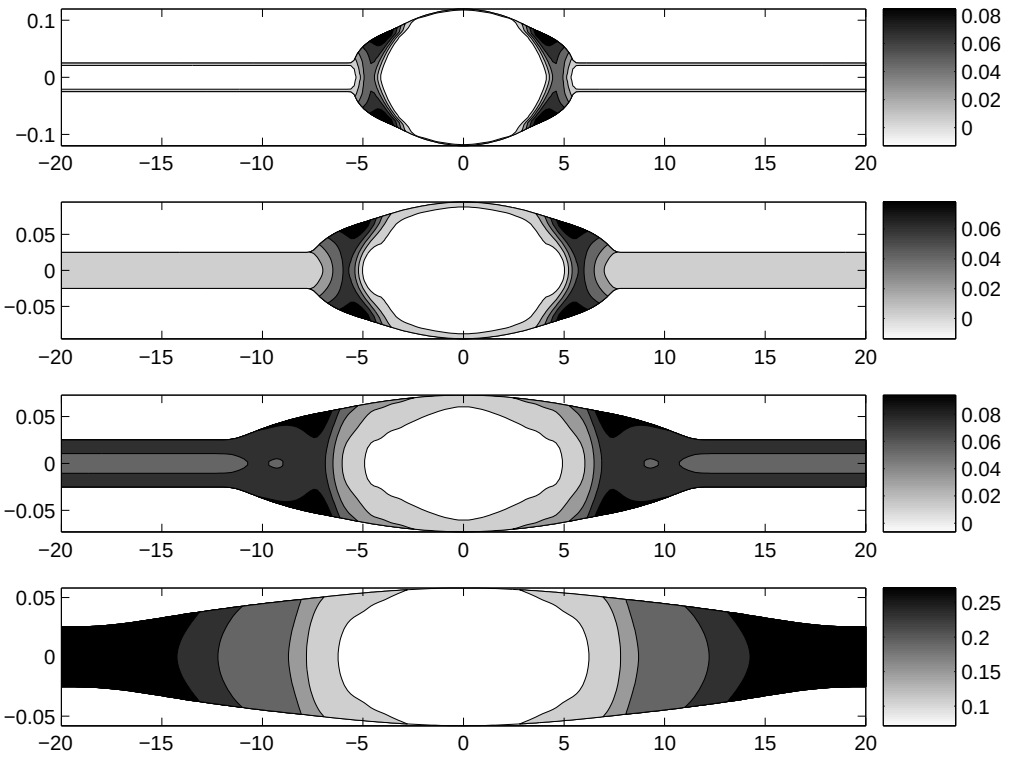

Figure 2.12. ($D = 10^{-6}\ cm^2/s$). Contour plot for volume fraction of vaginal fluid at 1 minute, 5 minutes, 30 minutes, and 2 hours (top to bottom). Note different contour levels in different panels.

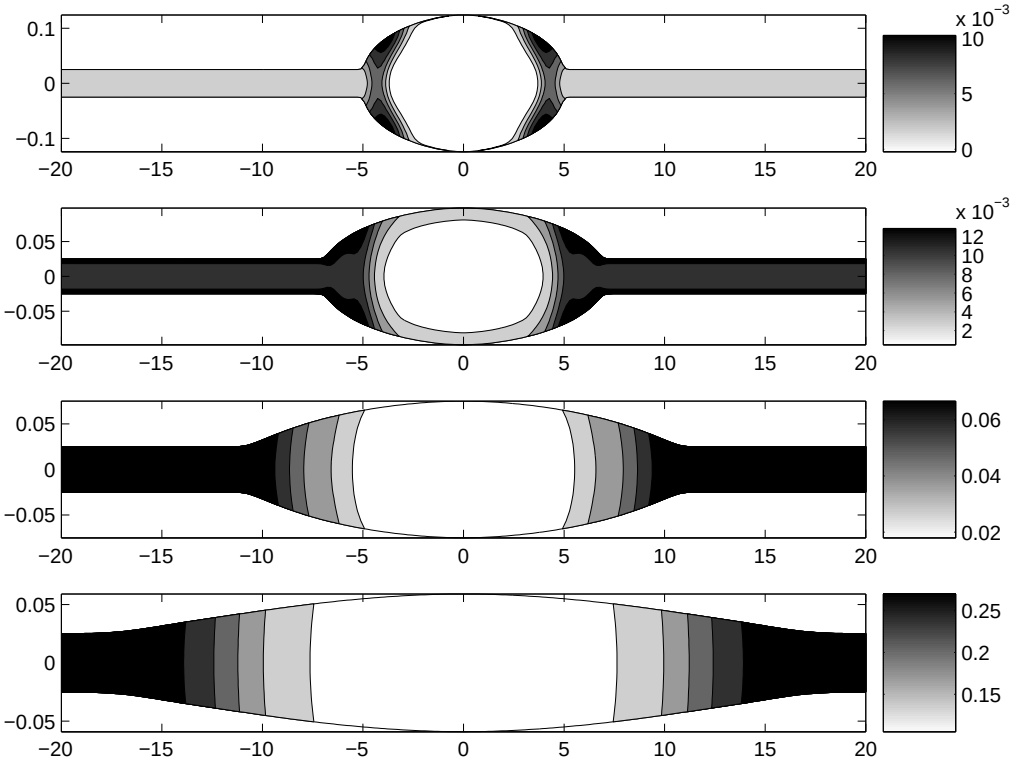

Figure 2.13. ($D = 10^{-5}\ cm^2/s$). Contour plot for volume fraction of vaginal fluid at 1 minute, 5 minutes, 30 minutes, and 2 hours (top to bottom). Note different contour levels in different panels.

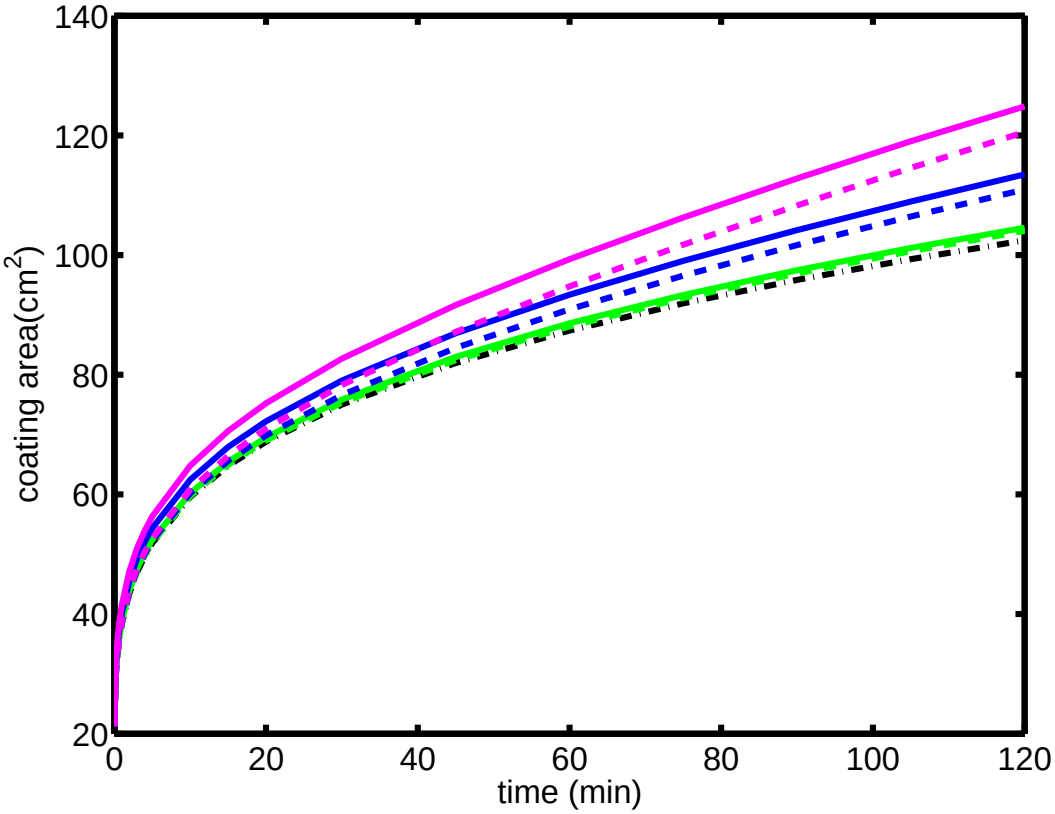

Figure 2.14. Coating area of the gel on the surface for $q = 0\ m/s$ (dashed-dot), 1×10^{-9} m/s, $5 \times 10^{-9}\ m/s$, $1 \times 10^{-8}\ m/s$ ($D = 10^{-5}\ cm^2/s$ (dashed) and $10^{-6}\ cm^2/s$ (solid)).

Case	mean of $\|u\|(mm/s)$	mean of $1/F(\tau_{xy})(Pa.s)$	coating area (cm^2)
1	0.0145	622.58	102.48
5	0.0262	618.04	104.57
6	0.0761	601.57	113.48
7	0.0827	583.74	124.86

Table 2.3. ($D_0 = 10^{-6} cm^2/s$) Averages of velocity profiles at $x = 5\ cm$ and averages of effective viscosities at 1 minute, and final coating areas.

Case	mean of $\|u\|(mm/s)$	mean of $1/F(\tau_{xy})(Pa.s)$	coating area (cm^2)
1	0.0145	622.58	102.48
5	0.0156	621.47	104.04
6	0.0207	617.06	110.97
7	0.0288	611.61	120.57

Table 2.4. ($D_0 = 10^{-5} cm^2/s$) Averages of velocity profiles at $x = 5\ cm$ and averages of effective viscosities at 1 minute, and final coating areas.

2.4.3 Velocity profile and effective viscosity

From Reynolds lubrication equation, the velocity profile has the form,

$$u_1 = M \int_{-h}^{y} F(\tau_{xy}) \frac{\partial h}{\partial x} y dy \tag{2.13}$$

The magnitude of the velocity is proportional to the function $F(\tau_{xy})$, which is the inverse of the effective viscosity, and the gradient of the height profile in the x-direction. Clearly, the gradient of the height profile in the x-direction has similar values for all cases in table 2.2 (see Fig. 2.8 and 2.10). The mean values of the effective viscosity, or the inverse of the function $F(\tau_{xy})$, are shown in Tables 2.3 and 2.4. The magnitude of the velocity increases when the effective viscosity decreases. Note that the increase in velocity is higher for the lower $D_0 = 10^{-6}\ cm^2/s$ due to larger decrease in effective viscosity near the wall.

2.4.4 Effective viscosity and volume fraction of vaginal fluid

The parameters of the function $F(\tau_{xy})$ are determined by the volume fraction of vaginal fluid (see Eq. (2.11)). As noted above, in the more diluted gel, in which the volume fraction of diluent is higher, the effective viscosity is relatively small. From Table 2.2, we see that the mean volume fraction is higher in the case of the larger wall flux. Hence, the larger wall flux corresponds to the smaller effective viscosity in Tables 2.3 and 2.4.

In conclusion, we have presented a new model of an internal elastohydrodynamic flow of a non-Newtonian fluid that is being continuously diluted due to flux of another fluid at its boundary. Inhomogeneous boundary dilution clearly provides the potential for significant acceleration of the coating flow; for example, from Fig. 2.9 one can observe a decrease by nearly 50% in the time required to coat an area of 100 cm^2 at the highest boundary flux rates. Thus, understanding

boundary dilution is critical to understanding the physical processes underlying the pharmacokinetics. This may have applications in a number of biomedical flow problems of interest, e.g. in the respiratory and musculo-skeletal systems. Our primary focus is upon vaginal coating flows of anti-HIV microbicide gels. Results here improve the accuracy with which those flows can be modeled. Vaginal fluid production can vary due to a number of factors, including progression of the menstrual cycle and age. This new model incorporates such fluid production, and is amenable to input of spatial (along the vaginal canal) and temporal variations in that production. It can be used in methodology that provides objective evaluations of microbicide gel performance and in the design of new, improved gels (e.g. [72]).

Chapter 3

The consequences of yield stress on deployment of a non-Newtonian anti-HIV microbicide gel

3.1 Introduction

Elastohydrodynamic flow theory can be used to model a number of flows of biomedical interest [43]–[47]. In this regard, a relatively recent and compelling problem is application of vaginal gels for delivery of mucosal antigens or of topical 'microbicide' molecules to inhibit infection by sexually transmitted pathogens such as HIV [43], [48], [50]–[52]. This low-cost modality could have substantial biomedical and epidemiological importance, enabling women to control their susceptibility to infection. Very recently, use of a vaginal gel formulation of the antiretroviral drug Tenofovir has shown significant reduction in HIV transmission in a clinical trial [3]. This is the first time that a topical microbicide gel has shown significant efficacy, and comes after failures of several other gels in prior trials. This initial success notwithstanding, there is widespread agreement that more effective microbicide delivery vehicles must be developed. This should be based, in part, upon a better understanding of how gel spreading and retention in the vagina govern successful anti-HIV drug delivery. Once that understanding is developed, specific gels can be created with characteristics designed to optimize their spreading, retention and drug delivery [72].

The vaginal gel coating flow problem involves: significant deformation of tissue accompanying the flow; little alteration of gel physical properties associated with pressure and temperature changes [73]; non-Newtonian gel behavior; and oftentimes yield stress behavior (depending upon the composition of the gel [72]). There are multiple mechanisms by which current microbicides act to prevent infection by genital pathogens. For all of these, a deeper physical understanding and mathematical modeling of vaginal coating flow is clearly needed. Recently, we developed a framework

for understanding the transluminal flow (along the vaginal canal) of microbicide vehicles driven by combined elastic squeezing and gravitational sliding [34]. These are believed to be the primary forces acting to drive such flow [54]. We then enhanced our model with a convective-diffusive transport equation to characterize water transport into the gel and, thus, spatially inhomogeneous gel dilution in chapter 2. Neither of these initial studies took into account yield stress behavior of the fluids, despite the fact that many current microbicide gels do exhibit such behavior. The goal of the present chapter is to incorporate such yield stress behavior into the biomechanics of vaginal coating by non-Newtonian gels.

Coating by a microbicide vehicle is a physically diverse process in which several factors interact to govern the flow. Among these are gravity, transvaginal pressure gradients due to contractility of the supporting viscera, the transverse squeezing forces from the distended epithelium, the possible yield stress as a rheological property of the microbicide gel, and the dilution by vaginal fluids being exuded from the boundaries (i.e. tissue surfaces). There have been initial fluid mechanical studies of intravaginal vehicle flows; these have focused on the individual effects of gravity or epithelial squeezing [55]–[57]. These initial studies are instructive in developing a physical understanding of the mechanisms of intravaginal vehicle deployment flows. The model developed in [34] incorporates simultaneous effects of a longitudinally directed force along the vaginal canal, e.g., gravity, and transversely directed epithelial squeezing in a lubrication flow analysis. Both non-Newtonian (in the form of Carreau constitutive model) and Newtonian fluid behaviors were considered. The Carreau model was chosen because microbicide gels (which are highly hydrated) are shear thinning and typically exhibit a plateau at low shear strain rates in a log-log plot of shear stress vs. shear strain rate. Because vaginal coating flows are slow flows in which much of the flow field experiences low shear strain rates, it is important to employ a constitutive equation that embodies such plateau behavior. The Carreau model does precisely this, while the Power Law model overestimates shear stress at the biologically relevant low shear strain rates. In our prior analysis, a single dimensionless number, independent of viscosity, was derived to characterize the relative influences of squeezing and gravitational acceleration on the coating flow in the Newtonian case. A second scale, involving viscosity, was used to determine the spreading rate. In the case of a shear-thinning fluid, the Carreau number also played a role. More recently, we extended this analysis, incorporating the effects of gel dilution due to contact with vaginal fluid produced at the gel-tissue interface [1]. Here, the model developed in [34] was supplemented by a convective-diffusive transport equation to characterize water transport into the gel, and, thus, local gel dilution. The problem was solved using a multi-step numerical scheme in a moving domain. The association between local dilution of the gel and its rheological properties was obtained experimentally, delineating the way constitutive parameters of a shear thinning gel were modified by dilution.

In the present study, we add yield stress behavior of microbicide vehicles to the elastohydrodynamic lubrication model of [34]. A microbicide gel can be designed to have a yield stress, e.g. by including derivatives of polyacrylic acid such as Carbopol and/or polycarbophil in its composition. In a limiting case, a yield stress fluid is a viscoplastic material that behaves as a rigid body at low applied stress but flows as a viscous fluid at higher stress, i.e. behaving as a Bingham fluid [74]. The physical basis of such behavior is that the liquid contains particles (e.g., clay), or large molecules (e.g., polymers) that interact, creating a weak solid structure; a certain amount of stress is required to break this structure. Yield stress fluids are used, for example, as mathematical models of the flow of mud in offshore engineering, and in the analysis of slurries.

The flows of yield stress fluids have been investigated under a range of conditions in the literature [35], [36]. It is common for flows of these fluids to exhibit complex, spatially inhomogeneous

behavior, i.e., mixed flows of rigid body and viscous flow simultaneously. Details depend upon the absolute value of local stress throughout the fluid. This suggests the concept of the yield surface, over which the value of stress is equal to the yield stress. A yield stress fluid follows a different constitutive equation when the absolute value of stress exceeds the yield stress, delineated by the location of the yield surface. Due to such rheological behavior, yield stress fluids can be analyzed in separate domains of validity for each constitutive equation, as determined by the absolute local value of stress. As an alternative, Smyrnaios et al. used a continuous rheological model for yield stress fluids [75], which spans the entire domain with a single constitutive model [76]. Here, the yield surface does not have to be placed within the domain [77]. Such an approach was originally proposed by Papanastasiou [78]. In the present chapter, we employ another continuous rheological model, i.e. the biviscosity model [79], implemented for a Carreau-like fluid.

Although fundamental, the developments here will be useful to the microbicide community. The concept of a yield stress fluid as the gel delivery vehicle for an intravaginal microbicide is attractive because such a material may tend to stay in place after coating vulnerable surfaces (when shear stresses are sufficiently small) and not be prone to leakage from the vagina. In addition to being more cosmetically acceptable to users, this may be an important factor in sustaining drug delivery, and also providing a physical barrier to HIV migration from semen to tissue [80].

3.2 Problem formulation

In this section, we first discuss the physics of the flow problem, and then explain a certain yield stress paradox observed in lubrication flows. We then determine conditions that render the lubrication theory of elastic wall squeezing flow consistent with the study of a yield stress fluid, using scaling analysis. We present a biviscosity model of a Carreau-like fluid with a yield stress, and the Reynolds lubrication equation as an evolution equation for the shape of a bolus of non-Newtonian fluid. The equations are developed in the symmetric domain $-h(x,t) \leq y \leq h(x,t)$ and a body force is included in the x-direction. The physical problem and computational domain are sketched in Fig. 3.1. The model is formulated in a 2D Cartesian domain. The simplification of two-dimensional flow is quite relevant anatomically; the cross section of the undistended human vaginal canal is "H" shaped, with the transverse dimension large compared to the vertical openings on its two sides [62].

3.2.1 Physics of the Flow Problem

The elastohydrodynamic flow of microbicide gels is driven by initial distention of elastic surfaces (squeezing) and potentially, gravitational acceleration which depends on the woman's posture. Following the placement of a gel into the vagina, the vaginal walls distend and this creates an elastic restoring force and leads to a pressure-gradient along the vaginal canal in the longitudinal direction. For the absence of a yield stress, for a non-Newtonian fluid, we make use of the lubrication approximation, obtaining the governing equation as [34],

$$\begin{aligned}\frac{\partial h}{\partial t} &= \frac{2^{-2-1/n}h}{3Cr(1+2n)\beta(W-4h_{,x})}\{6(1+2n)(W-4h_{,x}) \\ &\quad \times[-\beta hCr(W-4h_{,x})]^{1/n}\,h_{,x} + 2^{2+1/n}Cr(1+2n)\end{aligned}$$

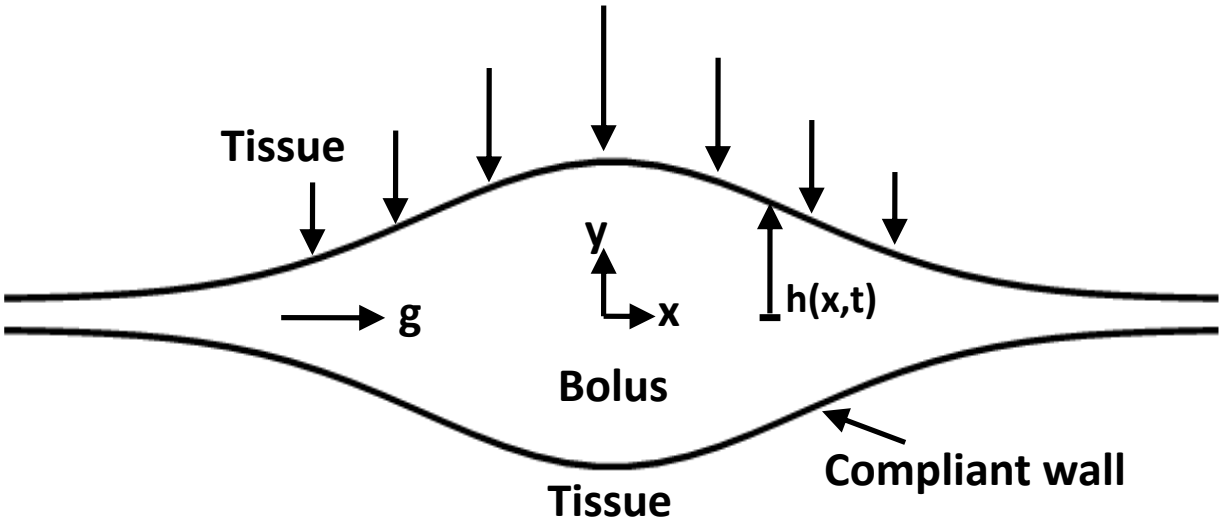

Figure 3.1. Definition sketch of the vaginal canal, emphasizing the longitudinal direction. The introitus is to the right. The transverse direction has an "H" shaped cross section; see text.

$$\times\beta(W-4h_{,x})h^2h_{,xx}-3h\left\{2^{1/n}Cr(1+2n)\right.$$
$$\left.+\ \beta(W-4h_{,x})^2h_{,x}+8\left[-\beta hCr(W-4h_{,x})\right]^{1/n}h_{,xx}\right\}\right\} \tag{3.1}$$

where $Cr \equiv \frac{\tilde{m}_0^{1/(1-n)}}{\tilde{m}^{1/(1-n)}}\frac{\tilde{U}}{\tilde{H}} = \tilde{\lambda}\frac{\tilde{U}}{\tilde{H}}$ is the Carreau number and $W = E\tilde{\rho}\tilde{g}/\tilde{M}$ is a dimensionless group comparing gravitational and squeezing effects which drive the flow. The sign of b is chosen so as to render absolute value of $\tilde{\tau}_{xy}$ positive. The constitutive model relates the shear-rate and the shear stress, $\dot{\tilde{\gamma}}_{xy} = \tilde{\tau}_{xy}\tilde{F}(\tilde{\tau}_{xy})$, where $F(\tilde{\tau}) = \frac{1}{\tilde{m}_0} + \frac{1}{\tilde{m}}\left(\frac{|\tilde{\tau}|}{\tilde{m}}\right)^{(1-n)/n}$ for a Carreau-like fluid. This features shear thinning with a plateau at low shear rates, leading to a finite viscosity at zero-shear rate. The highly hydrated gels applied vaginally tend to exhibit such behavior. In the case of a Newtonian fluid, $F(\tilde{\tau}) = 1/\tilde{m}_0$ (or $n = 1$ in the Carreau-like model), and the governing equation reduces to,

$$\frac{\partial h}{\partial t} + \frac{W}{4}h^2\frac{\partial h}{\partial x} - \left\{h^2\left(\frac{\partial h}{\partial x}\right)^2 + \frac{1}{3}h^3\frac{\partial^2 h}{\partial x^2}\right\} = 0 \tag{3.2}$$

Details of these derivations can be found in [34]. Note that dimensional variables were indicated with a tilde in [34]. Here and in the model that we present below, we have made use of the one dimensional constrained continuum model [64] approximation to account for the elastic forces of the vaginal walls. In this approximation, the fluid pressure near a compliant wall is linearly related to the local deformation of that wall. In general, for a deformation h, the fluid pressure is given by $p = (E/T)h \equiv Mh$. Here, E is the elastic (Young's) modulus of the compliant layer, T is its thickness, and M is termed the compliance of the elastic wall.

The presence of a yield stress complicates the problem in the form of a yield stress paradox, which is discussed in the next section. In solving the yield stress case we again make use of the lubrication approximation. In this analysis, we seek a method of reasonable and consistent approximation for the fluid mechanics, which will be amenable to rapid solutions, such as one would need in microbicide gel design. The constrained continuum model has been previously used by Lighthill and colleagues in the analysis of deformation effects in lubrication theory based blood flow [44], [81]. Given our limited understanding of vaginal wall mechanics, we believe it is reasonable to use that model here. As an improved understanding of those mechanics emerges, then more accurate numerical approaches to solution of the fluid mechanics will become appropriate.

3.2.2 Yield stress paradox

Previous analyses of squeezing flows of Bingham fluids with the lubrication approximation have produced conflicting results [82]. One must expect an un-yielded region of the yield stress fluid near the plane of symmetry, which would not flow; that is, this region should behave like a solid according to the rheological properties of a yield stress fluid, (e.g., Bingham fluid, Herschel-Bulkley fluid). However, owing to the fact that the apposed walls are approaching one another, there must be a corresponding flow, in the longitudinal direction. This paradox originates in the neglect of the normal stresses compared with the shear stresses while following the lubrication approximation. Hence, normal stresses should be considered for the squeeze flow of a Bingham fluid, i.e., lubrication theory might not be applicable when the behavior of a yield stress fluid is analyzed [75].

The presence of the rate of strain in the denominator of the constitutive equation of a Bingham fluid renders this model singular as the yield surface is approached. The biviscosity model is one

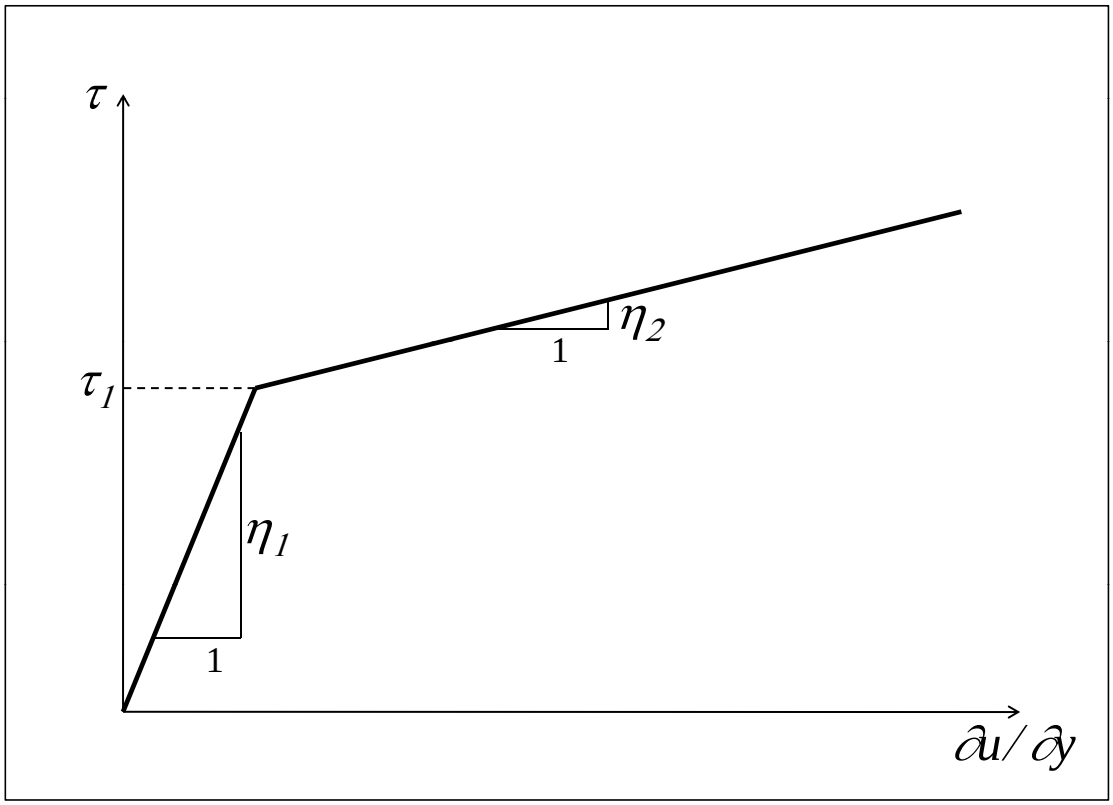

Figure 3.2. Stress-strain-rate curve of the biviscosity model of a Newtonian fluid.

of the models proposed in order to remove this singularity [79], [83]. That model allows for the determination of certain conditions under which lubrication theory may be applied to the squeezing flow of the yield stress fluid. The constitutive equation of the biviscosity model of a Newtonian fluid with yield stress is written,

$$\tau_{xy} = \begin{cases} \eta_1 \frac{\partial u}{\partial y} & \text{if } |\tau| < |\tau_1| \\ \eta_2 \frac{\partial u}{\partial y} + \tau_y & \text{otherwise} \end{cases} \tag{3.3}$$

where, $\tau_y = \tau_1(1-\delta)$ and δ is the viscosity ratio, $\delta = \eta_2/\eta_1$. Fig. 3.2 shows the stress-strain-rate curve of the biviscosity model of a Newtonian fluid. The simple Newtonian case is recovered when $\delta = 1$. The case of a Bingham fluid [74] is approached in the limit $\delta \to 0$. Wilson [83] determined conditions that make use of lubrication theory consistent with the analysis of a biviscosity yield stress fluid, by using scaling analysis. The condition is derived for the fluid squeezed between two solid disks. An analogous set of conditions consistent with the elastic wall squeezing flow is required for use in the problem of interest here.

3.2.3 Elastohydrodynamic lubrication theory with a biviscosity yield stress fluid

We begin by sketching what may be called standard lubrication theory. The balance of linear momentum for the x- and the y-directions is written as,

$$\frac{\partial p}{\partial x} = \frac{\partial \tau_{xy}}{\partial y} \tag{3.4}$$

$$\frac{\partial p}{\partial y} = 0 \tag{3.5}$$

Hence, with appropriate boundary conditions,

$$\tau_{xy} = \frac{\partial p}{\partial x} y \tag{3.6}$$

Yield surfaces, where the fluid starts yielding, can be located with Eq. 3.6. For the surface in the interval $0 < y \leq h(x,t)$, the result is y_1, where

$$y_1 = \tau_1 / (\partial p / \partial x) \tag{3.7}$$

Eq. 3.3, the constitutive equation of the biviscosity model with constant viscosity, is used here, with appropriate boundary and interface conditions. This leads to an expression for the axial velocity u:

$$u = \begin{cases} \frac{1}{2\eta_2}\frac{\partial p}{\partial x}(y^2 - h(x,t)^2) - \frac{\tau_y}{\eta_2}(y - h(x,t)) & \text{if } y > y_1 \\ \frac{1}{2\eta_1}\frac{\partial p}{\partial x}(y^2 - y_1^2) + \frac{1}{2\eta_2}\frac{\partial p}{\partial x}(y_1^2 - h(x,t)^2) - \frac{\tau_y}{\eta_2}(y_1 - h(x,t)) & \text{otherwise} \end{cases} \tag{3.8}$$

The order of the axial normal stress τ_{xx} can be obtained from the axial velocity u.

$$\tau_{xx} = \begin{cases} O\left(\eta_2 \frac{\partial u}{\partial x}\right) & \text{if } y > y_1 \\ O\left(\eta_1 \frac{\partial u}{\partial x}\right) & \text{otherwise} \end{cases} \tag{3.9}$$

The group of scales of the axial normal stress τ_{xx} is calculated in terms of other known scales, with careful manipulation of (3.8) and (3.9).

$$\left(G\frac{H^2}{L}, \frac{\tau_y H}{L}, G\frac{H^2}{L}\frac{\eta_1}{\eta_2}, \frac{\tau_y H}{L}\frac{\eta_1}{\eta_2} \right) \tag{3.10}$$

Here, H and L are length scales for the transverse (thickness) and longitudinal directions, respectively, and $G = \partial p / \partial x$. On the other hand, the scale of shear stress τ_{xy} is obtained from (3.6).

$$(GH)\, or\, (PH/L) \tag{3.11}$$

In order to neglect normal stress, i.e., for the lubrication approximation to be valid, $O(\tau_{xx})$ should be much smaller than $O(\tau_{xy})$. This leads to the requirement

$$\left(\epsilon, \frac{\tau_y}{P}, \frac{\epsilon}{\delta}, \frac{\tau_y}{P}\frac{1}{\delta} \right) \ll 1 \tag{3.12}$$

where $\epsilon = H/L$, and $\delta = \eta_2/\eta_1$.

Hence, it is self-consistent to analyze a biviscosity yield stress fluid with the lubrication approximation when (3.12) is satisfied. In particular, we require τ_y to be small enough and δ to be not too small.

3.2.4 A constitutive equation of a Carreau-like model with a yield stress

The 'purest' representative rheological model of a yield stress fluid is the Bingham model [33]:

$$\begin{array}{ll} \tau = \mu\dot{\gamma} + \tau_y & \text{if } |\tau| > \tau_y \\ \dot{\gamma} = 0 & \text{otherwise} \end{array} \tag{3.13}$$

As noted above, we have found it useful to work with a Carreau-like model to account for details of shear-thinning behavior evident in most gel delivery vehicles [34]. The original Carreau model can be written as $\eta/\eta_0 = \left(1 + (\lambda\dot{\gamma})^2\right)^{(n-1)/2}$. Here, η is viscosity, η_0 is the zero shear viscosity, λ is the relaxation time of the fluid, $\dot{\gamma}$ is the shear rate invariant and n is the power index. The parameters of the Carreau model can be converted into those of Carreau-like model asymptotically [34] in the relationship $m_0 = \eta_0$ and $m = \eta_0/\lambda^{1-n}$. We can alter the constitutive equation of a Carreau-like model to include a true yield stress through simple modification, as based on the Bingham model. This constitutive equation of a Carreau-like model with a yield stress would then read,

$$\dot{\gamma}_{xy} = \begin{cases} (\tau_{xy} - \tau_y)\, F(\tau_{xy}) & \text{if } |\tau_{xy}| > \tau_y \\ 0 & \text{otherwise} \end{cases} \tag{3.14}$$

Here,

$$F(\tau_{xy}) = \begin{cases} \frac{1}{m_0} + \frac{1}{m}\left(\frac{|\tau_{xy}| - \tau_y}{m}\right)^{(1-n)/n} & \text{if } |\tau_{xy}| > \tau_y \\ 0 & \text{otherwise} \end{cases} \tag{3.15}$$

The Carreau-like model is effective in the region where $|\tau_{xy}| > \tau_y$. When $|\tau_{xy}| < \tau_y$, the fluid behaves like a solid.

3.2.5 Biviscosity model of a Carreau-like fluid with a yield stress

Now we follow the lead of Wilson [83], and define a biviscosity model of a Carreau-like fluid with a yield stress. As we shall show, the biviscosity captures more realistic yield stress behavior for the specific types of fluids we are considering. The model (cf. Eq 3.3) may be written

$$\tau = \begin{cases} \eta_1 \frac{\partial u}{\partial y} & \text{if } |\tau| < |\tau_1| \\ \frac{1}{F(\tau_{xy})}\frac{\partial u}{\partial y} + \tau_y & \text{otherwise} \end{cases} \tag{3.16}$$

where, such that τ_y is yield stress, and $\tau_y = \tau_1(1-\delta)$. Here, δ is the viscosity ratio, $\delta = 1/\eta_1 F(\tau_{xy})$. We plot the stress-strain curve of the biviscosity model of a Carreau-like fluid at Fig. 3.3. Here, the exponent n of the function $F(\tau_{xy})$ is assumed to be less than one, which means that a Carreau-like fluid is a shear-thinning fluid. $F(\tau_{xy})$ can be written through modification of (3.15).

$$F(\tau_{xy}) = \frac{1}{m_0} + \frac{1}{m}\left(\frac{|\tau_{xy}| - \tau_y}{m}\right)^{(1-n)/n} \quad \text{if } |\tau_{xy}| > \tau_1 \tag{3.17}$$

Next, we present the Reynolds lubrication equation into which our constitutive model is substituted:

$$\frac{\partial h}{\partial t} + \frac{1}{2}\frac{\partial}{\partial x}\left[\left(M\frac{\partial h}{\partial x} - \rho g\right) m_2\right] = 0 \tag{3.18}$$

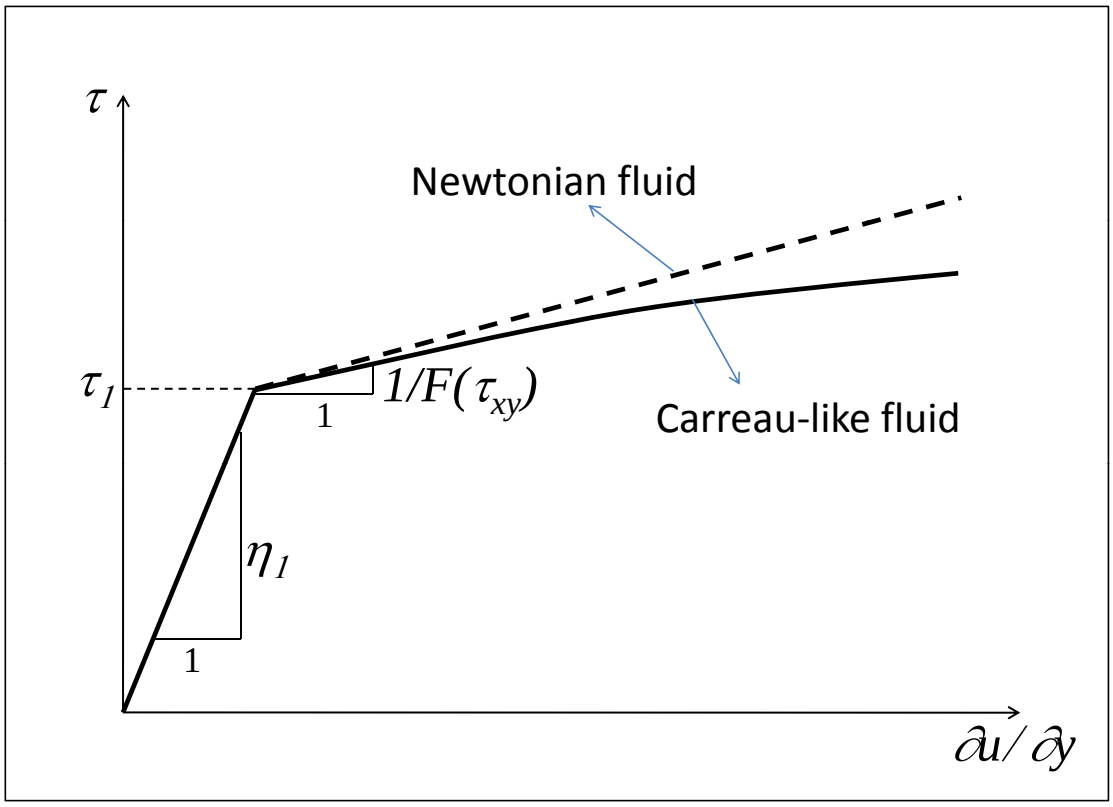

Figure 3.3. Stress-strain curve of the biviscosity model of a (shear-thinning) Carreau-like fluid.

where,

$$m_2 = \begin{cases} \int_{-h}^{h} \left[\int_{-h}^{y} (1/\eta_1) y dy \right] dy = -2h^3/3\eta_1 & \text{if } |\tau| < |\tau_1| \\ \int_{-h}^{h} \left[\int_{-h}^{y} F(\tau_{xy}) y dy \right] dy & \text{otherwise} \end{cases} \tag{3.19}$$

We have developed the governing equations accounting for the gravitational forces. However, in further developments here we shall neglect gravity for the following reasons. There is no standard way of inserting these microbicide gels. Gravitational effects can therefore be transient and act in any direction, as determined by the user's posture during and after gel insertion.

In the present analysis, the elastohydrodynamic flow is driven by initial distention of elastic surfaces and the resultant squeezing of the fluid bolus, which is initially at rest. This distention leads to pressure gradients and, eventually, fluid flow. We first integrate the x-momentum equation in the y-direction to obtain the shear stresses. Neglecting gravity and using the lubrication approximation, this equation becomes ($\partial p/\partial x = \partial \tau/\partial y$). Here, shear stress can be obtained as, ($\tau = y\partial p/\partial x = yM\partial h/\partial x$). Note that at $y = 0, \tau = 0$ due to symmetry. Then by substituting shear stresses into Eq. (3.17) and (3.19), m_2 values are obtained. Integrating the x-momentum equation in the y-direction twice, u_1 values are obtained. Velocities in the y-direction (u_2) are easily extracted from the incompressibility condition. In the mean time, m_2 values are substituted into the Reynolds lubrication equation, Eq. (3.18), and new height profile is obtained. Iteration proceeds and updated height profile is used to evaluate new shear stresses. The Reynolds lubrication equation, Eq. (3.18) is solved explicitly. As a partial check on accuracy, an asymptotic analysis of a closely related problem was given in [34]. Another check on accuracy was presented in [84] which tracks the integral balance of linear momentum. Stability also should be checked because the Reynolds lubrication equation is solved explicitly in time. A stability analysis including the influence of the Deborah number was presented in [84].

The representative viscosity of the Carreau-like model with a yield stress, m_0, can be used in the scaling analysis. Hence, the ratio of the yielded fluid viscosity to the un-yielded fluid viscosity, δ, is written in $\delta = m_0/\eta_1$. Applying the condition, $\epsilon/\delta \ll 1$, one of Eqs. (3.12), the use of lubrication theory is self-consistent in the case when

$$\eta_1 \ll m_0/\epsilon \tag{3.20}$$

The pressure scale should also be considered here. Given the limitations on magnitude of the Reynolds number and the thin layer assumption, pressure is made dimensionless by use of a scale constructed from the shear stress, $P = (m_0 U/H)/\epsilon$.

The velocity scale U is chosen to be the centerline velocity for flow due only to the compliance of the surfaces, i.e., the velocity scale when gravity is zero [34]. For Newtonian fluids with viscosity μ, the centerline velocity of pressure driven flow is $u = \frac{1}{\mu}\frac{\partial p}{\partial x}\frac{h^2}{2}$, where $\frac{\partial p}{\partial x}$ is pressure gradient, h is the height of the channel in which fluid is flowing. The equation of the compliance of the elastic wall, $p = (E/T)h \equiv Mh$, can be applied to here, which leads to $\frac{1}{\mu}M\frac{\partial h}{\partial x}\frac{h^2}{2}$. Hence, the velocity scale is $U = MH^3/(2\mu L)$ for Newtonian fluids. In the case of a Carreau-like model, this can be written $U = MH^3/(2m_0 L)$.

The pressure scale is found to be $P = (MH)/2$ for the elastic wall boundaries with compliance, M. Hence, one of the conditions for the neglect of the normal stresses is obtained from (3.12), which is

$$\left(\frac{\tau_y}{P} = \frac{2\tau_y}{MH} \right) \ll 1 \tag{3.21}$$

The last term of Eq. (3.12) can be written,

$$\left(\frac{\tau_y}{P}\frac{1}{\delta} = \frac{2\tau_y}{MH}\frac{\eta_1}{m_0}\right) \ll 1 \tag{3.22}$$

The normal stresses of the fluid should be considered when (3.20-3.22) are not satisfied. The first condition of (3.12) must be satisfied in all cases due to the use of lubrication theory here.

3.3 Results & Discussion

Overall, the use of lubrication theory in the analysis of elastohydrodynamic flow of a Carreau-like fluid with a yield stress is self-consistent, provided that four conditions are satisfied: $\epsilon \ll 1$ and (3.20-3.22). However, five rheological parameters: yield stress τ_y, first viscosity η_1, power index n, zero shear viscosity of Carreau-like model m_0, modified viscosity of Carreau-like model m, must be known in order to evaluate these conditions.

The measurement of yield stress has been historically problematical [35]–[38]. In the present study, we used the method given by Kulicke et al. [85] as applied to a test gel that was constructed using hydroxyethylcellulose and Carbopol. The presence of the latter macromolecule is what gives rise to yield stress behavior in this gel [72]. This is a relatively high viscosity gel, in the context of prototypes for use as vaginal microbicide vehicles. Fig. 3.4 illustrates results of application of the Kulicke method to this gel. In the method, a plot is created of stress vs. strain (not strain-rate) for a gel, during unidirectional rotation in a rheometer with a parallel plate configuration. We used a TA Instruments (New Castle, DE) 1500ex rheometer, and measurements were performed at body temperature (37^oC). The yield stress is defined as the value of stress in which there is an abrupt change in slope of the stress vs. strain curve. This point was found by stepwise numerical computation of the slope of the plot of stress vs. strain. This same rheometer was used to obtain viscosity as a function of shear rate (at 37^oC), using a controlled stress protocol that enabled measurements at shear rates down to about 10^{-3} sec^{-1}. These data were processed to obtain the values of the parameters in the Carreau model [58], after first subtracting the value of measured yield stress from the set of stress measurements obtained by the rheometer.

The data in Figure 3.4 are the superposition of results from two experiments. In the first, our collaborators acquired individual data over a larger time step than in the second experiment (apparent in Fig. 3.4). The intent in the second experiment was to obtain a more refined picture of the change in slope. However, this second rheometric protocol created a different time history of mechanical conditions for the gel. Denn [37] has pointed out that this can lead to differences in configuration of the gel microstructure which give rise to differences in quantitative macro-scale stress vs. strain data. In both rheometric experiments there are abrupt changes in the slope of the curve and these occur at points that are relatively close. The distinction is not important to the theoretical developments of the analyses presented here. We have shown both sets of experimental results to illustrate the challenges of measuring yield stress.

We now propose a means by which to extract the five constitutive parameters from the experimental data. The thickness of the gel, h, in the rheometer is small compared to the length scale in the direction of applied stress. Therefore, the lubrication approximation can be employed to model the flow in the rheometer. Hence, we assume that pressure gradients are negligible in the direction of applied stress, and consequently a linear velocity profile is obtained, i.e. Couette flow.

$\tau_y\ (Pa)$	$\eta_1\ (Pa.s)$	n	$m\ (Pa.s^n)$	$m_0\ (Pa.s)$
109.35	37268.1	0.4222	44.43	742.43

Table 3.1. Parameters of the constitutive equation for undiluted test gel

$\epsilon \ll 1$	$\frac{\epsilon\eta_1}{m_0} \ll 1$	$\frac{2\tau_y}{MH} \ll 1$	$\frac{2\tau_y}{MH}\frac{\eta_1}{m_0} \ll 1$
0.0125	0.6275	0.0044	0.2196

Table 3.2. Conditions given by (3.20-3.22) and the resulting values after the parameters given in Table 3.1 are substituted.

This is a good approximation because the strain at 60 seconds, γ_{60}, has a linear dependence on applied stress for small values of stress. Note that any significant pressure gradient would result in at least a quadratic change in velocity, leading to a curved relation between γ_{60} and applied stress for a Newtonian fluid. Substitution of the biviscosity model of a Carreau-like fluid with a yield stress, Eq. (3.16), into the velocity profile enables us to determine the velocity profile and, thus total strain at 60 s, γ_{60}, as follows,

$$\gamma_{60} = \begin{cases} \frac{60\tau h}{\eta_1} & \text{if } \tau < \frac{\tau_y}{1-\frac{m_0}{\eta_1}} \\ 60(\tau-\tau_y)\left(\frac{1}{m_0} + \frac{\left(\frac{\tau-\tau_y}{m}\right)^{(1-n)/n}}{m}\right) & \text{otherwise} \end{cases} \tag{3.23}$$

Experimental data obtained following the methods of [72] and the fit of (3.23) into the experimental data are shown in Fig. 3.4. The fitted values of the rheological parameters are given in Table 3.1.

Now that we have determined the constitutive parameters from the straightforward analysis of the rheometer flow, we can turn to examining the validity conditions for lubrication analysis of the vaginal flow. Table 3.2 shows the resulting values after the parameters in Table 3.1 are substituted into the conditions: $\epsilon \ll 1$ and (3.20-3.22). In keeping with the need to develop a rapidly solvable approximation to this flow for use in design calculations, we shall accept as reasonably well-satisfied the criteria of (3.12).

Two of the conditions, $\frac{\epsilon\eta_1}{m_0} \ll 1$ and $\frac{2\tau_y}{MH}\frac{\eta_1}{m_0} \ll 1$ are more critical. The first and third conditions, $\epsilon \ll 1$ and $\frac{2\tau_y}{MH}$, are satisfied as long as the second and fourth conditions are satisfied separately, owing to the small value of $\delta = m_0/\eta_1$, i.e. $\delta \ll 1$.

Given these experimental results, and having addressed (at least approximately) the conditions of validity of the lubrication approximation, we now consider a simulation of the coating flow of this gel driven by squeezing from the distended vaginal walls.

The initial condition for the shape of the bolus is taken as,

$$h(x, t=0) = h_\infty + b\ exp\left[-(x/a)^2\right] \tag{3.24}$$

The fluid volume of such a bolus (above the offset h_∞) is $V_b = 2abc\sqrt{\pi}$, where c is the vaginal width, i.e. 2 cm. The volume of the bolus here is 3 mL. As a scale for the height H, we choose 0.5 cm; this scale is of the order of magnitude of the maximum height of the bolus at time zero. Here we choose $h_\infty = 0.05H$ and $b = 0.45H$, and obtain $a = V_b/2bc\sqrt{\pi}$.

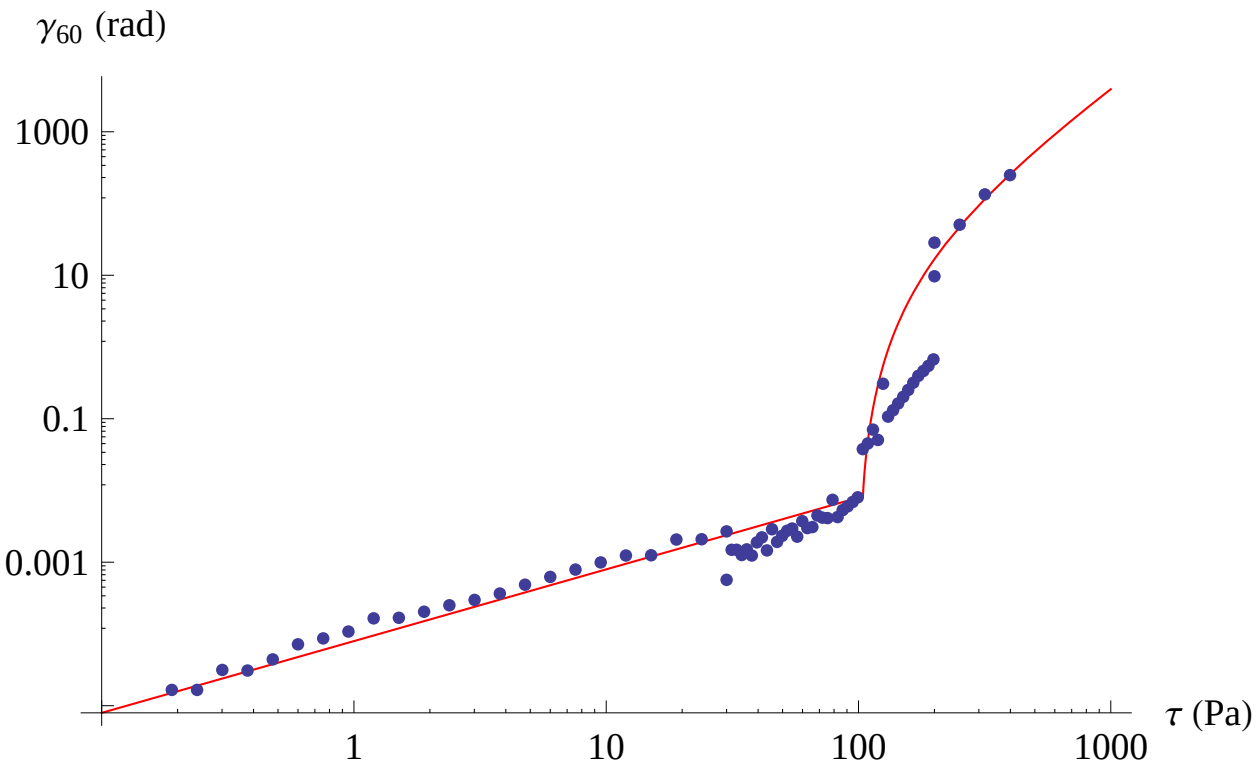

Figure 3.4. Strain at 60 seconds as a function of applied stress. The dots show experimental data; the solid line shows the best-fit rheological parameters in the Eq. (3.23).

The boundary conditions at the outlets of the channel far from the gel bolus are given as:

$$\text{at } x = \mp L : \frac{\partial h}{\partial x} = 0 \; ; \; \frac{\partial^2 h}{\partial x^2} = 0 \tag{3.25}$$

Here, L is the half of the vaginal length, and taken as 20 cm.

The applied stress depends on several parameters such as the pressure gradient and gel rheological properties. As the gel bolus coats the vaginal surface, gradients in height (i.e. thickness), and thus pressure gradients, become smaller. Therefore the shear stress, which is proportional to the pressure gradient, decreases. This enlarges the un-yielded region within the bolus and affects the coating process. Fig. 3.5 illustrates the growth of the un-yielded region within the gel over time. The contours of the shear stresses (Pa) are plotted in Fig. 3.5 at 10 seconds, 1, 5, 30, 90, and 120 minutes (left-to-right, top-to-bottom). Here, the yield surface (dashed line) within the bolus is defined by Eq. 3.7. According to Eq. 3.7, an un-yielded zone occurs below the dashed line, while the yielded region is located between the dashed line and the surface of the bolus (solid line). The graphs are plotted only for the upper half of the bolus because the domain is symmetric with respect to the x-axis. Thus, the coating flow of the gel bolus begins as a flow of mostly yielding material. There is a gradual transition to un-yielded material which, in this biviscosity model, flows much more sluggishly. The gel in this study (termed a "bolus gel") was designed with the intent that it does not spread appreciably along the vaginal canal. This design goal derives from the hypothesis that such limited gel flow could improve retention within the canal over time. The present analysis demonstrates this theoretically. However, the spatial extent of gel spreading may be quite limited if the yield stress is excessive.

3.4 Conclusions

In summary, we have studied an important biological problem with significance related to efforts to prevent infection by HIV. The problem reduces to flow of a shear thinning fluid, with a yield stress, along a two-dimensional channel, as driven by the elastic squeezing forces of the distended channel walls. This problem is in the spirit of a large body of work on flows of yield stress fluids, but has a number of features not previously considered and/or combined, for example: (1) the constitutive equation is an alternative to the Power Law model (we used the Carreau model) to account for the low shear rate behavior of the types of fluids relevant to this specific problem; and (2) the elastic forces driving the flow are coupled to the flow. We investigated conditions under which lubrication analysis is valid for the flow, and developed four conditions for self-consistency of our approach, two of which dominate: $\frac{\epsilon\eta_1}{m_0} \ll 1$ and $\frac{2\tau_y}{MH}\frac{\eta_1}{m_0} \ll 1$, when $\delta = m_0/\eta_1 \ll 1$. In addition, we illustrated the extraction of five rheological parameters from rheometric data for a test gel which is an actual prototype gel for vaginal delivery of anti-HIV molecules: yield stress τ_y, first viscosity η_1, power index n, zero shear viscosity of Carreau-like model m_0, and modified viscosity of the Carreau-like model m. We presented reasonable validation of the self-consistency conditions in the model, in keeping with the goals of the effort to obtain a rapidly solvable model suitable for use in design calculations. Finally, the yield surface and height profile of a spreading bolus of the gel were obtained. These showed growth of the un-yielded region of gel due to the decreasing pressure gradients that accompany the flow. Beyond the application to vaginal coating by microbicide gel vehicles, this chapter represents, more generally, extension of the work of Wilson [83] to resolve the yield stress paradox, here for elastohydrodynamic squeezing flows of a yield stress fluid.

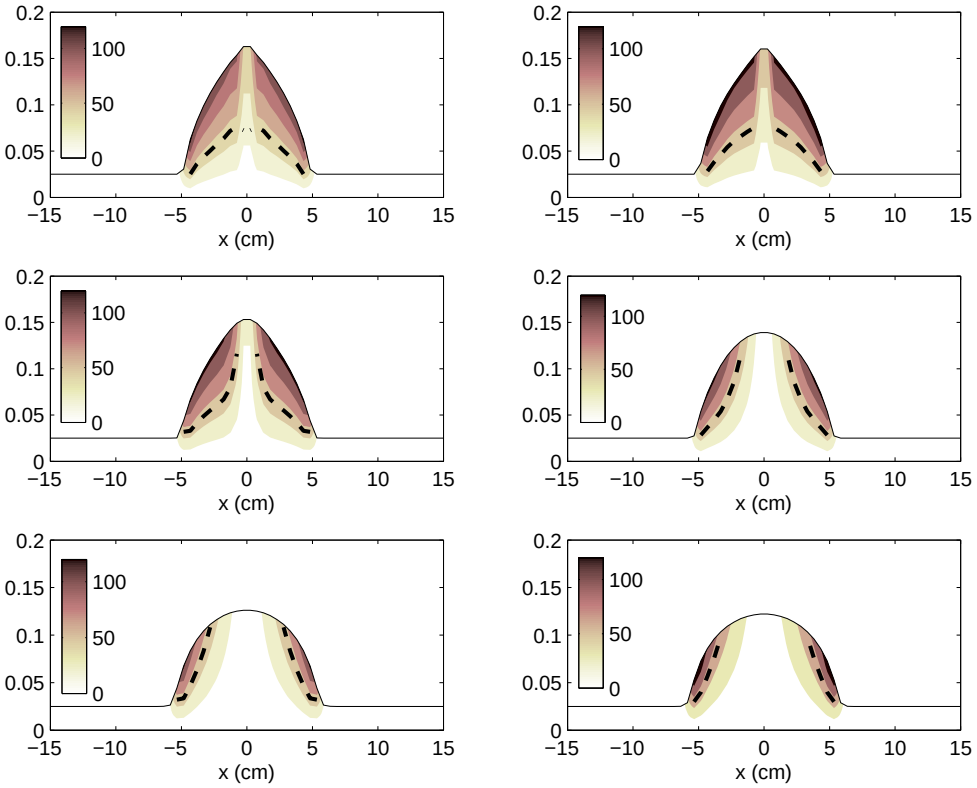

Figure 3.5. Contour plots of the shear stresses (Pa) along the channel (cm) at 10 seconds, 1, 5, 30, 90, and 120 minutes (from left-to-right, top-to-bottom). Yield surfaces, Eq. 3.7, are plotted as dashed lines. The un-yielded zone occurs below the dashed line, while the yielded region is located between the dashed line and the surface of the bolus (solid line). Note that dashed lines are exaggerated. In reality, they are simply lines of infinitesimal thickness, and represent the interface between the yielded and the un-yielded regions.

Chapter 4

Transient spreading and swelling behavior of a gel deploying an anti-HIV topical microbicide

4.1 Introduction

The prevention of transmission of HIV and other sexually transmitted pathogens remains a major global health priority. Although the consistent use of male and of female condoms is highly effective in combating transmission, in many developing countries women have little or no say in their sexual practices, and their partners are often not willing to use condoms [13]. According to a United Nations Population Division estimate [14], only 6.1% of married women of reproductive age –globally– use condoms regularly. This ratio decreases to 1.7% in the continent of Africa. At present, topical microbicides present one of the most promising strategies to fight against the transmission of HIV/AIDS. A recently completed clinical study [3] has shown significant effectiveness of the anti-HIV compound tenofovir –deployed via a gel delivery vehicle– in blocking sexual transmission of HIV in women.

A primary delivery modality of anti-HIV microbicides is their application in fluid vehicles that coat the vulnerable epithelial surfaces of the vaginal lumen prior to intercourse. This coating provides a surface over which active microbicidal ingredients are delivered to the vaginal environment. Drugs such as tenofovir (a reverse transcriptase inhibitor) must migrate down through vaginal epithelium to the underlying lamina propria, within which they function to inhibit HIV transmission [86]. The biophysics of the vaginal coating process can be studied using a mathematical model that combines elastohydrodynamic flow of the bolus of fluid (the gel) along the vaginal lumen, mass transfer due to inhomogeneous gel dilution from the moving epithelial surface boundary, and time- and space-varying rheological properties of the fluid. The effectiveness of the microbi-

cide gel product derives from the completeness and durability of coating, as well as the potency of the active ingredients. The coating process of microbicide gel vehicles is governed by several factors [54]–[58]. Gravity, transvaginal pressure gradients due to contractility of the supporting viscera, and transverse squeezing forces from the distended epithelium, drive the flow. Salient gel rheological properties, which also govern the flow, involve shear thinning (common in these gels) and the possible existence of a yield stress; both of these can be altered significantly by dilution [58].

There have been initial fluid mechanical studies of intravaginal fluid flows; these focused on the individual effects of gravity or epithelial squeezing [55]–[57]. Those initial studies are instructive in developing a physical understanding of the mechanisms of intravaginal vehicle coating flows. The second-generation model developed by our group [34] involves simultaneous effects of a longitudinally directed force along the vaginal canal, e.g., gravity, and transversely directed elastic epithelial squeezing, in a lubrication flow analysis. In follow up, we supplemented our elastohydrodynamic lubrication model [34] with a convective-diffusive transport equation to model limited amounts of dilution that is inhomogeneously distributed throughout the flowing non-Newtonian fluid [1]. However, this model neglected significant swelling of the gel, owing to restrictions derived from the techniques employed in the analysis. Recently, we have analyzed the effects of a yield stress in the elastohydrodynamic flow problem, in the absence of dilution. A yield stress, which constrains gel flow under weak forcing, is emerging as an important property of gel vehicles for microbicide deployment [87]. While it may limit the initial extent of gel coating, it also acts to retain that coating.

In the present chapter, we return to the study of inhomogeneous boundary dilution but now account for the important presence of significant swelling of the gel by absorption of vaginal fluid. In order to approach this problem, a source term is included within the Reynolds lubrication equation, to account for the mass transfer that takes place across the moving epithelial surface and into the gel bolus. We supplement the lubrication equation with a mass conservation equation for the gel component in the presence of entering water. This treatment derives from multi-component mass transfer theory. It provides the dilution distribution within the non-Newtonian gel-water solution, and is not restricted to modest dilutions as was necessary in chapter 2.

The resulting theory models fluid flow driven by a longitudinal force (e.g., gravity) and a transversal force (e.g., wall compliance). The gel flow influences transport of fluid from the boundary, which, in turn, causes swelling of the gel. In this analysis we make, and validate, the reasonable approximation that the concentration of water imbibed by the gel is uniform across the height of the thin layer, over timescales of relevance to the overall coating flow. We begin by considering a boundary condition in which the fluid velocity at the boundary is constant in time and space. Values of this velocity derive from experimental data on production of human vaginal fluid. This was the boundary condition applied in chapter 2. We compare the new results here with our initial ones: these did include a 2-D concentration field solution [1], albeit in the absence of swelling. Finally, and perhaps most significantly, we explore several plausible mechanisms that may explain fluid transport across the epithelial surface boundary. These consist of a time and space varying boundary velocity as a function of: (1) hydrodynamic pressure difference; (2) osmotic gradient; and (3) electroosmotic forces. The governing Reynolds lubrication equation and convective-diffusive transport equation are solved simultaneously using an implicit multi-step numerical scheme, for each of these cases.

The theory developed here will help shed improved light on the specific problem of fluid uptake by a microbicide gel and its impact on the course of the gel's vaginal deployment. As such, it will improve our understanding of delivery of anti-HIV microbicides, and other molecules, by vaginal

gels. More, generally, we have created a framework in which to analyze transient swelling of non-Newtonian fluids during boundary dilution. This may have broader applicability in fluid mechanics, and in other biological flows that may involve swelling, e.g. in the cornea.

4.2 Problem formulation

In this section, we derive a Reynolds lubrication equation, appropriate to a multi-component mass transfer problem, and which includes a term accounting for the solution of gel and water. This must be supplemented by a separate mass conservation equation for gel. The equations are developed in the symmetric domain $-h(x,t) \leq y \leq h(x,t)$ and a body force is included in the x-direction. The physical problem and computational domain are sketched in Fig. 4.1. The model is formulated in a two-dimensional Cartesian domain. The simplification of two-dimensional flow is quite relevant anatomically; the cross section of the undistended human vaginal canal is "H" shaped, with the transverse dimension large compared to the vertical openings on its two sides [62].

For the constitutive model we take the form,

$$\dot{\gamma}_{xy} = \tau_{xy} F(\tau_{xy}) \tag{4.1}$$

Here, $\dot{\gamma}_{xy}$ is the shear rate and τ_{xy} is the shear stress. One can choose $F(\tau_{xy}) = 1/m_0$ for a Newtonian fluid or, as we do below and have done in chapter 2 and 3,

$$F(\tau) = \frac{1}{m_0} + \frac{1}{m}\left(\frac{|\tau|}{m}\right)^{(1-n)/n} \tag{4.2}$$

This is a Carreau-like fluid which exhibits shear thinning and a finite viscosity at zero-shear rate, m_0. Here, m is a viscosity parameter of the Carreau-like fluid and n is the power index. The original Carreau model can be written as $\eta/\eta_0 = (1 + (\lambda\dot{\gamma})^2)^{(n-1)/2}$. Here, η is the viscosity of the Carreau model, η_0 is the zero shear viscosity, and λ is the relaxation time of the fluid. The parameters of the Carreau model can be converted into those of Carreau-like model asymptotically [34] in the relationship $m_0 = \eta_0$ and $m = \eta_0/\lambda^{1-n}$. The two models may be matched at small and large strain rates although they are not exactly equivalent.

The primary assumption in the lubrication approximation is that the thickness of the gel bolus is small relative to its longitudinal extent, i.e. $\epsilon = H/L \ll 1$, where H and L are length scales for the transverse (thickness) and longitudinal directions, respectively. In the usual way, we take the limits $\epsilon Re \to 0$ and $\epsilon \to 0$ to obtain the lubrication approximation. The Reynolds number is $Re = HU/\nu$, where ν is a representative kinematic viscosity and U is velocity scale in the longitudinal dimension. The magnitude of the Reynolds number is small. Given the small magnitude of the Reynolds number and the thin layer assumption, a pressure scale is constructed from the shear stress as $P = (m_0 U)/H$. After making the lubrication approximation, the balance of linear momentum in the x-direction is integrated with respect to y to obtain

$$\left[-\frac{\partial p}{\partial x} + \sum_{i=1}^{r} \rho_i g\right] y + \frac{1}{F(\tau_{xy})}\frac{\partial u}{\partial y} + c_1 = 0 \tag{4.3}$$

where r is the total number of components in the solution (here $r = 2$), ρ_i is the density of the i^{th} component, and u is the mass-average velocity. By symmetry, $\partial u/\partial y = 0$ on $y = 0$; hence the

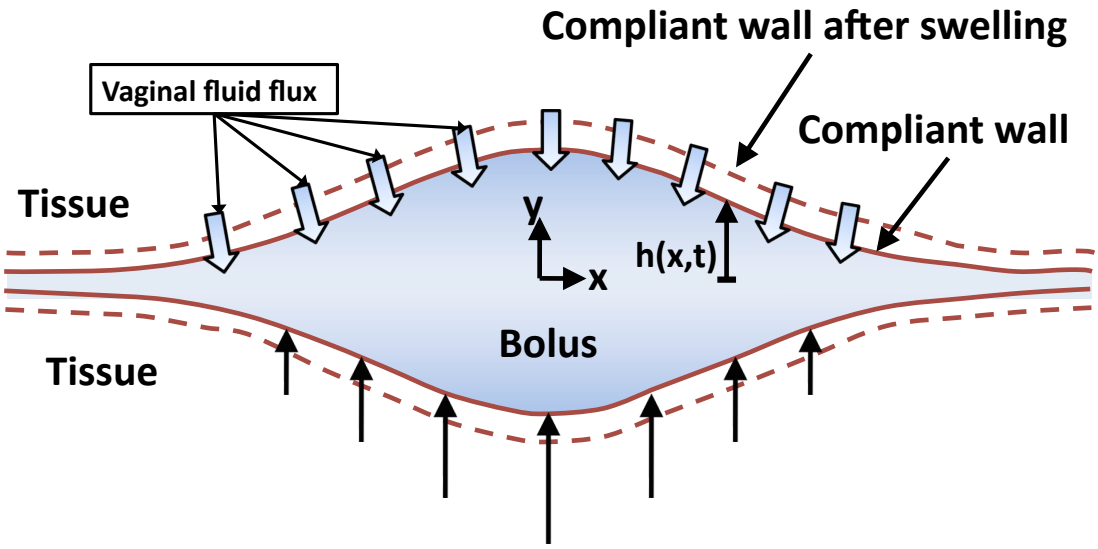

Figure 4.1. Definition sketch of the vaginal canal, emphasizing the longitudinal direction. The introitus is to the right. The transverse direction has an "H" shaped cross section; see text.

constant of integration $c_1 = 0$. Next we solve this equation for $\partial u/\partial y$, integrate with respect to y, and use the boundary condition $u(x, y = -h(x,t), t) = 0$. This yields

$$u = \int_{-h}^{y} F(\tau_{xy}) \left[\frac{\partial p}{\partial x} - \sum_{i=1}^{r} \rho_i g \right] y dy \tag{4.4}$$

The global mass conservation equation and gel mass conservation equation can be written as [88],

$$\begin{aligned} \frac{\partial \rho}{\partial t} + \vec{\nabla} \cdot (\rho \vec{u}) &= -\vec{\nabla} \cdot (\rho \vec{\psi}) \\ \frac{\partial \rho_g}{\partial t} + \vec{\nabla} \cdot (\rho_g \vec{u}) &= \vec{\nabla} \cdot \rho D_{gw} \vec{\nabla} w_g \end{aligned} \tag{4.5}$$

where, ρ and ρ_g are the densities of the solution and the gel, respectively, and D_{gw} $(= D_{wg})$ is the mutual diffusion coefficient. Here, $\vec{\psi}$ is the incoming boundary fluid velocity vector, w_g is the density ratio of the gel to the gel-water combination (ρ_g/ρ) and, $\vec{u}$ is the velocity vector $(= u\hat{\imath} + v\hat{\jmath})$. We assume that the incoming flux is directed only in the y-direction, i.e. $\vec{\psi} = \psi\hat{\jmath}$ with $\psi|_{y=\pm h} = q(x,t)$. In the following, we consider a prototype gel that is composed of 97% water and 3% hydroxyethylcellulose. The densities of both gel and water are very close to 1 g/cm^3. Therefore, for simplicity, we assume that the density of the solution remains constant during dilution and swelling. Then, global mass conservation and gel mass conservation read

$$\begin{aligned} \vec{\nabla} \cdot \vec{u} &= -\frac{\partial \psi}{\partial y} \\ \frac{\partial \phi}{\partial t} + \vec{\nabla} \cdot (\phi \vec{u}) &= \vec{\nabla} \cdot D_{gw} \vec{\nabla} \phi \end{aligned} \tag{4.6}$$

Here, $q(x,t)$ is the local vaginal wall flux, which is negative for swelling, and $\phi(x,t)$ is the local volume fraction of the gel. After substituting Eq. 4.4 into Eq. 4.6 and integrating Eq. 4.6 in the y-direction from $-h$ to h, global mass conservation and gel mass conservation read

$$\begin{aligned} \frac{\partial h}{\partial t} + \frac{1}{2}\frac{\partial}{\partial x}\left[\left(M\frac{\partial h}{\partial x} - \rho g \right) m_2 \right] &= -q \\ \frac{\partial (\phi h)}{\partial t} + \frac{1}{2}\frac{\partial}{\partial x}\left[\phi \left(M\frac{\partial h}{\partial x} - \rho g \right) m_2 \right] &= \frac{\partial}{\partial x}\left(h D_{gw} \frac{\partial \phi}{\partial x} \right) \\ m_2 &= \int_{-h}^{h} \left[\int_{-h}^{y} F(\tau) y dy \right] dy \end{aligned} \tag{4.7}$$

Here, we make the reasonable approximation that the concentration of the gel and water are uniform across the gel thickness, over the timescales of relevance. As in earlier chapters, we employ the one-dimensional constrained continuum model [64] approximation to model vaginal wall elasticity. In this approximation, the fluid pressure near a compliant wall is proportional to the local deformation of that wall. In general, for a deformation h, the fluid pressure is given by $p = (E/T)\, h \equiv Mh$. Here, E is the elastic (Young's) modulus of the compliant layer, T is its thickness, and M is the compliance of the elastic wall. We take for that compliance the value $10^4/0.5$ Pa/cm and consider a bolus volume of 3 mL, as in earlier chapters. We also neglect effects of gravity; these are small compared to the squeezing of the elastic wall [34], and such neglect does not detract from the focus of the analysis here.

The boundary fluid velocity, $q(x,t)$ is a quantity that is not well understood. There is remarkably little research on the presence and flow of human vaginal fluid [65], [89], [90]. This fluid

is produced primarily by a transudation process through the vaginal epithelium [65]. In general it is believed that the rate of fluid percolation through the vaginal epithelium may be variable, depending upon the time of day, the phase of the menstrual cycle, and/or other factors. It is also increased during sexual stimulation [89]. In principle, one might expect that vaginal fluid flow out from the epithelial surface and into a gel coating may be affected by osmotic phenomena, and/or by the hydrodynamic pressure in the vaginal lumen. Here, absent more detailed physiological information, four cases will be studied. In these, we seek to span a range of possible mechanisms, which, unfortunately, remain to be elucidated. First, the boundary fluid velocity is taken as constant. This provides a simple baseline for analysis, and is also the condition utilized in chapter 2. Thereafter the fluid velocity across the epithelial surface boundary is taken as being produced by three candidate mechanisms: (1) the hydrodynamic pressure difference, (2) the osmotic pressure gradient, and (3) electroosmotic forces. At the end of the chapter we discuss relevant measurements that need to be performed in order to progress further in this problem.

The concentration of gel (and therefore of water) is assumed to be uniform over the gel thickness, over relevant timescales. Indeed, taking into account a 2-D concentration field in the analysis would render the model unnecessarily complex, especially with a deformable interface. We studied the 2-D concentration distribution problem in [1] in the limit of modest fluid uptake by the gel, i.e. without accounting for gel swelling behavior. The global mass conservation equation of the solution was solved explicitly. On the other hand, the mass conservation equation for the gel was solved implicitly by Crank-Nicolson method. The Thomas algorithm was used to solve the resulting tri-diagonal linear systems. Central differences were used for the first and second order spatial derivatives.

The initial condition for the shape of the bolus is taken as [34],

$$h(x, t = 0) = h_\infty + b \cdot exp[-(x/a)^2] \tag{4.8}$$

This shape is a mathematical convenience and the details have little effect on the evolution of the fluid flow and dilution profile [34]. The fluid volume of such a bolus (above the offset h_∞) is $V_b = 2abc\sqrt{\pi}$, where c is the vaginal width, i.e. 2 cm. We take the volume to be 3 mL, which is a value typical of microbicide gels. As a scale for the height H, we choose 0.5 cm; this is of the order of magnitude of the maximum height of the bolus at time zero. We choose $h_\infty = 0.05H$ and $b = 0.45H$, and obtain $a = V_b/2bc\sqrt{\pi}$. The boundary conditions at the outlets of the channel far from the gel bolus are given as:

$$\text{at } x = \mp L : \frac{\partial h}{\partial x} = 0 \; ; \; \frac{\partial^2 h}{\partial x^2} = 0 \; ; \; \frac{\partial \phi}{\partial x} = 0 \tag{4.9}$$

Here, L is the half of the vaginal length, and taken as 20 cm.

4.3 Results

4.3.1 Constant boundary flux

The volume of native vaginal fluid present in the vagina is estimated as approximately $0.5-0.75$ mL [65]. The production of fluid is measured as $1-10$ cm^3/day, depending on the phase of the menstrual cycle [90]. If we take the vaginal surface area as about 100 cm^2, this corresponds to a

fluid velocity at the boundary of $q \approx 10^{-9} - 10^{-8}\ m/s$. Hence, for a typical gel vehicle volume of 3 mL the range of dilution by vaginal secretions is 10% to 30% [58]. It is possible that in this case, a theory that applies for modest dilutions and neglects swelling may be appropriate. Thus, we treat such a case here in order to draw parallels between the present theory −which can account for significant transient swelling− and our earlier theory, which cannot.

In order to conduct these analyses, the effect of dilution by vaginal secretions on an actual gel, that is biologically relevant, must be included. We obtained data for an aqueous gel containing 3% hydroxyethylcellulose; this gel is very similar to the placebo gel used in the successful microbicide trial [3]. Gel rheological properties at body temperature (37^oC) were obtained for serial dilutions of the gel with vaginal fluid simulant [65], using a constant stress protocol on a TA Instruments model AR 1500ex rheometer, with a 4^o cone and 20 cm plate configuration. Shear rates ranged from $10^{-4} - 42\ sec^{-1}$ and data were fitted to the Carreau-like model. Measurements were performed for serial dilutions of the gel (with thorough mixing) with vaginal fluid simulant [65] in 5% increments from 0% to 75%. Parameters of the constitutive equation were obtained for each dilution. Then, these data were fit to a polynomial representation of effects of dilution [1], which took the form,

$$\begin{aligned} m_0 &= -2274.02\nu^3 + 4922.72\nu^2 - 3437.98\nu + 786.04 \\ n &= -0.6905\nu^3 + 1.9704\nu^2 - 0.9217\nu + 0.6601 \\ \lambda &= 27936.58\nu^3 - 18847.95\nu^2 + 1847.44\nu + 382.10 \end{aligned} \tag{4.10}$$

We have taken the value $D = 10^{-6}\ cm^2/sec$ for the diffusion coefficient of water through the gel [1].

Evolution of the height profile of the bolus is plotted in Fig. 4.2. Here, as an upper bound, q is set to $1 \times 10^{-7}\ m/s$. This exceeds somewhat the physiologically estimated mean boundary flux ($q \approx 10^{-9} - 10^{-8}\ m/s$); we have applied it so that swelling can be easily observed in the analysis. At 30 minutes, the net percent increase of volume of the gel-solvent mixture is 94%, owing to water uptake from the boundaries. Next, we check the accuracy of our assumption that the concentrations of the gel and water are uniform over the gel thickness. The assumption requires the following to be true:

$$t_D \ll t_{flow}\ ;\ \frac{H^2}{D} \ll \frac{L}{U}\ ;\ \epsilon^2 = \frac{H^2}{L^2} \ll \frac{1}{Pe} \tag{4.11}$$

where the Péclet number $Pe = UL/D$ and $U = (MH^3)/(2m_0L)$. Here, we choose L as a physiological value for the size of the domain in x, i.e. 20 cm, while H is chosen as maximum height of the bolus, which is not fixed, i.e. $H = 0.25\ cm$ at $t = 0$, and $H = 0.1\ cm$ at 5 minutes. At $t = 0$, $\epsilon^2 \sim 10^{-4}$ and $1/Pe \sim 10^{-6}$. After 2 elapsed minutes, the parameters are: $\epsilon^2 \sim 10^{-5}$ and $1/Pe \sim 10^{-5}$. For the rest of the computation, H keeps decreasing. Note that, Eq. 4.11 can be written as, $H^5 \ll 2m_0DL^2/M$; thus the left-hand-side decreases by the power 5. Consequently, we conclude that over the timescales of interest, the assumption of uniform concentrations over the height of the cross section is well motivated. Moreover, this case is for the highest boundary velocity of fluid, and is a therefore a conservative test of the assumption. For the remainder of the analyses here, lower and more physiologically realistic fluid velocity values at the boundary will be used, which will further support the assumption regarding the concentration profile in y.

The evolution of the volume fraction as a function of longitudinal position in the gel is plotted in Fig. 4.3. As can be seen, the decrease in gel fractions at the spreading edges of the bolus is more rapid, due to the smaller thickness of the gel there.

Next, we analyze a physiological range of boundary fluid velocities that derives from the data on mean production rates of human vaginal fluid. The height profile of the bolus at 2 hours and

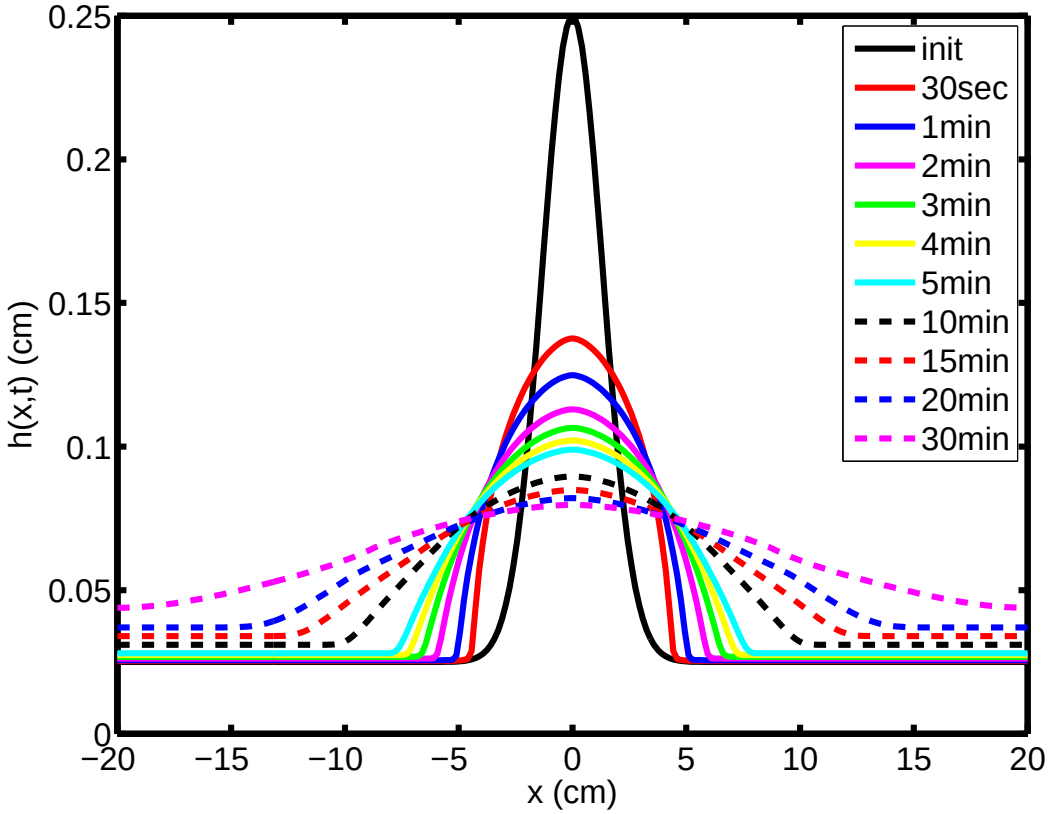

Figure 4.2. Height profile of bolus at $t = 0, 30$ sec, 1 to 30 minutes ($q = 1 \times 10^{-7}\ m/s$ and $D = 10^{-6}\ cm^2/s$).

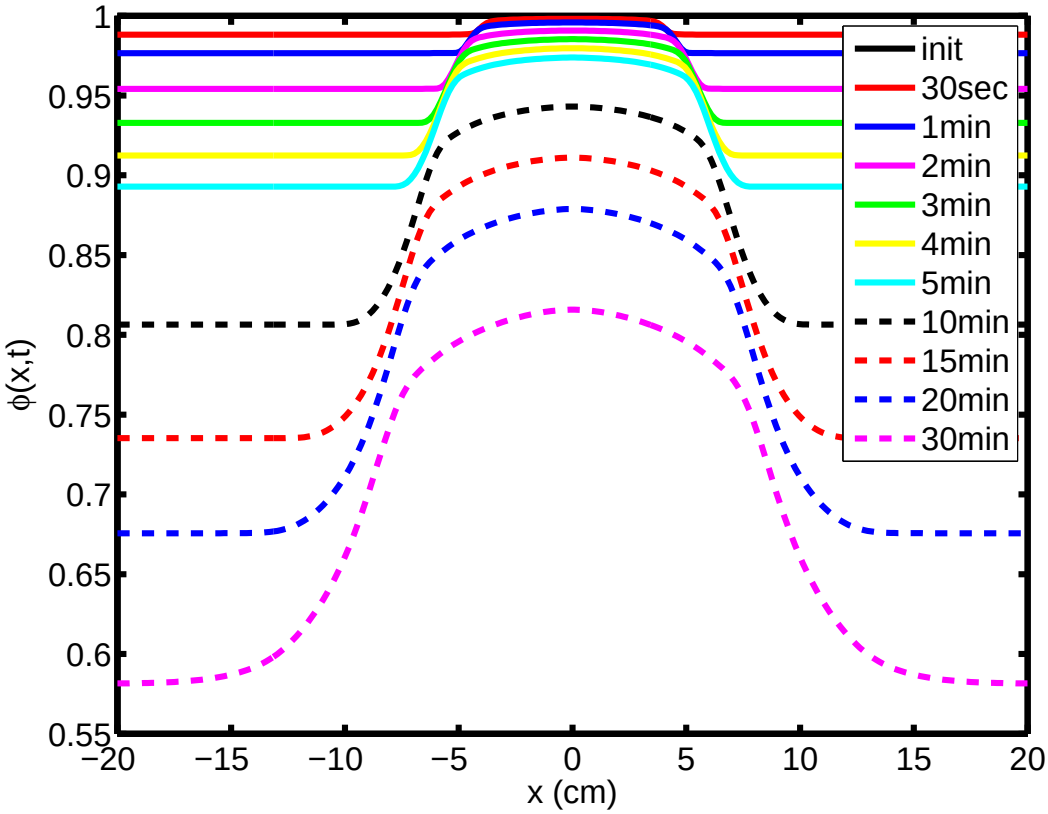

Figure 4.3. Volume fraction of gel vs. x (cm) at $t = 0, 30$ sec, 1 to 30 minutes ($q = 1 \times 10^{-7}$ m/s and $D = 10^{-6}$ cm^2/s).

coating area as a function of time are plotted for several boundary velocity values: $q = 0\ m/s$, $1 \times 10^{-9}\ m/s$, $5 \times 10^{-9}\ m/s$, and $1 \times 10^{-8}\ m/s$ in Figs. 4.4 and 4.5, respectively. As can be seen from the figures, as boundary flux increases the coated area grows more rapidly with respect to time.

4.3.2 Effect of Swelling

The effects of the swelling behavior of the gel on spreading are shown in Figs. 4.6 and 4.7. The height profile of the bolus is plotted for several boundary fluid velocity values (zero velocity, 1×10^{-9} m/s, $5 \times 10^{-9}\ m/s$, and $1 \times 10^{-8}\ m/s$); these are contrasted with our earlier results for these same cases, that did not account for swelling, but did allow for a 2-D concentration distribution field [1]. Here, we choose the higher diffusion coefficient cases ($D = 10^{-5}\ cm^2/s$), Fig. 10 and 11 in [1]. For $D = 10^{-5}\ cm^2/s$, the concentration is almost uniform across the thickness of the gel (see Fig. 13 in [1]) from the very first moment due to diffusion in y-direction. Therefore, we can easily compare the results of the same vaginal fluid fluxes and see the effects of swelling behavior. As can be seen from Figs. 4.6 and 4.7, the model here (that accounts for swelling behavior of the gel) indicates more rapid coating. This can be explained by the larger volume of the diluted bolus due to mass transfer and thus, enhanced squeezing forces.

4.3.3 Exploration of models for inhomogeneous boundary flux

It is known that vaginal fluid is produced primarily as the result of an exudation process across the vaginal epithelium [65]. As noted in the foregoing sections, there is insufficient experimental data at present to enable creation of a definitive fluid transport boundary condition on the surface of the vaginal epithelium. For this reason, we explore several possible models for the mechanism that produces vaginal fluid at the epithelial surface. We draw upon knowledge of related boundary conditions on other tissue surfaces.

Boundary flux dependent on the hydrodynamic pressure

In ultrafiltration models, pure solvent flux is governed by $\Delta P/R_m$ [91]. As one potential mechanism −and associated boundary condition− we consider the possibility that the hydrodynamic pressure difference across the epithelium drives the flux. In this approach, we assume that the boundary flux is governed by,

$$q(x,t) = \frac{\Delta P}{R_m} = \frac{P_{cell} - P_{soln}}{R_m} = \frac{P_{cell} - Mh}{R_m} \tag{4.12}$$

Here, ΔP is the hydrodynamic pressure difference, P_{cell} is the epithelial intracellular pressure, P_{soln} is the pressure of the gel-water solution at the boundary, and R_m is the membrane resistance. The vaginal epithelium is a stratified squamous epithelium resting on a lamina propria [92]. To our best knowledge, there is no experimental value of the intracellular pressure of epithelial cells. Here, as a biologically based estimate, we use the intracellular pressure of red blood cells, which is approximated as $\sim 20 - 30\ Pa$ [93], [94]. A typical membrane resistance is given as 5×10^{10} $Pa.s/m$ in [91].

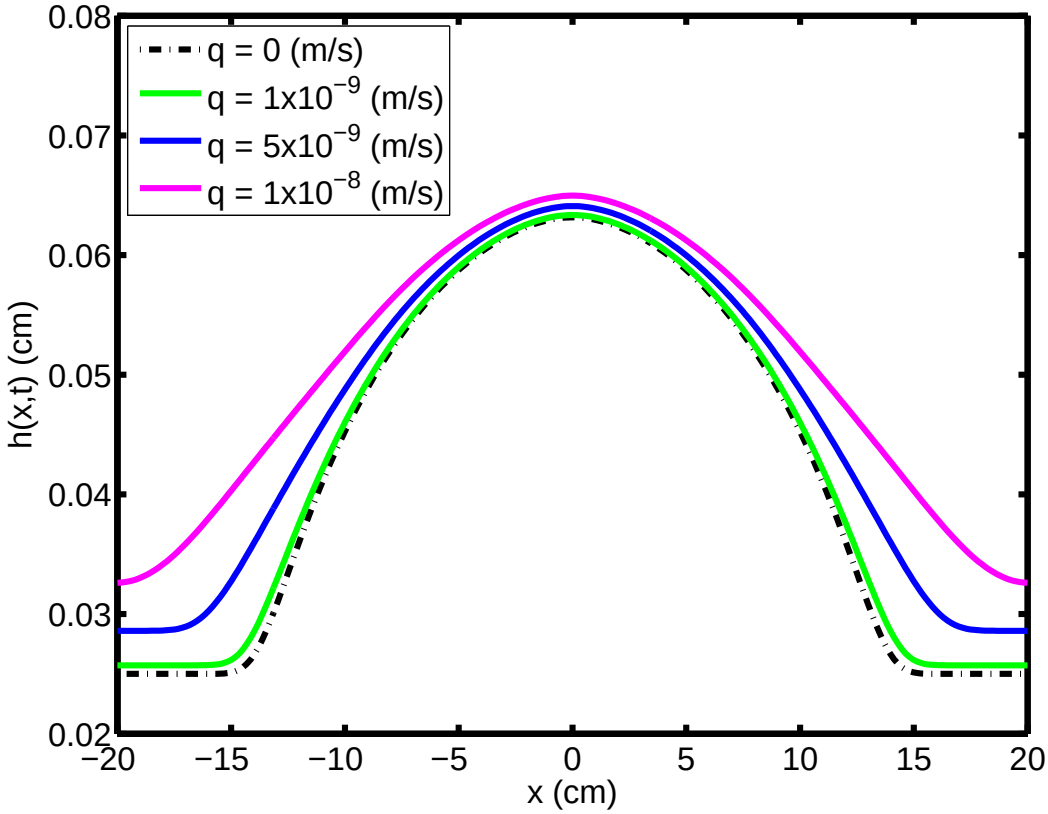

Figure 4.4. ($D = 10^{-6}\ cm^2/s$). Height profile of bolus at 120 minutes for $q = 0\ m/s$ (dash-dot), $1 \times 10^{-9}\ m/s$, $5 \times 10^{-9}\ m/s$, and $1 \times 10^{-8}\ m/s$.

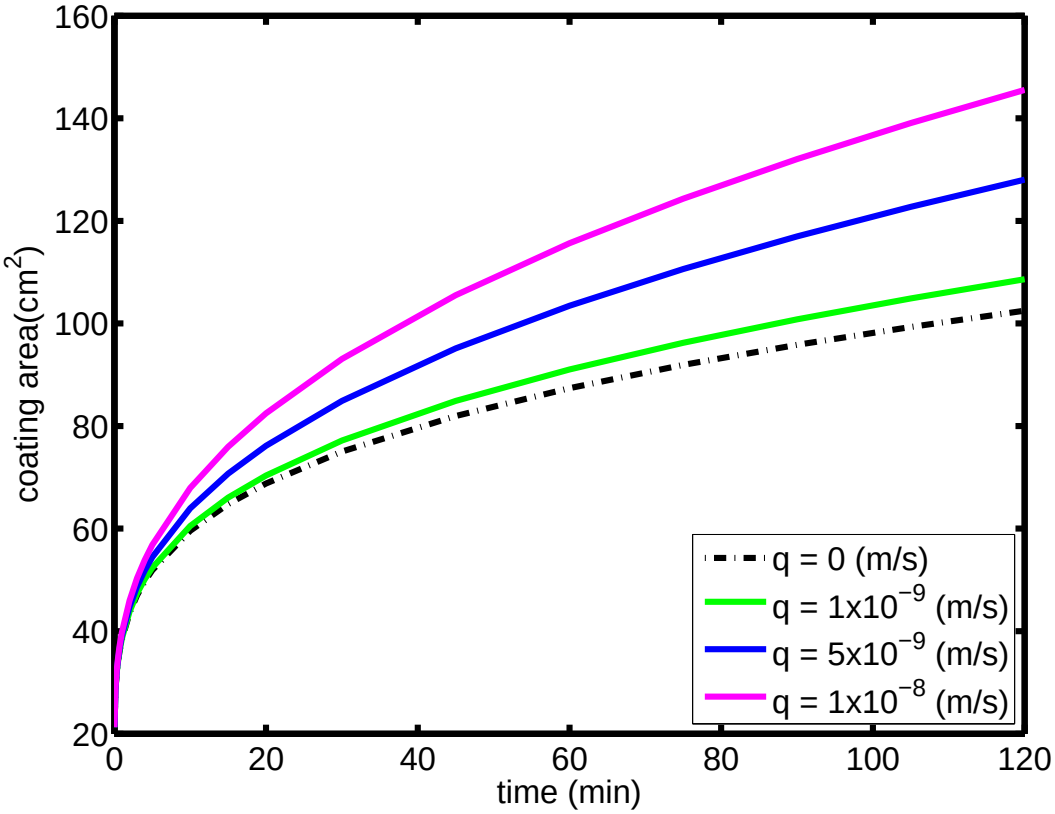

Figure 4.5. ($D = 10^{-6}\ cm^2/s$). Coating area of the gel on the surface for $q = 0\ m/s$ (dash-dot), $1 \times 10^{-9}\ m/s$, $5 \times 10^{-9}\ m/s$, and $1 \times 10^{-8}\ m/s$.

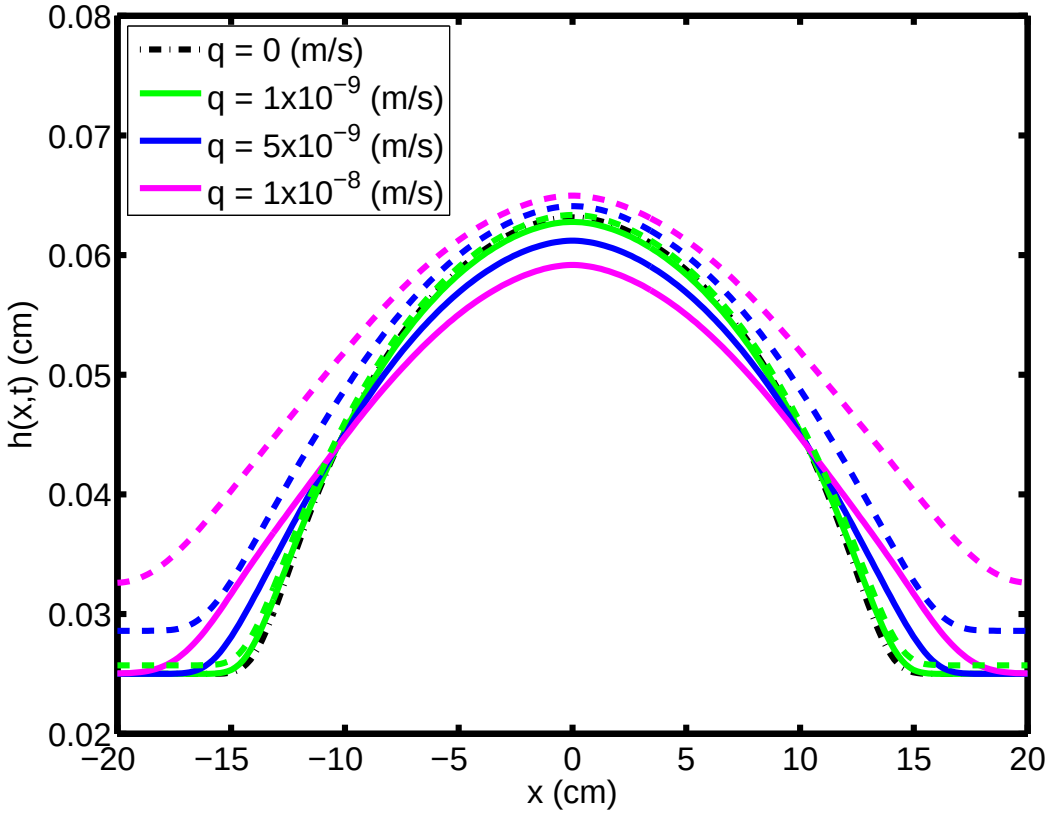

Figure 4.6. ($D = 10^{-5}\ cm^2/s$). Height profile of bolus at 120 minutes for $q = 0\ m/s$ (dash-dot), $1 \times 10^{-9}\ m/s$, $5 \times 10^{-9}\ m/s$, and $1 \times 10^{-8}\ m/s$. Solid lines are for the cases without swelling [1]. Dashed lines are for the cases with swelling.

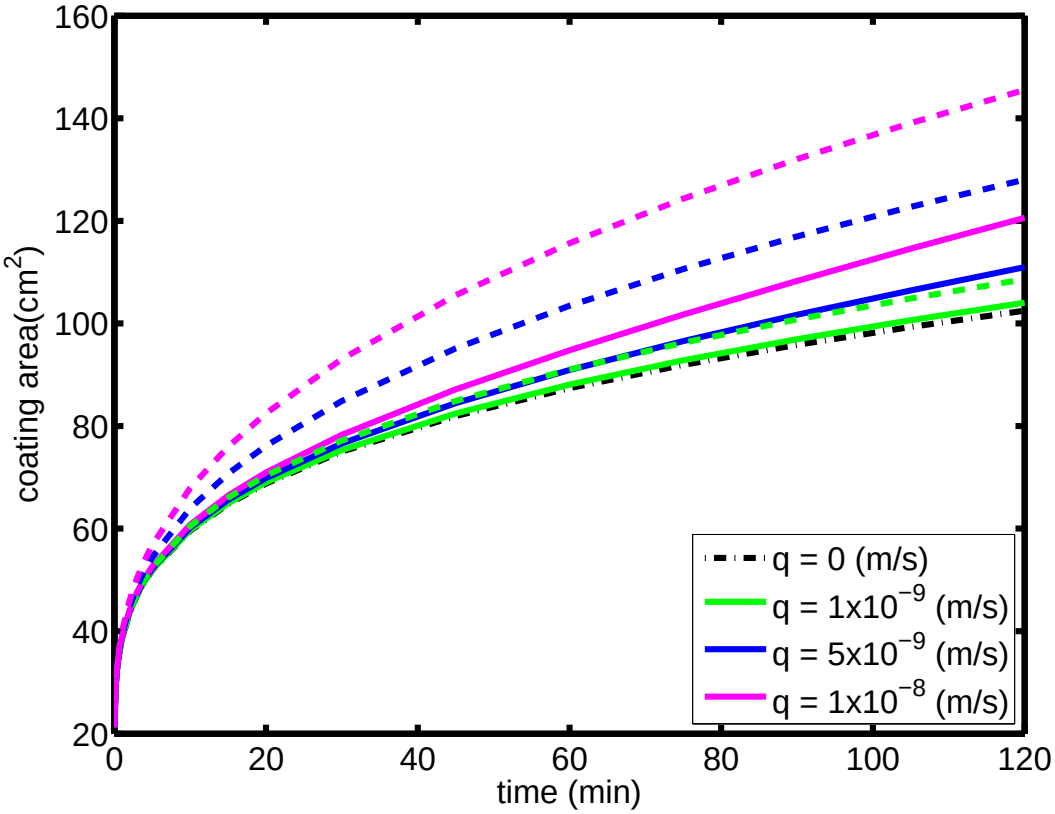

Figure 4.7. ($D = 10^{-5}\ cm^2/s$). Coating area of the gel on the surface for $q = 0\ m/s$ (dash-dot), $1 \times 10^{-9}\ m/s$, $5 \times 10^{-9}\ m/s$, and $1 \times 10^{-8}\ m/s$. Solid lines are for the cases without swelling [1]. Dashed lines are for the cases with swelling.

For this model, height profiles of the gel bolus at 2 hours, and coating area as a function of time, are plotted for several membrane resistance values: $5 \times 10^{10}\ Pa.s/m$, $1 \times 10^{11}\ Pa.s/m$, and $5 \times 10^{11}\ Pa.s/m$ in Fig. 4.8 and 4.9, respectively. As can be seen from figures, coating area decreases as epithelial membrane resistance increases.

This model, for a boundary fluid velocity that is based on membrane resistance and epithelial intracellular pressure, produces fluxes that lie within the range of mean values we mentioned have been measured in experimental work [90].

Boundary flux dependent on the osmotic gradient

Next, we consider a model in which the boundary flux is related to a significant osmotic gradient across the epithelial surface. We assume that vaginal epithelium, at the ultrastructural level, consists of long, narrow paracellular transport channels open at one end (apical/lumen side) and closed at the other (serosal side), see Fig. 4.10. Solute is actively transported into the lateral intercellular spaces (LIS) across its walls, making the channel fluid hypertonic. As solute diffuses towards the open mouth, more and more water enters the channel along its length due to the associated osmotic gradient. In the steady state a standing osmotic gradient would be maintained in the channel by active solute transport. We closely follow a model developed in [41]. However, the model is extended here to apply to the case where the external solution (at $z = L$) may have different osmolarity from the cell interiors. With this change, the governing equation for the velocity of fluid ν in the channel is given as,

$$N(z) + \frac{D_s r^2}{4P}\frac{d^3\nu}{dz^3} - \frac{r^2}{4P}\nu\frac{d^2\nu}{dz^2} - \frac{C_i r}{2}\frac{d\nu}{dz} - \frac{r^2}{4P}\left(\frac{d\nu}{dz}\right)^2 = 0 \tag{4.13}$$

Here, the independent parameters are:

- L = the length of the paracellular transport channel
- r = the radius of the channel
- P = the osmotic water permeability of the channel walls, defined as the volume of water crossing 1 cm^2 in 1 sec in response to an osmotic gradient of 1 milliosmol per cc or 1 osmol per liter
- C_i = the osmolarity of the water inside the epithelial cells
- C_{gel} = the osmolarity of the water at the open end (i.e. inside the gel, along the vaginal lumen)
- D_s = the diffusion coefficient of the actively transported solute
- $N(z)$ = the rate of active solute transport across the walls of the channel into its lumen at any height z, defined as milliosmols of solute transported in 1 sec across 1 cm^2 of channel wall area. (Passive solute movement across the channel walls is assumed to be negligible)
- $C(z)$ = the osmolarity of the water in the channel at a height z
- $v(z)$ = the linear velocity of water flow in the channel at height z, taken as positive in the direction $z = 0$ to $z = L$.

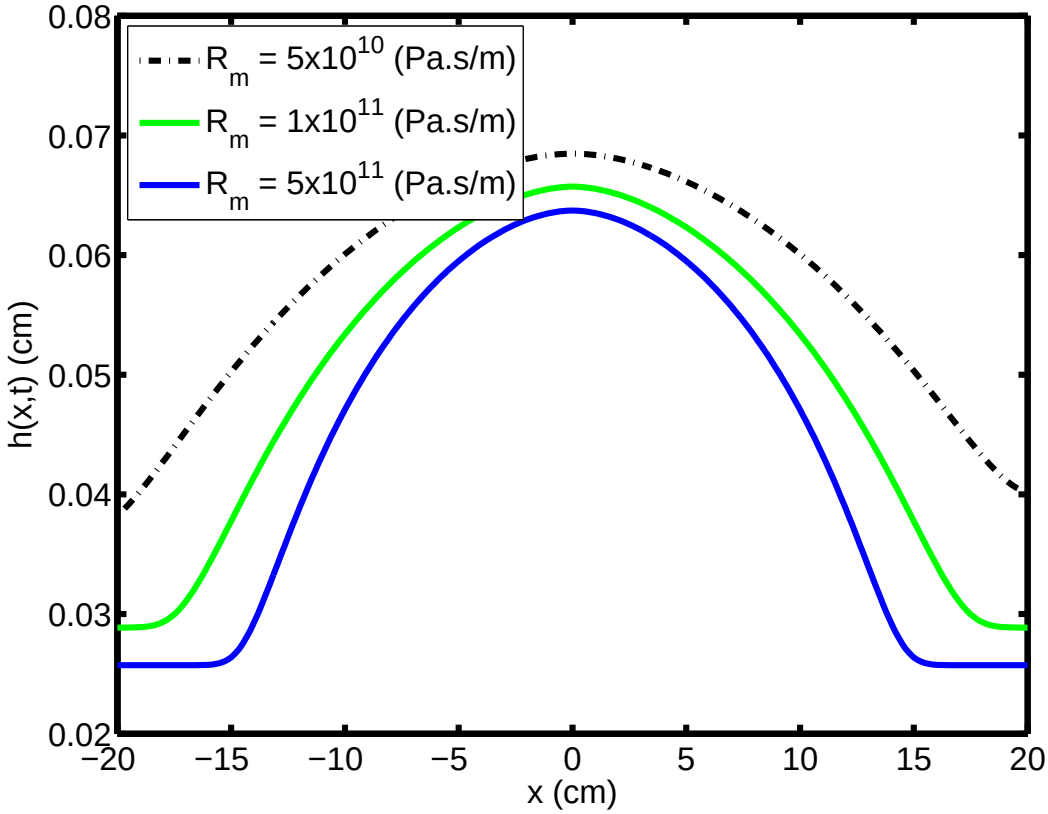

Figure 4.8. ($D = 10^{-6}\ cm^2/s$) Height profile of bolus at 120 minutes for $R_m = 5 \times 10^{10}$ $Pa.s/m$, 1×10^{11} $Pa.s/m$, and 5×10^{11} $Pa.s/m$.

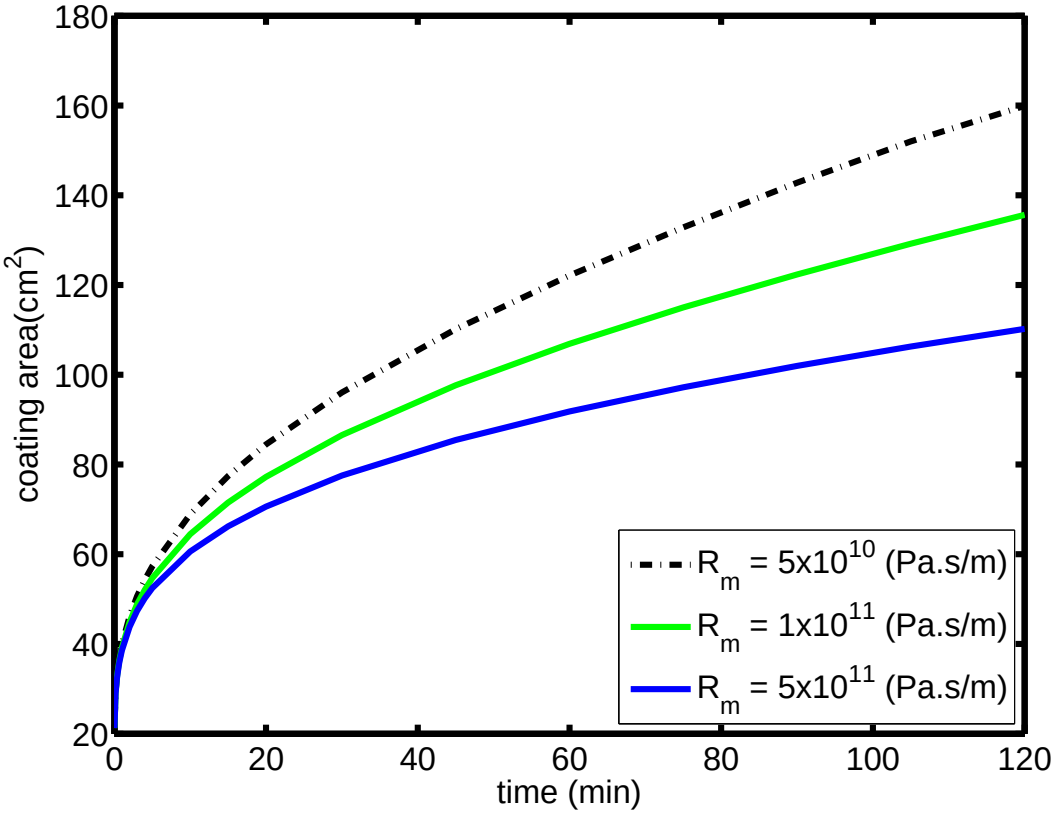

Figure 4.9. ($D = 10^{-6}\ cm^2/s$) Coating area of the gel on the surface for $R_m = 5 \times 10^{10}$ $Pa.s/m$, 1×10^{11} $Pa.s/m$, and 5×10^{11} $Pa.s/m$.

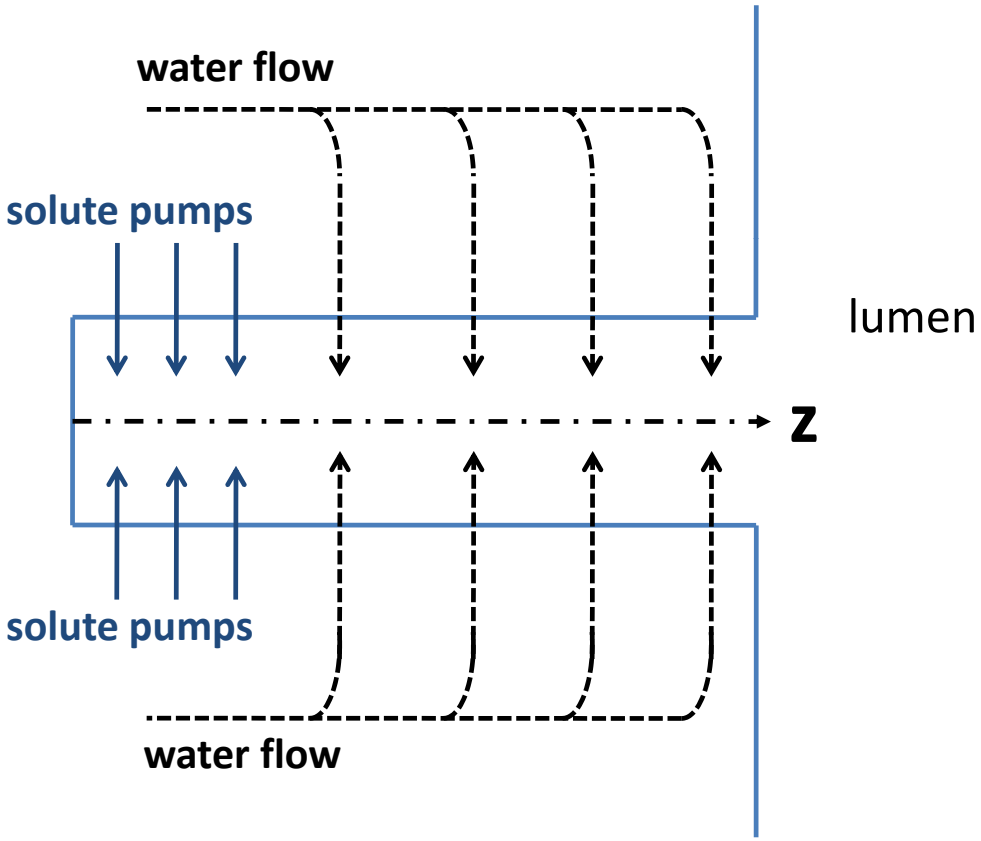

Figure 4.10. Sketch of a standing-gradient flow system.

The assumptions made in this analysis and the details of the derivation of this transport mechanism can be found in [41]. We have supplemented our bi-component, non-Newtonian, elastohydrodynamic flow model with the standing-gradient osmotic model in order to account for fluid that is being released into the gel. Boundary conditions for the standing-gradient osmotic model can be given as,

$$\begin{aligned} \text{at } z &= 0,\ \frac{dC}{dz} = \frac{d^2\nu}{dz^2} = 0 \\ \text{at } z &= 0,\ \nu = 0 \\ \text{at } z &= L,\ C = C_{gel},\ \frac{d\nu}{dz} = \frac{2P(C_{gel} - C_i)}{r} \end{aligned} \tag{4.14}$$

Note that the last boundary condition is defined in [41] as: at $z = L$, $C = C_i$, $d\nu/dz = 0$. Here, we assume that, at the open end, the osmolarity of the water moving inside the channels approaches the osmolarity of the water within the vaginal lumen, C_{gel}.

An effective length of the channel, L, has to be defined for stratified epithelium owing to its layer-over-layer structure. As the bolus is placed into the lumen, the bolus of fluid distends the vaginal epithelium. To the best of our knowledge, there are no experimental data on the geometrical deformation of the epithelium (e.g., change in orientation of epithelial cells). Here, we assume that the epithelium thickness between the serosal side and the apical side depends exponentially on the compliance ratio of the serosal side and the apical side. Thus, we supplement our model with an additional compliance, to account for the compression of the epithelium and thus the varying distance between the lumen and the serosal side. Then, the height profile of serosal side, h_2,

$$h_2(x,t) = h(x,t) + L_1 exp\left[-\frac{(h(x,t) - h_\infty)M_2}{HM_1}\right] \tag{4.15}$$

where, M_1/M_2 characterizes the thickness of the epithelium.

We solve Eq. 4.13 separately from the governing gel-water flow equation, Eq. 4.7. Eq. 4.13 is solved with the shooting method owing to the nature of the boundary conditions. This gives us the velocity at the open end of the channel for a specified L and C_{gel} value. Eq. 4.13 has been solved for a representative range of L, from 10 μm to 100 μm, and for a practical range of C_{gel}, from 0.3 Osm (isotonic) to 2 Osm (hypertonic). Then, $\nu(z = L)$ as a function of L for $C_{gel} = 0.3$, 0.6, 1 and 2 Osm, is plotted in Fig. 4.11. We set $r = 0.05$ μm, $C_i = 0.3$ Osm, $D = 10^{-6}$ cm^2/s, $N = 10^{-6}$ $mosmols/cm^2/s$ for $0 < z < 10$ μm and at zero for $z > 10$ μm, and $P = 10^{-6}$ $cm/Osm/s$, following [41]. Here, for different values of L, we confine all solute transport to the bottom tenth of the channel. Clearly, further experimental characterization of the vaginal wall is required for a more accurate set of parameters and a more sophisticated theoretical treatment of the varying distance of LIS across the epithelium.

The curve-fit of the results in Eq. 4.13 is found to be,

$$\log \nu(z = L) = p_0 + p_1 L + p_2 L^2 + p_3 L^3 + p_4 L^4 \tag{4.16}$$

where the coefficients of the curve-fits are given in Table 4.1.

Note that the water velocity in the channel is defined as, $q_{LIS} = \nu(z = L) = w \cdot q$. Here, w is the relevant factor or "porosity" of the epithelial layer. For vaginal epithelium, further experimental work is a prerequisite to determine the widths of the channels between the epithelial cells that can enable us to evaluate the porosity. Also accounting for the variability of the sizes of vaginal epithelial

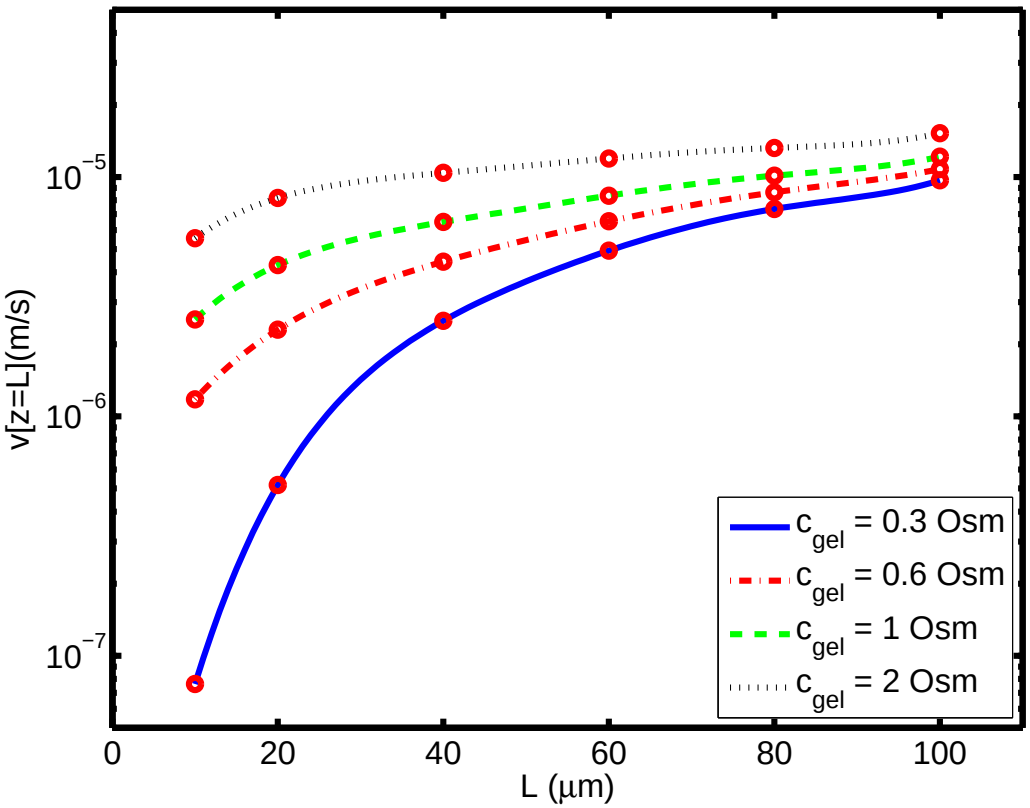

Figure 4.11. Velocity (circles) at the open end ($z = L$) obtained by Eq. 4.13 for several L and C_{gel} values. Solid lines are curve-fits.

C_{gel}	p_4	p_3	p_2	p_1	p_0
0.3	$-1.25e-07$	$3.39e-05$	$-3.42e-03$	0.16	-8.42
0.6	$-3.71e-08$	$1.00e-05$	$-1.01e-03$	0.05	-6.36
1	$-3.83e-08$	$1.01e-05$	$-9.62e-04$	0.04	-5.95
2	$-3.11e-08$	$8.32e-06$	$-7.91e-04$	0.03	-5.52

Table 4.1. The coefficients of the curve-fit for $C_{gel} = 0.3$ (isotonic), 0.6, 1, and 2 Osm.

cells due to its stratified structure, we use the porosity value of a relatively simpler structure, i.e. rabbit corneal epithelium (single layer squamous epithelium) $w \sim 100$ [89], [95], [96].

Following the derivation of the wall fluid velocity, we now consider a simulation of the coating flow of the gel. Height profiles of the bolus at 30 minutes and coating area as a function of time are plotted for a range of compliance ratios, $M_1/M_2 = 0.1$, 0.25, 1 and 100 in Fig. 4.12 and 4.13, respectively. Here, the water osmolarity at the open end, C_{gel} is set to 0.6, to account for the hypertonicity of the gel. As can be seen from the figures, as the compliance ratio increases, coating area increases. On the other hand, further increase of M_1/M_2, after unity, does not significantly change the coating area.

Next, we maintain the compliance ratio, M_1/M_2 at 0.1, and vary the water osmolarity at the open end, C_{gel}. Height profiles of the bolus at 30 minutes and coating area as a function of time are plotted for $C_{gel} = 0.3$ (isotonic), 0.6, 1 and 2 in Fig. 4.14 and 4.15, respectively. As can be seen from the figures, as the water osmolarity at the open end or "thirstiness" of the gel increases, coating area increases.

Of course, as more fluid is exuded from the vaginal wall, the dilution and hence also local osmolarity of the gel can be expected to change. We do not couple the local osmolarity with the C_{gel} in the following simulations, in view of the fairly significant assumptions that we have had to make regarding various physiological parameters. When the model can be improved with more relevant parameters, making the local osmolarity in the simulation respond to inhomogeneous boundary dilution is straightforward.

Boundary flux dependent on electro-osmotic effects

It is known that vaginal epithelial cells actively transfer Na^+ ions from the lumen into the blood [97]. This lumen-to-plasma ion transfer generates a potential difference, ΔV across the epithelium up to $30-40\ mV$ in women [98]. There are also relevant animal data on this phenomenon. The highest ΔV recorded in vivo value is at the time of ovulation ($38.2 + 1.8\ mV$) with the lowest value ($9.3 + 2.1\ mV$) [99]. Lower values of ΔV, on the order of $1\ mV$, were also reported in the literature [100], [101]. The transvaginal ΔVs measured in vitro, are always smaller than those observed in vivo, but do show an identical pattern [99]. Transvaginal ΔV renders the lumen negative and the blood or serosal side of the vagina positive. Details of these types of measurements, in vivo and in biopsy specimens in vitro across the vagina were described in [97].

Sanchez et al. [102] concluded that electro-osmotic coupling at LIS was insufficient to account for fluid flux in the case of the corneal endothelium. Within the vagina, the boundary fluid flux is estimated as $q \approx 10^{-9} - 10^{-8}\ m^3/s$ per unit area (m^2) of vaginal surface [90]; the associated

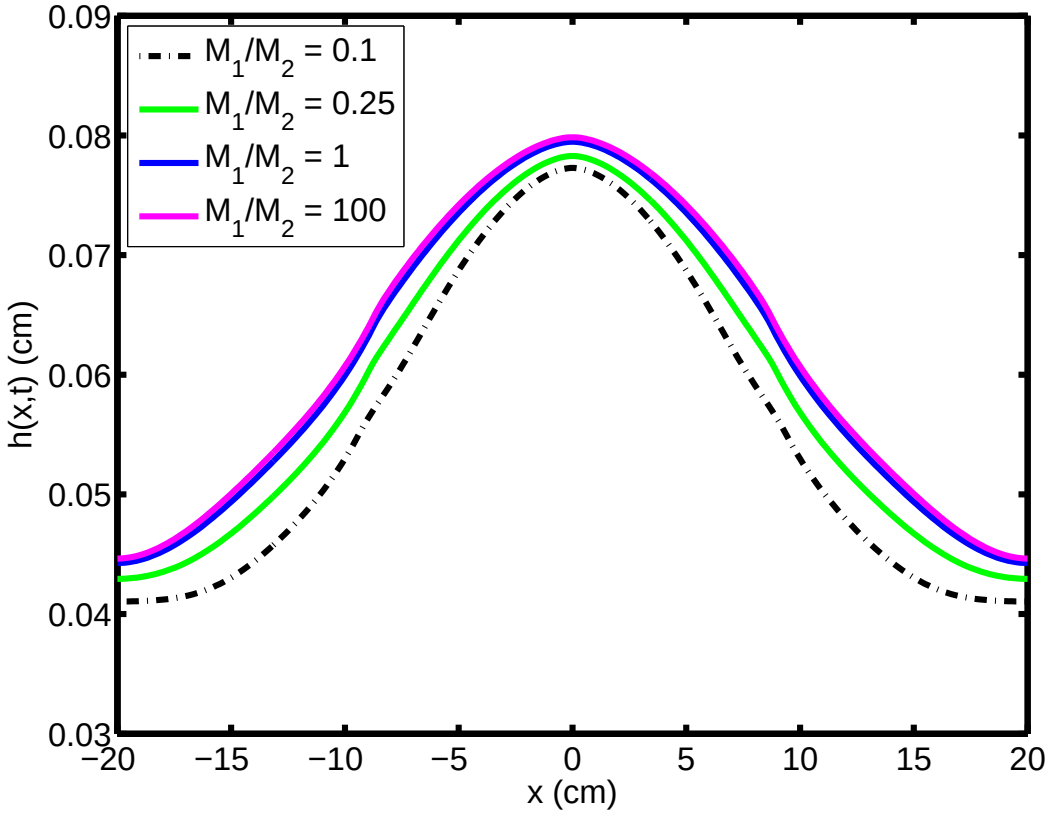

Figure 4.12. ($C_{gel} = 0.6$) Height profile of bolus at 30 minutes for $M_1/M_2 = 0.1$, 0.25, 1 and 100.

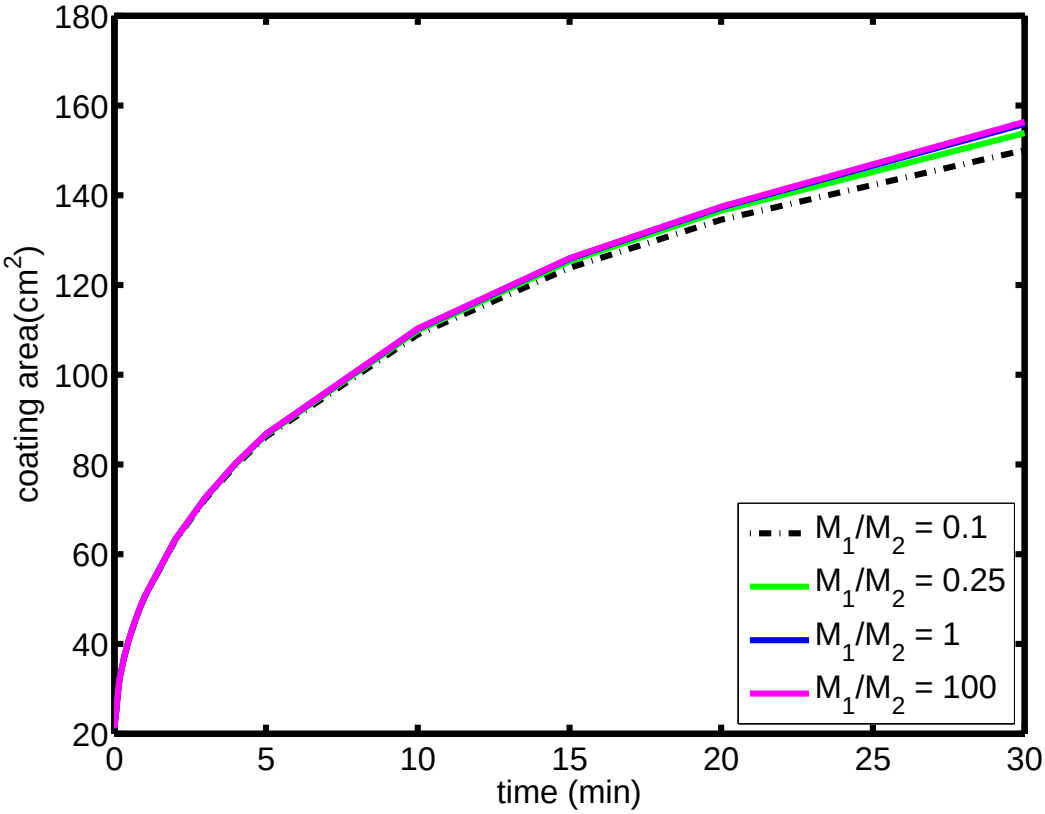

Figure 4.13. ($C_{gel} = 0.6$) Coating area of the gel on the surface for $M_1/M_2 = 0.1$, 0.25, 1 and 100.

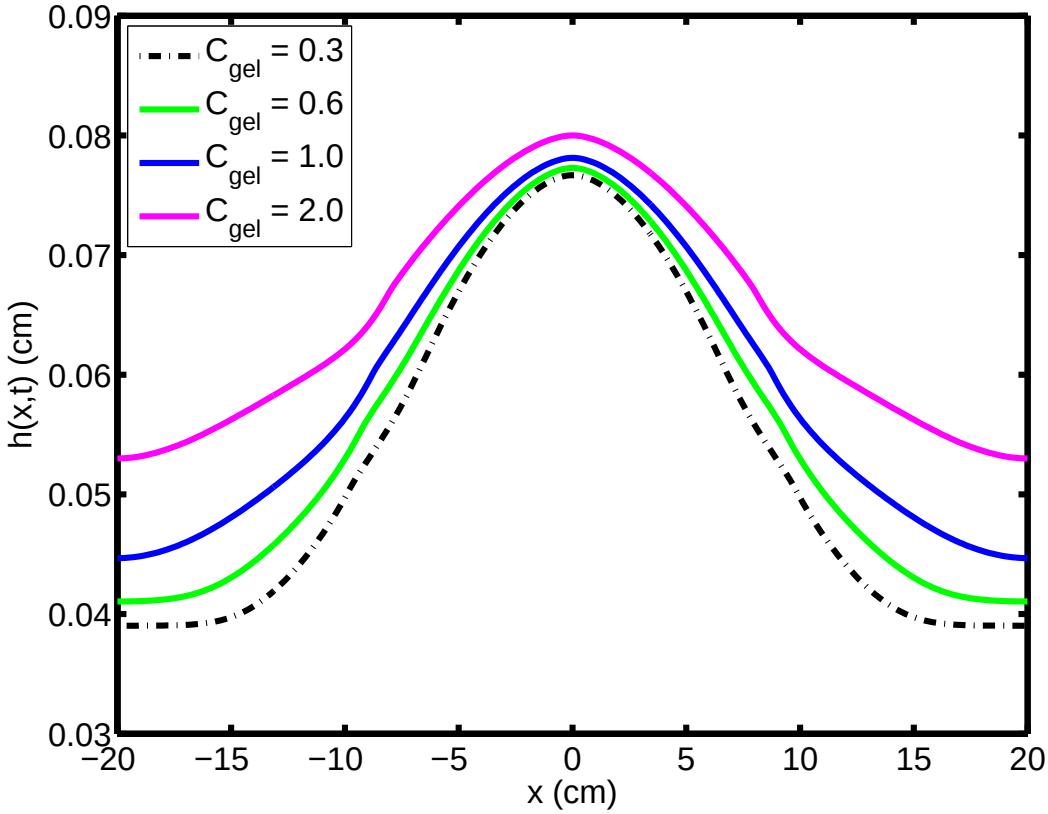

Figure 4.14. ($M_1/M_2 = 0.1$) Height profile of bolus at 30 minutes for $C_{gel} = 0.3$, 0.6, 1 and 2.

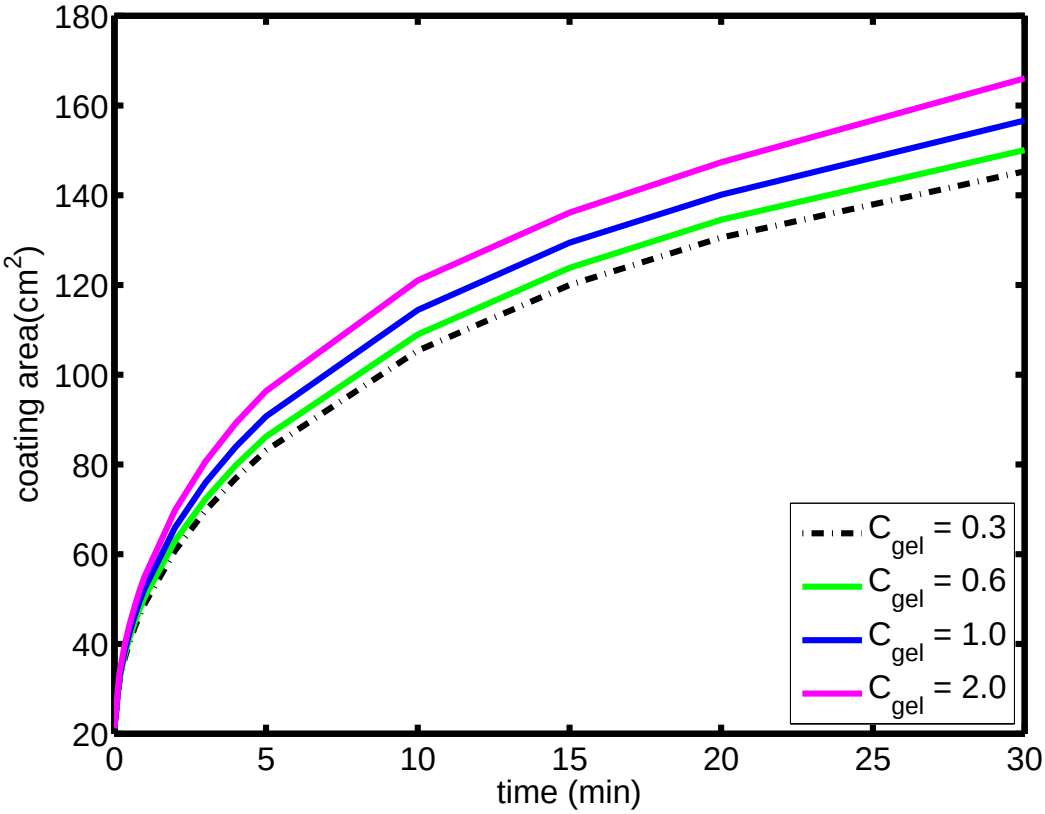

Figure 4.15. ($M_1/M_2 = 0.1$) Coating area of the gel on the surface for $C_{gel} = 0.3$, 0.6, 1 and 2.

fluid velocity in the LIS would be, $q_{LIS} = w \cdot q \approx 10^{-7} - 10^{-6}\ m^3/s$. We now explore whether this mechanism may explain the fluid flux at the vaginal wall.

Here, we employ Helmholtz-Smoluchowski (HS) model. This model assumes a configuration of idealized fluid capillaries with smooth surfaces to represent the spaces between the vaginal epithelial cells,

$$q_1 = -\frac{\epsilon\epsilon_0 E_1 \zeta_1}{\eta} \tag{4.17}$$

where, ϵ is the dielectric constant (relative permittivity), ϵ_0 is vacuum permittivity; these are taken as 78.5 and 8.85 pF/m, respectively, following [42]. The zeta potential is ζ_1, and η is viscosity, $\eta = 6.9 \cdot 10^{-3}$ poise. The zeta potential (ζ_1) of typical cell membranes is approximately -15 mV [103]. And E_1 is the electrical field along the LIS, which and can be found as $E_1 \approx -\Delta V/L_1$. Here, ΔV is taken as $1 - 40\ mV$. L_1 is the thickness of the LIS.

For the range of ΔV: 1 to 40 mV, the Helmholtz-Smoluchowski model gives the boundary fluid velocity in the LIS as, $q_1 \sim 7 \cdot 10^{-8} - 3 \cdot 10^{-6}\ m/s$ for a constant thickness of the LIS, 100 μm. Hence, the range of boundary fluid velocity estimation by the HS model matches well with the experimentally deduced average range, q_{LIS}.

We expect that distention of the vaginal surface leads to intercellular pathways being squeezed and becoming proximate to each other. This would lead to shorter delays along the channels between layers connecting these intercellular pathways. Here, Eq. 4.15 is employed again, accounting for moving boundary of the epithelial surface, and thus the varying distance between the negatively charged lumen and the positively charged serosal side. Then, the HS model can be written as,

$$q_1 = -\frac{\epsilon\epsilon_0 \Delta V \zeta_1}{\eta\left[h_2(x,t) - h(x,t)\right]} \tag{4.18}$$

where $h_2(x,t)$ is defined by Eq. 4.15.

Height profiles of the bolus at 2 hours and coating area as a function of time are plotted for the potential difference, $\Delta V = 1$ and 10 mV in Fig. 4.16 and 4.17, respectively. For $\Delta V = 1\ mV$, results are very similar for a wide range of compliance ratio, $M_1/M_2 = 0.1$, 0.25, 1 and 100. As ΔV increases, boundary flux and coating area increase, and the effects of compliance ratio become evident. As can be seen from the figures, as the compliance ratio decreases, coating area increases. On the other hand, further increase of M_1/M_2, after unity, does not significantly change the coating area.

4.4 Discussion

In this analysis, we improved our model to take into account finite volume changes in a gel associated with imbibed fluid during the course of an elastohydrodynamic squeezing flow. This flow simulates vaginal deployment of a non-Newtonian gel, intended for delivery of topically acting drugs such as anti-HIV microbicides. To model this problem, we added a source term in the Reynolds lubrication equation, to account for the mass transfer that takes place across the moving epithelial surface and into the gel bolus. We supplemented the lubrication equation with a mass conservation equation of the gel component, in a treatment that derives from multi-component mass transfer theory. This provided the dilution distribution within the non-Newtonian gel-water

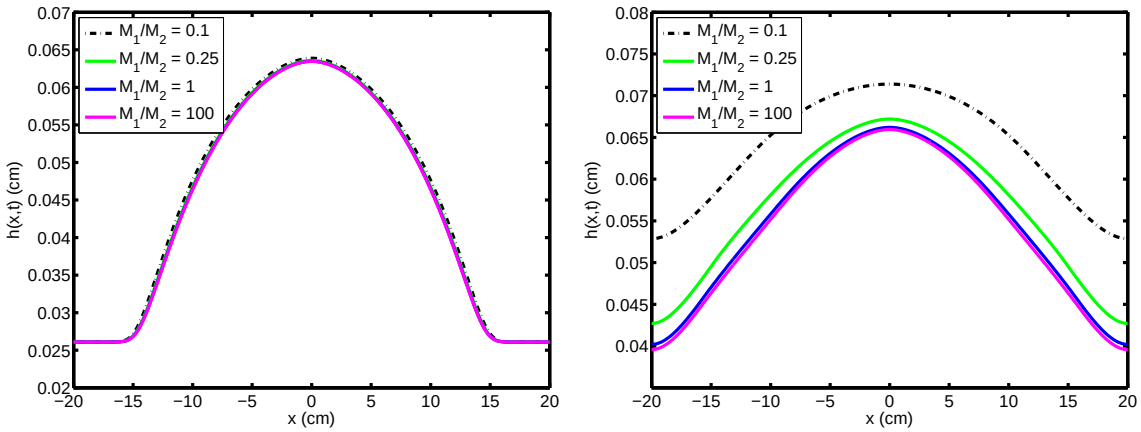

Figure 4.16. Height profile of bolus at 120 minutes for $M_1/M_2 = 0.1$, 0.25, 1 and 100.

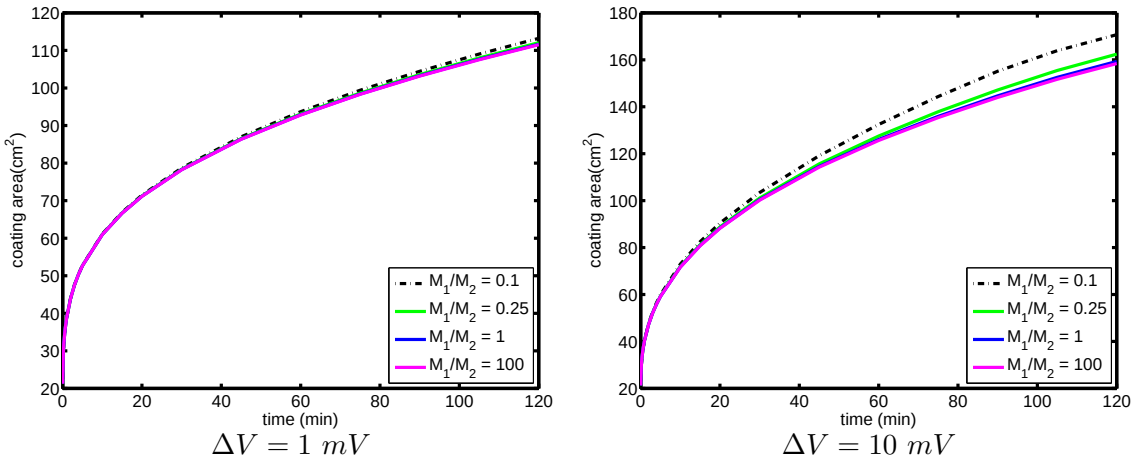

Figure 4.17. Coating area of the gel on the surface for $M_1/M_2 = 0.1$, 0.25, 1 and 100.

solution, and overcomes the restriction of modest dilutions that was inherent in chapter 2. The resulting theory models fluid flow driven by a longitudinal force (e.g., gravity) and a transversal force (e.g., wall compliance), although in the examples here we considered only the transverse squeezing force (which is a more complex problem than flow due to gravity alone). This flow influences transport of the fluid from the boundary, which is responsible for the swelling of the gel. In order to conduct analysis of the consequences of inhomogeneous boundary dilution, the parameters of the constitutive equation and the volume fraction of vaginal fluid were linked to data from the rheological measurements of a test vaginal gel used in human microbicide research.

We first checked the accuracy of our assumption that the concentrations of the gel and water are uniform across the height of the thin layer. We adapted a conservative approach, actually applying a boundary flux that exceeds somewhat the physiologically estimated mean boundary flux. We concluded that over the timescales of interest, the assumption of uniform concentrations is well motivated.

Scientific inquiry into the mechanism behind the flux from the vaginal wall has scarcely begun. Such flux vary depending upon the time of day, or the phase of the ovulation cycle. We first employed a fluid flux at the boundary that is constant in time and space; values of this flux were derived from data on the mean production rate of human vaginal fluid. As boundary flux increased, the coated area was logically found to grow more rapidly with time. This phenomenon of boundary dilution is therefore important to understand from the point of view of the application we have in mind. The model including swelling shows more rapid coating −i.e. larger coating areas− than when swelling is neglected. This can be explained by an increase in the volume of the bolus due to transient swelling and, consequently, increased squeezing forces that drive the spreading process.

We then explored three mechanisms that may explain the boundary flux from the vaginal walls; each mechanism has an associated time- and space-varying boundary condition. First we considered a model where flux is a function of hydrodynamic pressure difference across the membrane of epithelium. This simple model leads to estimates the vaginal flux in the experimentally measured range. However, it is questionable whether the fluid supply from the first cell layers at the apical side into the lumen can be sustainable. These cells will be depleted as reservoirs of fluid unless upper layers transfer fluid into them over the timescales of relevance.

The second mechanism we explored explains the flux as a consequence of standing osmotic gradients in the tortuous channels between epithelial cells. To study this, we modified a standing-gradient osmotic flow model [41] to account for osmotic gradients that may drive fluid through the epithelial tissue underlying a hypertonic gel. This flow is thus due to active transportation of solute into the LIS, diffusion towards the open mouth and (possibly hyperosmolar) gel. We note that vaginal boundary flux can be defined in two different ways: flux per LIS and flux per unit area of the vaginal surface. To convert from one to another, a factor called porosity, w, is used [95] and the following formula, $q_{LIS} = w \cdot q$, is employed. The simple structure of corneal endothelium allows one to calculate its geometry and thus the porosity in a plausible manner [89], [95]. However, the structure and geometry of vaginal epithelium is relatively complex. To the best of our knowledge, useful detail about the widths of the channels between the vaginal epithelial cells is lacking. Absent such measurements, we used the porosity value of a relatively simpler structure, i.e. rabbit corneal epithelium. With this assumption, the standing-gradient osmotic model leads to vaginal fluid fluxes at rates, $q_{LIS} \approx 10^{-7} - 10^{-5}\ m/s$ or dividing q_{LIS} by porosity, $q \approx 10^{-9} - 10^{-7}\ m/s$ −comparable to experimental data on such production. We accounted for the potential hypertonic property of microbicide gels by changing the boundary condition of the standing-gradient osmotic flow model at the open end of the paracellular transport channels. Although we did not couple the evolving

water concentration of the gel, which is evaluated at each time step by the present model, with the osmolarity at the open end of channels, it is straightforward as long as the osmotic coefficient is known for the specific gel employed. Here, instead we set constant values, from isotonic (0.3 Osm) to hypertonic (0.6, 1 and 2 Osm), for the osmolarity at the open end of channels.

In the final mechanism, we accounted for electroosmotic forces as a driver of fluid flux out from the vaginal epithelial surface. The vaginal fluid production was estimated with Helmholtz-Smoluchowski model by assuming the case of idealized capillaries with smooth surfaces for spaces between the vaginal epithelial cells. This estimated the boundary fluid velocity as, $q_1 \approx 1.4 \cdot 10^{-7} - 6 \cdot 10^{-6}\ m/s$ for a constant thickness of the LIS, 100 μm. Hence, the range of boundary fluid velocity estimation by the HS model matched well with the experimentally deduced average range, q_{LIS}. In recent years, there have been several contributions to the literature on tight junctions for paracellular flow in the corneal endothelium [42]. Given the more limited understanding of vaginal wall anatomy and physiology, a more parameter-demanding tight junction model is not employed here.

We cannot emphasize enough that there is a dearth of physiological information about the parameters of osmotic and electo-osmotic forces across the vaginal epithelium. The parameters that characterize such phenomena are summarized in the foregoing sections. For the purposes of this inquiry, the associated parameters have been estimated from those of relatively simpler epithelia such as the corneal epithelium. Clearly, such information for vaginal epithelium would not only improve the biophysical accuracy of the modeling here, but be of broad relevance to further research in womens health. In addition, for both osmotic and electoosmotic boundary fluxes, a simple model is employed in the present chapter to evaluate varying distance between the apical and the serosal side of vaginal epithelium. This provided the effective lengths of the channels along the vaginal lumen. Further experimental study of the effects of compression on the lengths of lateral intracellular spaces is required for more sophisticated numerical models of transport across the vaginal epithelium, and in general, any stratified epithelium.

The theory developed here for a swelling microbicide gel and its impact on the course of the gel's vaginal deployment will be useful to the microbicide community. The theory developed here improves our understanding of the biophysics of microbicide gel flows in vivo, which can lead to improved understanding of drug delivery by those gels. In addition, the theory here may find application in other elastohydrodynamic problems involve swelling, e.g. in the cornea.

Chapter 5

Transport processes in films that release anti-HIV microbicide molecules

5.1 Introduction

An alternative and promising method for blocking sexual tranmission of HIV today lies in the application of topical microbicides to mucosal surfaces. There is a widespread agreement that more effective and diverse drug delivery vehicles, as well as better active ingredients, must be developed to increase microbicide efficacy. In this setting, there is now great interest in developing different delivery vehicles such as vaginal rings, gels, and films. In this chapter, we study films. In many parts of the world, vaginal films are preferred over gels [104] due to their practical appeal. In addition, the films have several advantages of portability, ease of application (without applicator), easy storage and handling, feasibility of large scale production, and improved stability of drugs at extremes of temperature and humidity. Hence films may be more suitable than gels for tropical climates [105].

We first experimentally investigate the effects of dilution and swelling by ambient vaginal fluids on the rheological properties of the film formulations. The rheological parameters are obtained at equilibrium for plausible swelling ratios by our collaborators. We fit Carreau constitutive model to the rheological data. Then, we integrate the rheological data into a mathematical model of homogeneously diluted film spreading.

In a real application, a microbicide-bearing film dissolves by first imbibing (or taking up) solvent (vaginal fluid), whereupon its material structure changes in a way that frees individual polymer molecules in the film to move. The polymer structural relaxation via water uptake forms a two-phase, glassy-rubbery system, and eventually a single-phase rubbery system. Here, we assume that

the relaxation time scale of the polymer network is much smaller than the flow time scale, and neglect the transient dissolution of the film. We develop a mathematical/computational model of the spreading and swelling of a microbicide-bearing polymer film, and subsequent distribution of an active drug throughout the vaginal lumen. We propose two boundary conditions, namely (1) transcellular and (2) paracellular, for the absorption of drug molecules. The utility of the present model derives from its ability to model tradeoffs in film design as they affect the pharmacokinetics.

5.2 Swollen dissolved polymer films

As a preliminary analysis, swollen dissolved polymer films deploying anti-HIV microbicides will be considered. We first experimentally investigate the effects of dilution and swelling by ambient vaginal fluids on the rheological properties of the film formulations designed for vaginal microbicide drug delivery. The extent to which film swells depends on the amount of vaginal fluid absorbed and can be defined using the parameter called the swelling ratio. The degree of swelling of films was calculated according to the following expression

$$\text{Swelling Ratio} = \frac{\text{mass of imbibed fluid}}{\text{mass of dry film}} \tag{5.1}$$

5.2.1 Experimental methods

The amount of ambient fluid present in the vaginal canals varies among individuals, ranging from 0.5 g to 0.75 g (assuming the vaginal fluid density of 1 g/cm^3). Current applications of vaginal films apply the materials in a size of approximately 4 in^2. The weight of our film formulation of this size is approximately 0.17 g. Therefore, assuming complete dissolution by only already-available vaginal fluid, the net swelling ratio of films in vaginal fluid in real application can be estimated as ranging from 3 to 5. If other vaginal fluid is recruited via the mechanisms explored in chapter 4, the swelling ratio may be larger.

Film and DI water were appropriately massed to obtain the desired dilutions. The film was then dissolved in the water in a microtube. The film solutions were homogenized via mixing by vortexing. The diluted solutions were capped and allowed to equilibrate for approximately 24 hours before taking measurements. Multiple batches of samples were prepared. For each dilution, results were averaged from 3 independent batches.

The measurements of the rheological properties of the film were obtained from a TA Instruments model AR 1500ex rheometer using a 40 cone and 20 cm diameter plate by our collaborators. Measurements were taken at 37^{o}C over shear rates in the range of $0.01-500$ s^{-1} in order to simulate the shear rates in which materials (gel and gel-like materials) experience in real application. That is, the materials experience shear rates of less than 0.1 s^{-1} during passive seeping and shear rates approximately 100 s^{-1} during coitus [58]. Yield stress measurements were taken from measuring the residual stress at 37^oC with a Brookfield model 5 HB DV-III Ultra rheometer.

5.2.2 Experimental results

The log-log plot of viscosity vs. shear rate of the film dilution samples is given in Fig. 5.1.

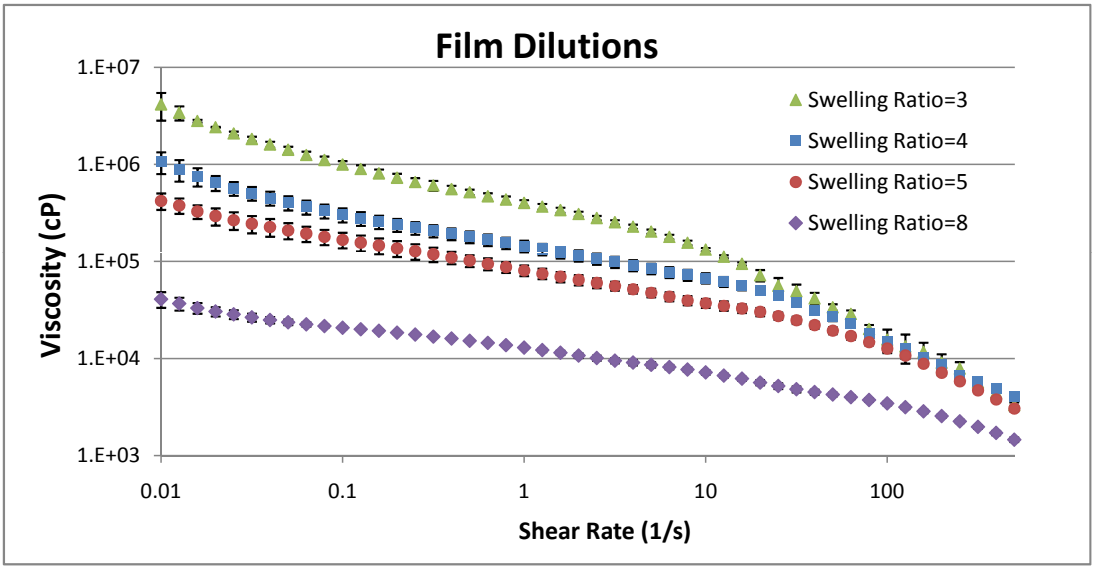

Figure 5.1. The log-log plot of viscosity vs. shear rate of film dilutions (3 batches for each dilution)

Yield stress is obtained by measuring the residual stress of each film dilution sample. Results show that the film begins to lose its yield stress as the degree of dilution increases. For this particular film, it completely loses its yield stress when the swelling ratio becomes greater than 4. Results are given in Table 5.1.

Swelling ratio	Yield Stress τ_0(Pa)
3	23.81
4	2.94
5	0
8	0

Table 5.1. Yield stress of the film dilution samples (1 batch for each dilution)

5.2.3 Constitutive model

For the constitutive model we take the form,

$$\dot{\gamma}_{xy} = \tau_{xy} F(\tau_{xy}) \tag{5.2}$$

Here, $\dot{\gamma}_{xy}$ is the shear rate and τ_{xy} is the shear stress. One can choose $F(\tau) = 1/m_0$ for a Newtonian fluid or, as we do below,

$$F(\tau) = \frac{1}{m_0} + \frac{1}{m}\left(\frac{|\tau|}{m}\right)^{(1-n)/n} \tag{5.3}$$

for a Carreau-like fluid which exhibits shear thinning and a finite viscosity at zero-shear rate, m_0. Here, m is the viscosity of the Carreau-like model and n is the power index. The original Carreau model can be written as $\eta/\eta_0 = (1 + (\lambda\dot{\gamma})^2)^{(n-1)/2}$. Here, η is the viscosity of the Carreau model, η_0 is the zero shear viscosity, and λ is the relaxation time of the fluid.

The log-log plots of viscosity vs. shear rate of films with swelling ratios: 3, 4, 5, and 8 are given in Fig.s 5.2, 5.3, 5.4, and 5.5, respectively. The solid (red) line is the fitted Carreau model.

The parameters of the Carreau model can be converted into those of Carreau-like model asymptotically [64] in the relationship $m_0 = \eta_0$ and $m = \eta_0/\lambda^{1-n}$. The two models may be matched at small and large strain rates although they are not precisely equivalent [34].

Table 5.2 shows that the zero shear viscosity m_0 decreases to one-tenth and the shear-thinning exponent n doubles as swelling ratio increases from 3 to 5, i.e. estimated range of swelling ratio in real applications.

5.2.4 Numerical model and results

Now, we integrate the rheological data of the film formulations into the mechanistic mathematical model. This is the Reynolds lubrication model with a Carreau-like constitutive equation

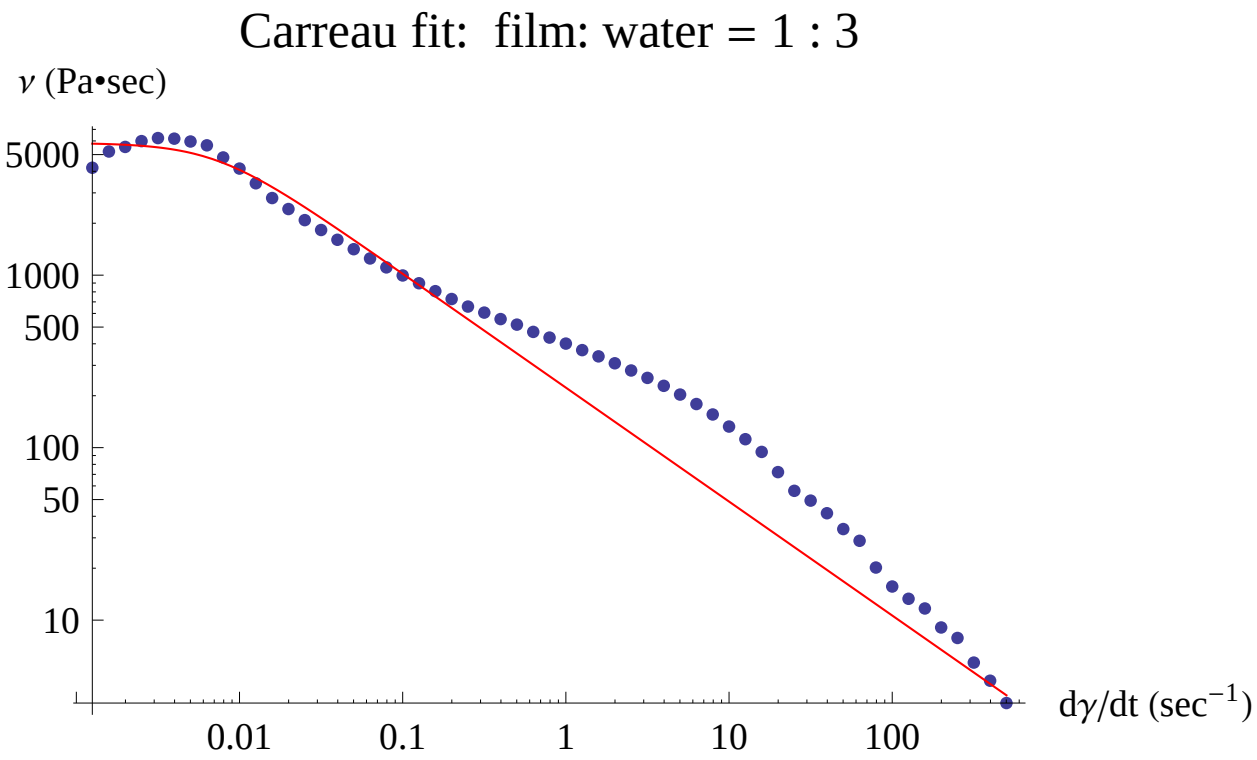

Figure 5.2. The log-log plot of viscosity vs. shear rate of a prototype film with swelling ratio: 3. Dots are experimental data, and the solid (red) line is the fitted Carreau model.

Swelling ratio	m_0 $(Pa \cdot s)$	n	m $(Pa \cdot s^n)$
3	5843.92	0.3394	222.82
4	1777.35	0.4960	104.21
5	671.077	0.6036	70.99
8	652.69	0.6628	10.65

Table 5.2. The parameters of the Carreau-like model for a dissolved prototype film.

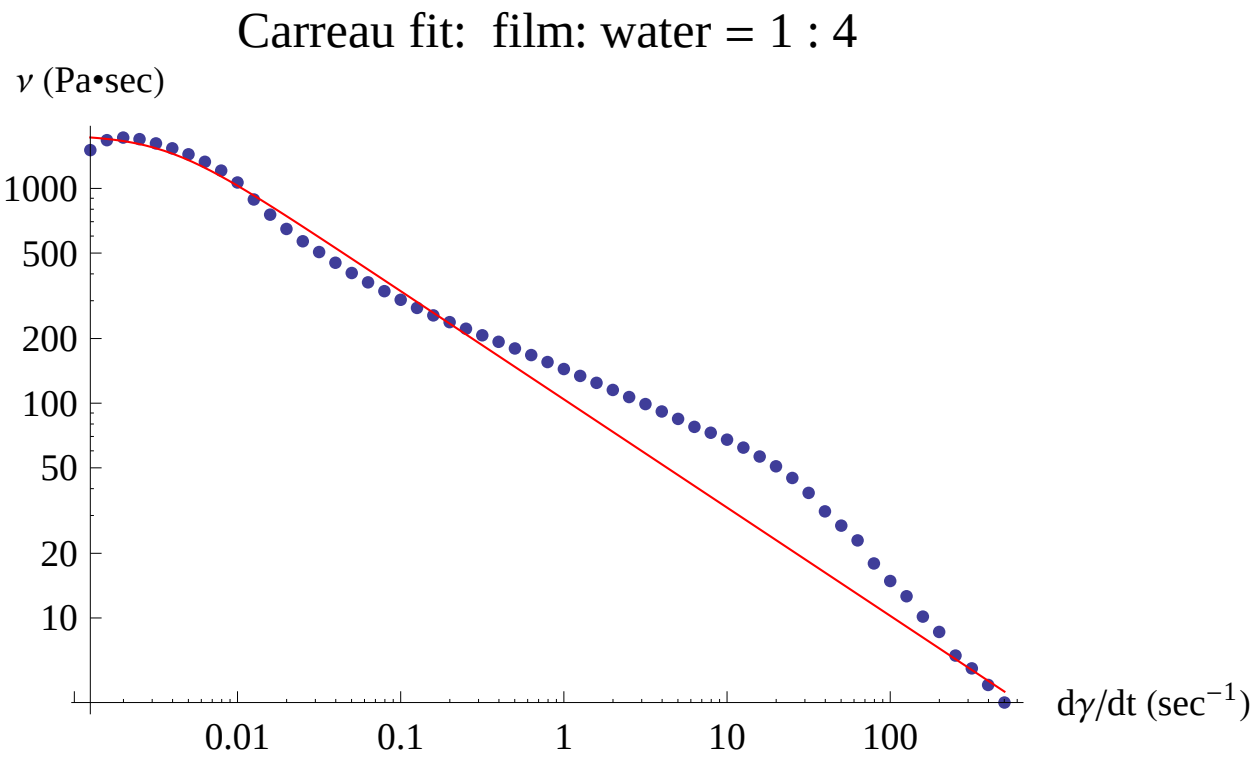

Figure 5.3. The log-log plot of viscosity vs. shear rate of a prototype film with swelling ratio: 4. Dots are experimental data, and the solid (red) line is the fitted Carreau model.

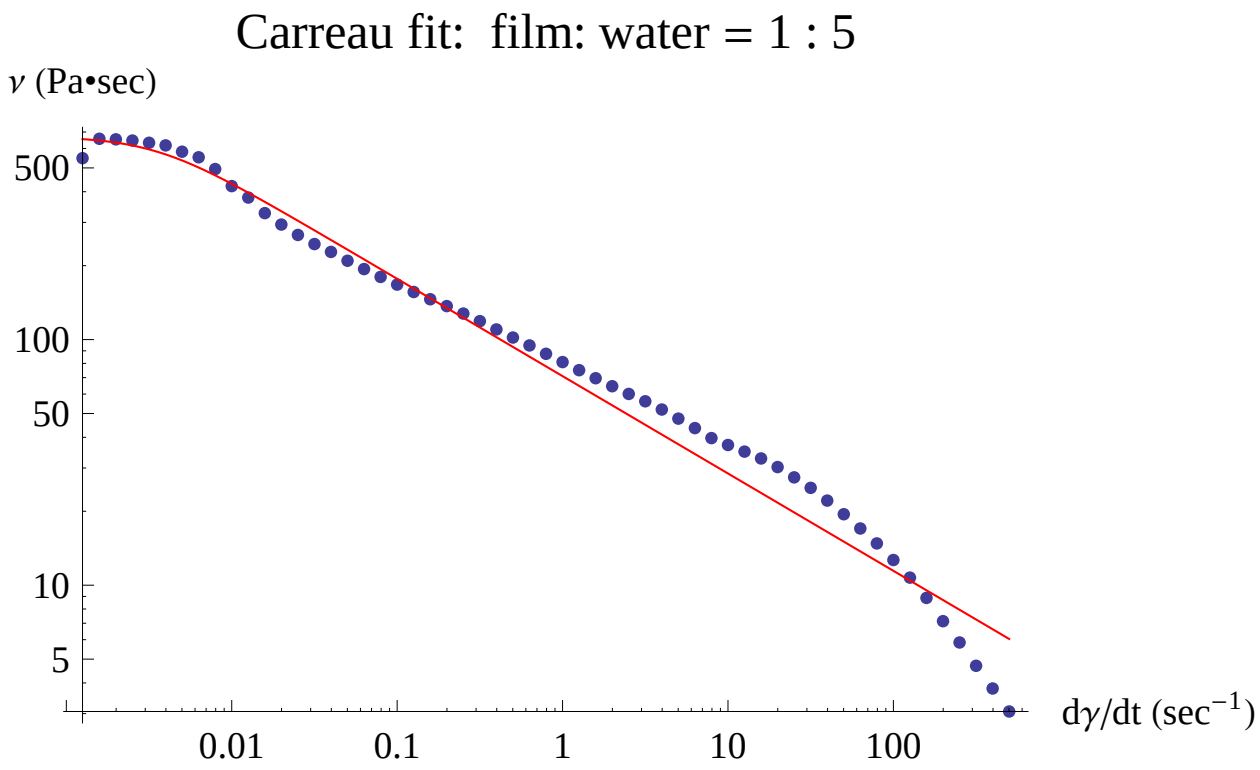

Figure 5.4. log-log plot of viscosity vs. shear rate of a prototype film with swelling ratio: 5. Dots are experimental data, and the solid (red) line is the fitted Carreau model.

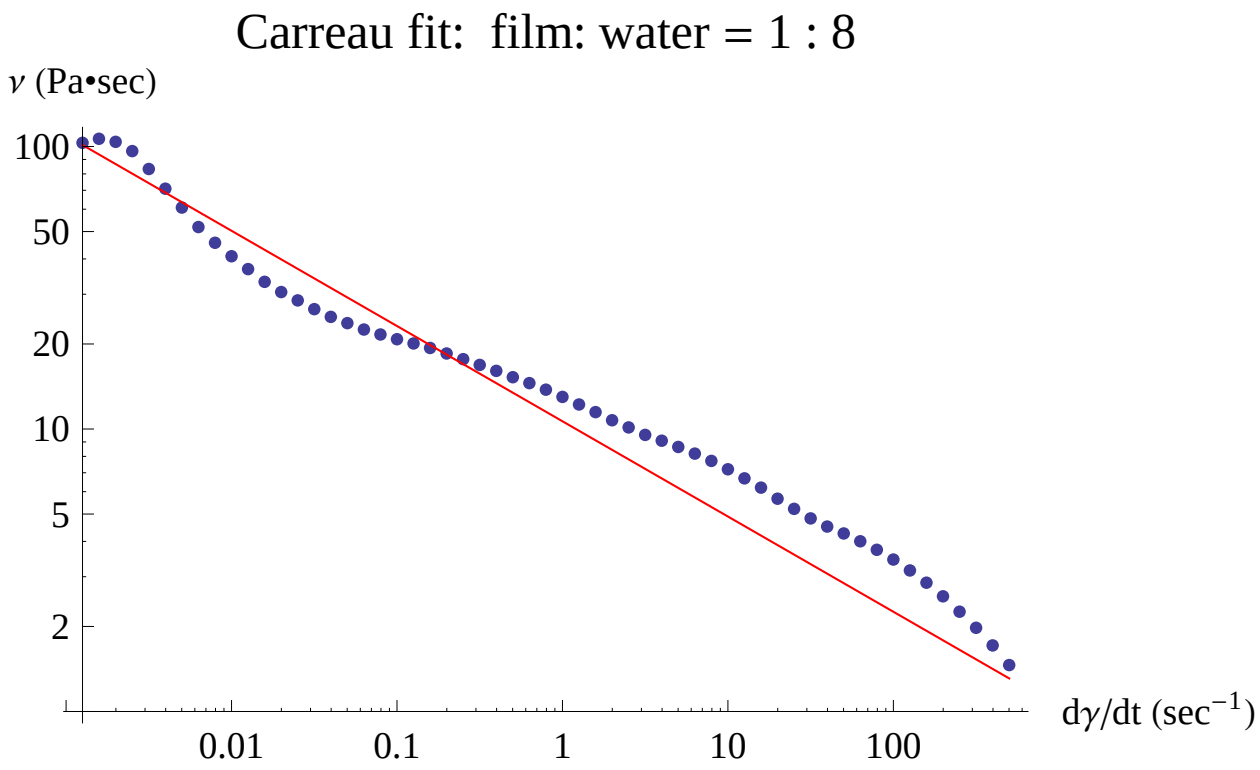

Figure 5.5. The log-log plot of viscosity vs. shear rate of a prototype film with swelling ratio: 8. Dots are experimental data, and the solid (red) line is the fitted Carreau model.

employed in chapter 2 (Eq. 2.3-2.4). However, initial condition has to be redefined. Here, initial condition for the height profile of a film read as,

$$h(x, t = 0) = \begin{cases} h_\infty & \text{if } x < -a/2 \text{ or } x > a/2 \\ b & \text{otherwise} \end{cases} \tag{5.4}$$

where, a is the width of the film, b is the initial height of the film ($= vbsr \times h_\infty$). Here, $vbsr$ is a volume-based swelling ratio, calculated by multiplying the original swelling ratio with the density ratio of film and water (ρ_f/ρ_w). To smooth the corners of the film at $x = \pm a/2$, an error function is used in a way that it covers ten grid points (1/40 of the grid points in the x-direction). Although it is not presented here, further increase in the number of grid points did not change the results.

As an initial approach to effects of film dilution on flow, we assume that the mixing ratio of film and vaginal secretions is constant and that dilution is homogeneous during the spreading process, as in the initial studies of dilution of gels [58]. Here, we assume that there is no further dilution after the onset of flow. The film formulations are already swollen, and ready to spread.

Results are illustrated in Fig. 5.6 for the profile of the film at 2 hours after the onset of flow. The height profiles are shown for swelling ratios = 3, 4, 5, and 8. The spreading length of the film increases with the extent of swelling ratio.

In order to quantify the effect of swelling ratio clearly, the coated area is shown in Fig. 5.7. The length of spreading of the film, which is proportional to the effective surface area coated, we define as four standard deviations of the film height profile. Then, this is multiplied with the physical width of the vagina, i.e. 2 cm. The effect is clearly significant; for example, a prototype film with swelling ratio 5, coats in 2 hours triple area with respect to a film with swelling ratio 3.

On the other hand, film formulations with a range of swelling ratio 3 to 5, i.e. estimated range in real applications, coat less area than which homogeneously diluted gels accomplish. This can be partially attributed to the rheology of the film formulations.

5.3 Transient swelling and spreading of a film deploying anti-HIV microbicide

A microbicide-bearing polymer film dissolves by first imbibing (or taking up) solvent (vaginal fluid), whereupon its material structure changes in a way that frees individual polymer molecules in the film to move. The polymer structural relaxation via water uptake forms a two-phase, glassy-rubbery system, and eventually one-phase, fully rubbery system. An important question arises here: Is this phenomena occurs under the conditions where the relaxation time of polymer molecules is significant with respect to the flow time scale?

We assume that the relaxation time scale of the polymer network is much smaller than the flow time scale, and neglect the transient dissolution of the film. Here, we develop a model for transient swelling and spreading of a film deploying anti-HIV microbicide. In our model, we account for further swelling of a dissolved film, and subsequent distribution of microbicides throughout the vaginal lumen. The association between swelling of film and rheological properties is obtained experimentally, delineating the way constitutive parameters are modified by swelling and dilution. The constitutive parameters, m_0, m and n, of the Carreau-like model are plotted in Fig.s 5.8, 5.9,

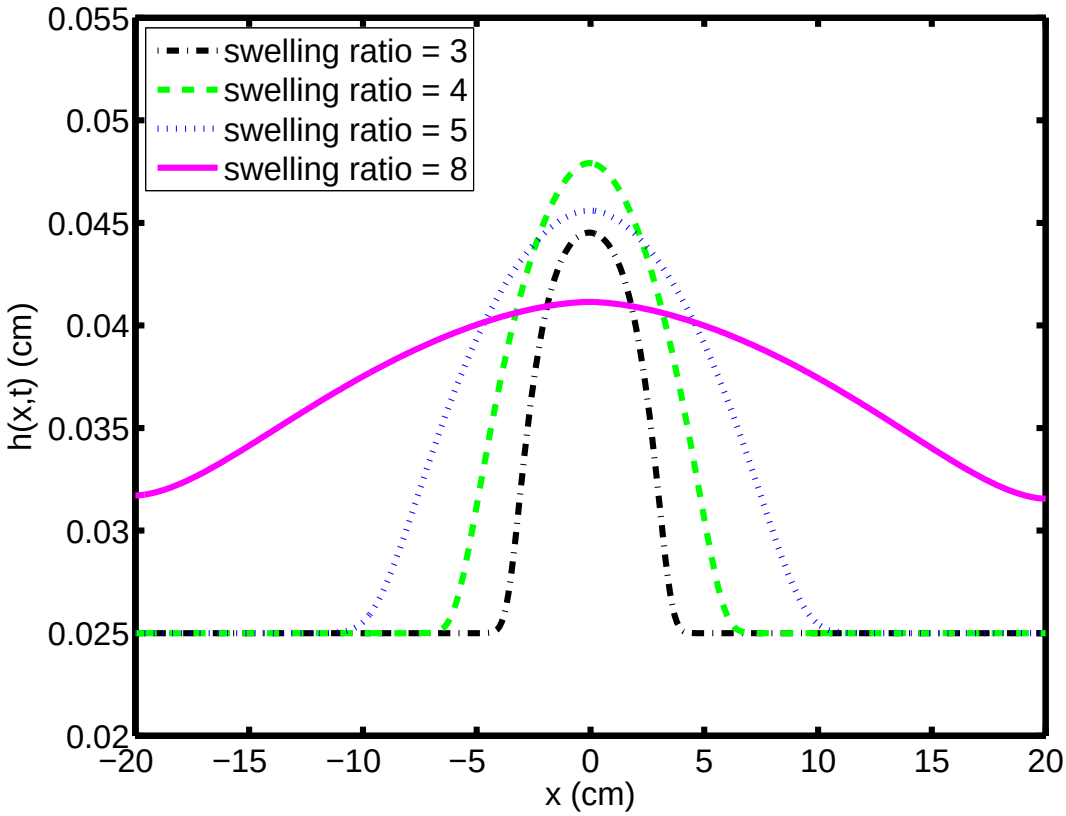

Figure 5.6. Height profile of films at 2 hours for swelling ratio = 3, 4, 5, and 8.

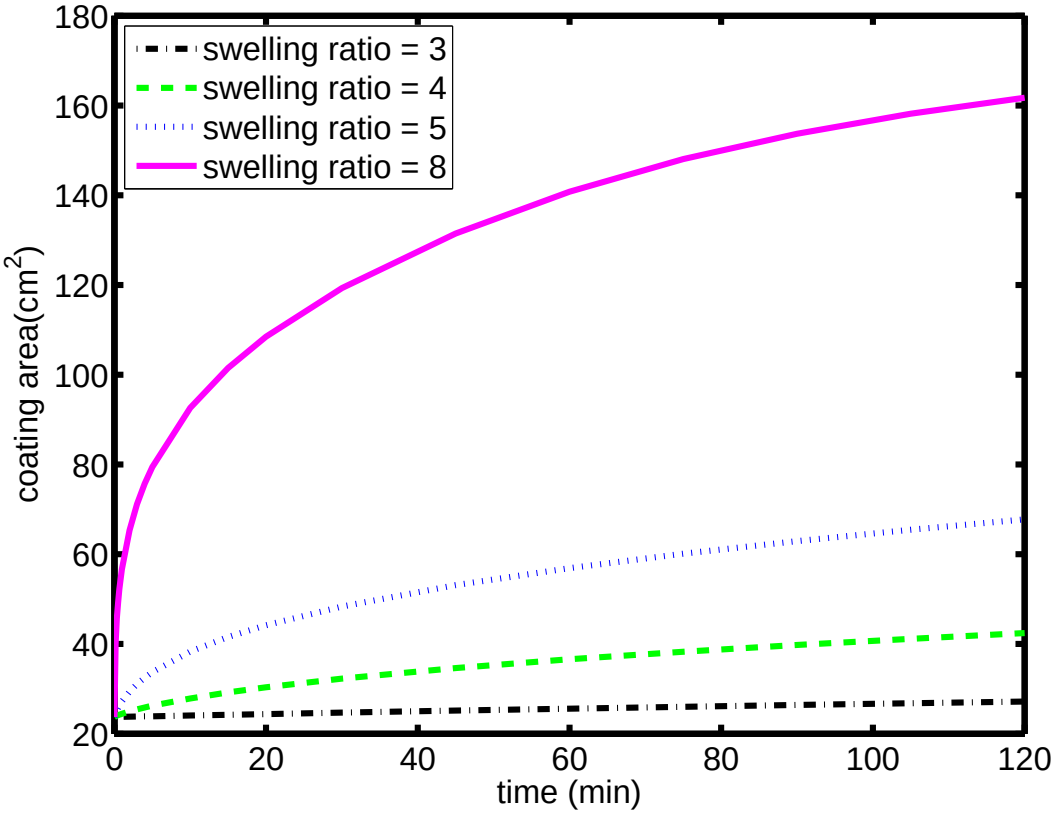

Figure 5.7. Coating area of the film on the surface for swelling ratio = 3, 4, 5, and 8.

and 5.10. Here, both quadratic (dashed) and hyperbolic (solid) curve-fits of the results are given. Note that a second or higher order polynomial curve-fit does not satisfy the conditions, e.g. $m_0 > 0$.

The hyperbolic curve-fits of the results given in Table 5.2 are found to be,

$$\begin{aligned} m_0 &= 562 - 0.908 \cdot sinh(-13.93 + 2.54 \cdot vbsr) \\ n &= 0.68 + 0.00084 \cdot sinh(-8.77 + 1.15 \cdot vbsr) \\ m &= -43.56 + 3.207 \cdot coth(-0.0146 + 0.0148 \cdot vbsr) \end{aligned} \tag{5.5}$$

where $vbsr$ is the volume-based swelling ratio.

5.3.1 Problem formulation

A recently completed study [3] has shown significant effectiveness of the anti-HIV compound Tenofovir in blocking HIV transmission in women. Here, we study a case of Tenofovir-bearing film formulations. Tenofovir belongs to a class of antiretroviral drugs and blocks reverse transcriptase, an enzyme crucial to viral production in HIV-infected people. The diffusion coefficient of Tenofovir in fluid is approximated using experimentally defined diffusion coefficients of a compound of similar molecular weight, fluorescein [106]. The moleculer weights, MW, of fluorescein, dapivirine, and Tenofovir are given in Table 5.3. Then, experimentally measured diffusion coefficients of water and

	MW (g/mol)
Fluorescein	332.3
Dapivirine	329.4
Tenofovir	287.2

Table 5.3. Molecular weights of some molecules

fluorescein in water are given in Table 5.4.

	Diffusion coefficient of molecules in water (cm^2/s)
Water	2.2×10^{-5}
Fluorescein	4.86×10^{-6}

Table 5.4. Diffusion coefficients of water and fluorescein in water

Therefore, this enables us to approximate the diffusion coefficient of Tenofovir molecules in water (and in dissolved film-water solution) as $D_T \approx 10^{-6}$ cm^2/s. On the other hand, diffusion coefficient of water molecules in water (and in dissolved film-water solution) is taken as $D_{fw} \approx 10^{-5}$ cm^2/s.

Following the assumption that we made in chapter 4, we attempt to simplify our present problem. Similarly, here we assume that the dissolved film-water solution has a homogenous concentration in the transverse direction. This requires the following, $\epsilon^2 \ll 1/Pe$, where $Pe = UL/D$ and $U = (MH^3)/(2m_0L)$. In chapter 4, after 2 elapsed minutes, the parameters satisfy the assumption. For films, m_0 is much higher than that of gels, cf. Table 2.1 and Table 5.2. Therefore,

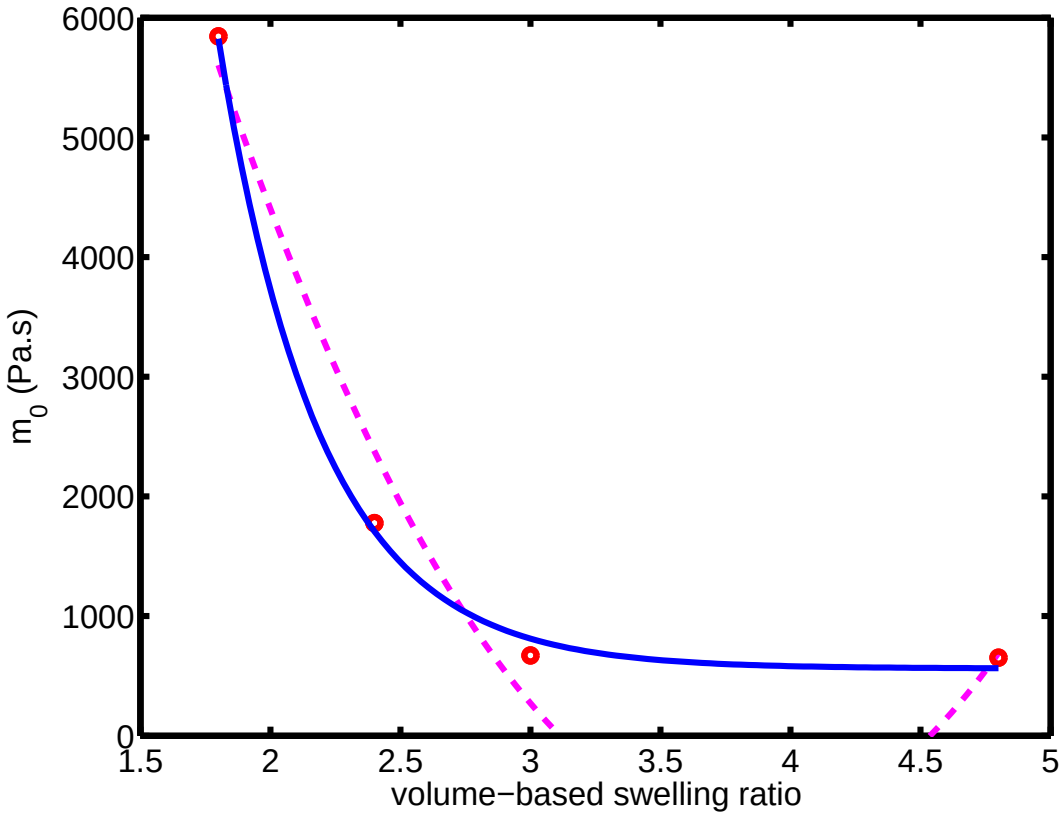

Figure 5.8. Curve fit to Carreau-like zero-shear viscosity data of a prototype film. Solid line is hyperbolic curve-fit and dashed line is quadratic curve-fit.

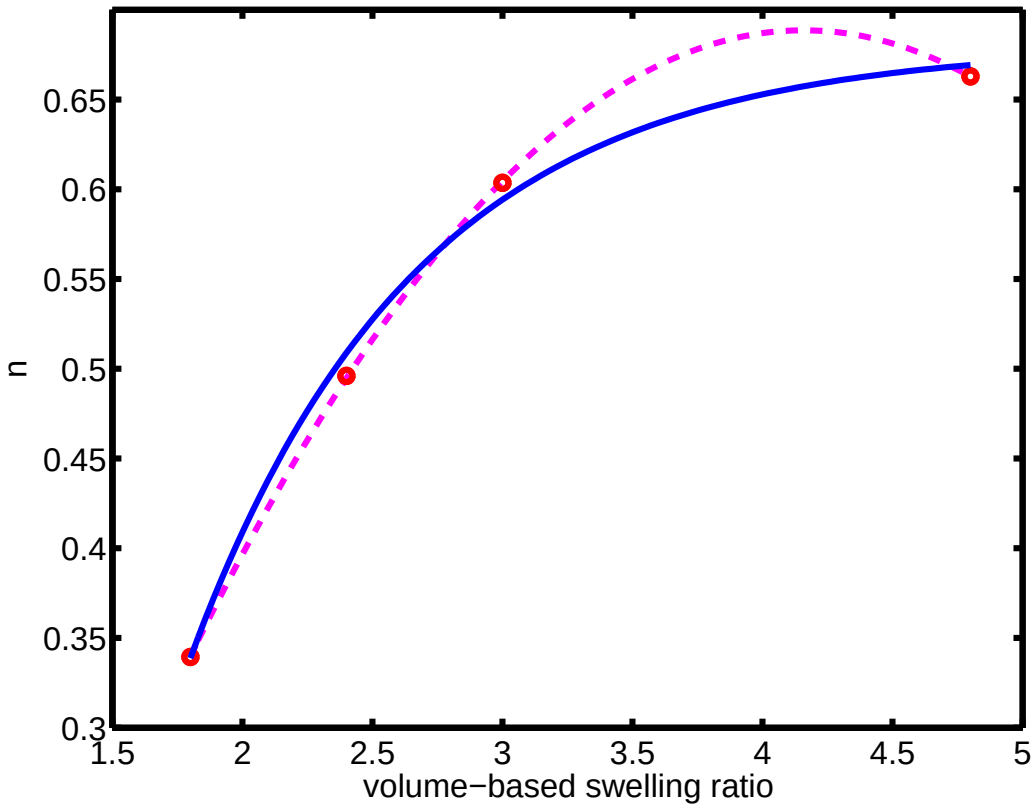

Figure 5.9. Curve fit to Carreau-like power index data of a prototype film. Solid line is hyperbolic curve-fit and dashed line is quadratic curve-fit.

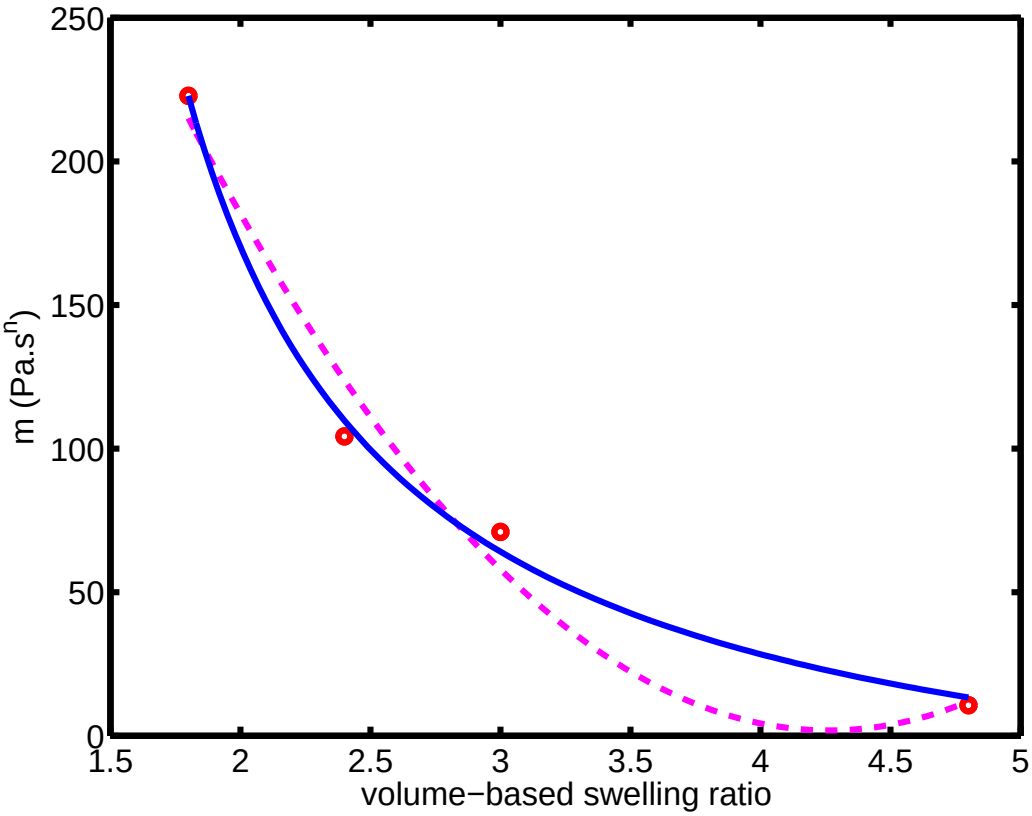

Figure 5.10. Curve fit to Carreau-like viscosity data of a prototype film. Solid line is hyperbolic curve-fit and dashed line is quadratic curve-fit.

the assumption is well motivated. Then, swelling and spreading of a dissolved film-water solution read as,

$$\begin{aligned} \frac{\partial h}{\partial t}+\frac{1}{2}\frac{\partial}{\partial x}\left[\left(M\frac{\partial h}{\partial x}-\rho g\right)m_2\right] &= -q \\ \frac{\partial(\phi h)}{\partial t}+\frac{1}{2}\frac{\partial}{\partial x}\left[\phi\left(M\frac{\partial h}{\partial x}-\rho g\right)m_2\right] &= \frac{\partial}{\partial x}\left(hD_{fw}\frac{\partial \phi}{\partial x}\right) \\ m_2 &= \int_{-h}^{h}\left[\int_{-h}^{y}F(\tau)ydy\right]dy \end{aligned} \tag{5.6}$$

As in our earlier work, we employ the one dimensional constrained continuum model [64] approximation to model vaginal wall elasticity. In this approximation, the fluid pressure near a compliant wall is proportional to the local deformation of that wall. In general, for a deformation h, the fluid pressure is given by $p=(E/T)\,h\equiv Mh$. Here, E is the elastic (Youngs) modulus of the compliant layer, T is its thickness, and M is the compliance of the elastic wall. We take for that compliance the value $10^4/0.5\ Pa/cm$.

The boundary fluid velocity, $q(x,t)$ is a quantity that is not well understood. There is remarkably little research on the presence and flow of human vaginal fluid [65], [89]. To take into consideration the very thirsty structure of vaginal films, we assume an exponential boundary fluid velocity depending on the volume fraction of film, $q=q_0\cdot exp(a_{th}\phi(x,t))$. Here, q_0 is a boundary flux constant, a_{th} is an exponential term, and $\phi(x,t)$ is the volume fraction of film along the vaginal lumen.

To model the subsequent distribution of Tenofovir throughout the vaginal lumen, simply we can add another mass conservation equation into our multi-component model. However, diffusion coefficient of Tenofovir, D_T is one-tenth of that of water in film-water solution, D_{fw}. Therefore, transport of Tenofovir molecules both in the x-direction and in the y-direction has to be accounted for.

Now, we return to the model that we developed in chapter 2 for 2-D water distribution with a moving boundary and for modest dilutions. We employ that model here for transport of Tenofovir molecules along the vaginal lumen and subsequent absorption of them at the vaginal wall. With the domain mapping, the two-dimensional convection-diffusion equation Eq. (2.5) in chapter 2 takes the form (equation is repeated here for completeness):

$$\begin{aligned} \frac{\partial V}{\partial t} &= -u_1\frac{\partial V}{\partial x}-\frac{1}{h}\frac{\partial V}{\partial \zeta}\left[u_2-\zeta\left(\frac{\partial h}{\partial t}+u_1\frac{\partial h}{\partial x}\right)\right]+\frac{D_0 exp(a_dV)}{h^2} \\ &\times\left\{-\zeta h(1+a_dV)\frac{\partial^2 h}{\partial x^2}\frac{\partial V}{\partial \zeta}+(2a_d+a_d^2V)\left(\frac{\partial V}{\partial \zeta}\right)^2+(1+a_dV)\frac{\partial^2 V}{\partial \zeta^2}\right. \\ &+\zeta\left(\frac{\partial h}{\partial x}\right)^2\left[2(1+a_dV)\frac{\partial V}{\partial \zeta}+(1+a_dV)\frac{\partial^2 V}{\partial \zeta^2}+a_d\zeta(2+a_dV)\right. \\ &\times\left.\left(\frac{\partial V}{\partial \zeta}\right)^2\right]-2\zeta h\frac{\partial h}{\partial x}\left[a_d(2+a_dV)\frac{\partial V}{\partial \zeta}\frac{\partial V}{\partial x}+(1+a_dV)\frac{\partial^2 V}{\partial \zeta\partial x}\right] \\ &\left.+h^2\left[a_d(2+a_dV)\left(\frac{\partial V}{\partial x}\right)^2+(1+a_dV)\frac{\partial^2 V}{\partial x^2}\right]\right\} \end{aligned} \tag{5.7}$$

where, $h=h(x,t)$, and velocity components in the x- and y-direction are $u_1=u_1(x,y,t)$ and $u_2=u_2(x,y,t)$, respectively. Here, V is the concentration of Tenofovir, and $V=V(x,\zeta,t)=$

$\nu(x, y, t)$. The flow equations, Eq. 5.6 and transport equation for Tenofovir molecule, Eq. 5.7 are solved together in a multi-step implicit numerical scheme.

We can take two boundary conditions for drug molecules:

1. Transcellular diffusion of drug molecules
2. Paracellular transport of drug molecules

For the former BC, a constant flux can be chosen and this can be connected to the derivative of V, such as $q = D_0 exp(a_d V) \frac{1}{h(x,t)} \frac{\partial V}{\partial \zeta}$ in the (x, ζ) domain. Here, the assumption that the diffusion coefficient of Tenofovir, D_T, is dependent on the volume fraction as $D_T = D_0 exp(a_d V)$, can enable us to model further interactions of Tenofovir with the vaginal wall.

For the latter BC, first the physical size of Tenofovir molecule should be estimated and then compared with the intercellular spaces between vaginal epithelial cells. The physical size of Tenofovir molecule is not reported in the literature. It is mainly composed of an adenine and a phosphonic acid. A simple length scale, l can be calculated by $l = (m/\rho/N_A)^{1/3}$. Here, N_A is avagadro number and $N_A = 6.022 \times 10^{23}\ mol^{-1}$. The molar masses, M, the densities, ρ and the calculated lengths, l, of these individual structures are given in Table 5.5.

	$M\ (g/mol)$	$\rho\ (g/cm^3)$	Length (A^o)
phosphonic acid	82	1.651	4
adenine	135.13	1.6	5.2

Table 5.5. The molar masses, the densities and the lengths of phosphonic acid and adenine

As can be seen from Table 5.5, the total length is $\sim$ 10 A^o. The intercellular spaces between vaginal epithelial cells differ from layer to layer [107]. To the best of our knowledge, there is not any reported value for the lateral intercellular spaces between vaginal epithelial cells. However, they are reported as $\sim$ 30 A^o for corneal endothelial cells [108], and $\sim$ 240 A^o for intestinal epithelial cells [109].

5.4 Results

5.4.1 The effects of boundary flux constant

We investigate the effects of boundary flux constant, q_0, on the coating area of films and the distribution of Tenefovir molecules. The evolution of the height profile of the film is plotted in Fig. 5.11. Initialy, the film is very 'thirsty' and the boundary flux near the film is considerably larger ($\sim \times 30$) than that at relatively less distended vaginal wall. This is due to the fact that the boundary flux is exponentially related to the volume fraction of film. As the film is hydrated more, boundary flux near the film decreases to $\sim \times 5$ of that takes place across the relatively less distended boundary. As can be seen from the figure, after elapsed 20 minutes, film begins to spread more due to varying rheology, e.g. lower zero-shear viscosity. The evolution of the volume fraction

of film as a function of longitudinal position is plotted in Fig. 5.12. At $t = 0$, film is already swollen and dissolved. The initial volume-based swelling ratio, $vbsr$, is 1.8. To switch from swelling ratio to volume fraction of film, $vbsr = (1 - \phi)/\phi$ is used. As time passes, volume fraction of film decreases due to the incoming water flux.

The height profile of a prototype film at 2 hours for $q_0 = 10^{-9}\ m/s$, $q_0 = 2 \times 10^{-9}\ m/s$, $q_0 = 5 \times 10^{-9}\ m/s$, and $q_0 = 10^{-8}\ m/s$ is given in Fig. 5.13. As boundary flux constant increases, spreading length increases. The effects of rheology can also be seen from the figure. For instance, for $q_0 = 10^{-9}\ m/s$ and $q_0 = 2 \times 10^{-9}\ m/s$, spreading is very slow during the entire 2 hours, while significant amount of swelling is taking place. In order to quantify the effect of boundary flux constant, q_0, clearly, the coating area is shown in Fig. 5.14. Higher boundary flux constant leads to more rapid coating.

The contours for concentration of Tenofovir molecules are plotted at $t = 0$, $t = 2$ minutes, $t = 30$ minutes, and $t = 2$ hours in Fig. 5.15. Boundary dilution decreases sharply near the edges of films due to the exponential term. Here, initially Tenofovir molecules are hardly carried by convection due to a rheology barrier, cf. 2 minutes. As film is diluted more, rheology enables Tenofovir molecules to move faster by increasing convective forces. The 'hat's that are observed at 30 minutes are most probably due to the convective effects that are felt more near the edges. Then diffusion smoothes, cf. 2 hours.

5.4.2 The effects of exponential or 'thirstiness of film'

Next, we investigate the effects of boundary flux exponential term, a_{th}, on the coating area of films and the distribution of Tenefovir molecules. The height profile of a prototype film at 2 hours for $a_{th} = 10$, $a_{th} = 15$, and $a_{th} = 20$ is given in Fig. 5.16. As can be seen from the figure, results for $a_{th} = 10$ and $a_{th} = 15$ are very close due to the relatively smaller flux constant and exponential factors. In order to quantify the effect of boundary flux exponential term, a_{th}, clearly, the coating area is shown in Fig. 5.17.

The contours for concentration of Tenofovir molecules are plotted at $t = 0$, $t = 2$ minutes, $t = 30$ minutes, and $t = 2$ hours in Fig. 5.15. A similar rheology barrier is also observed here for Tenofovir molecules.

5.5 Conclusions

There is a widespread agreement that more effective drug delivery vehicles with more alternatives, as well as better active ingredients, have to be developed to raise efficacy ratio. In this setting, there is now great interest in developing different delivery vehicles such as vaginal rings, gels, and films. In this chapter, we studied film formulations.

We first experimentally investigated the effects of dilution and swelling by ambient vaginal fluids on the rheological properties of the film formulations. The rheological parameters were obtained at equilibrium for plausible swelling ratios. The zero-shear viscosity, m_0, values were much higher than that of gels used in chapters 2-4. The Carreau constitutive model was fitted to the rheological data. Then, we integrated the rheological data into the mathematical model of the film spreading.

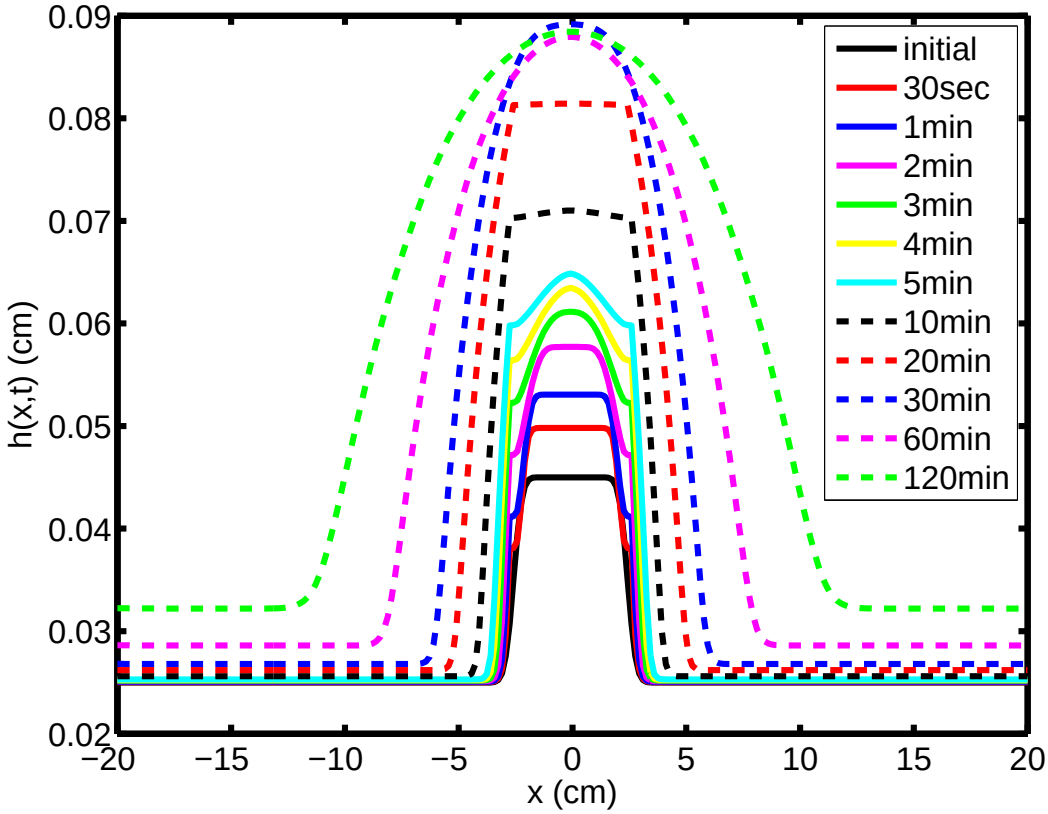

Figure 5.11. ($q_0 = 10^{-8}\ m/s$ and $a_{th} = 10$) Evolution of the height profile of a film-water solution.

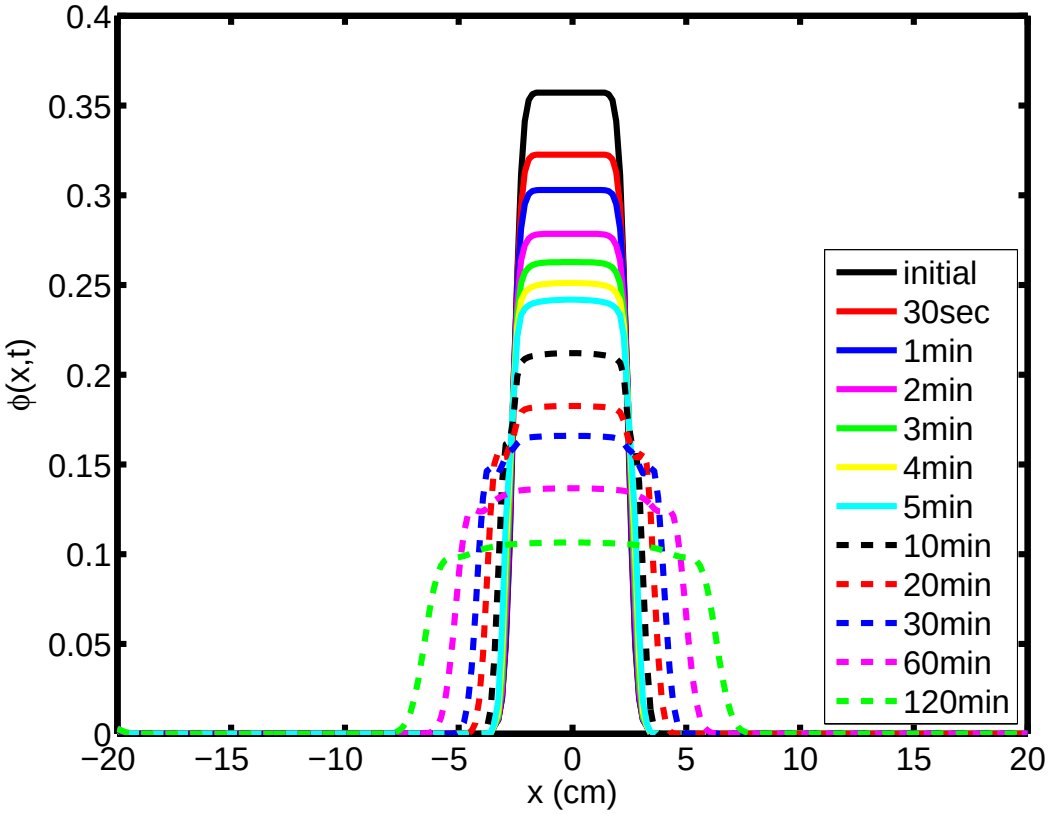

Figure 5.12. ($q_0 = 10^{-8}\ m/s$ and $a_{th} = 10$) Evolution of the volume fraction of film material.

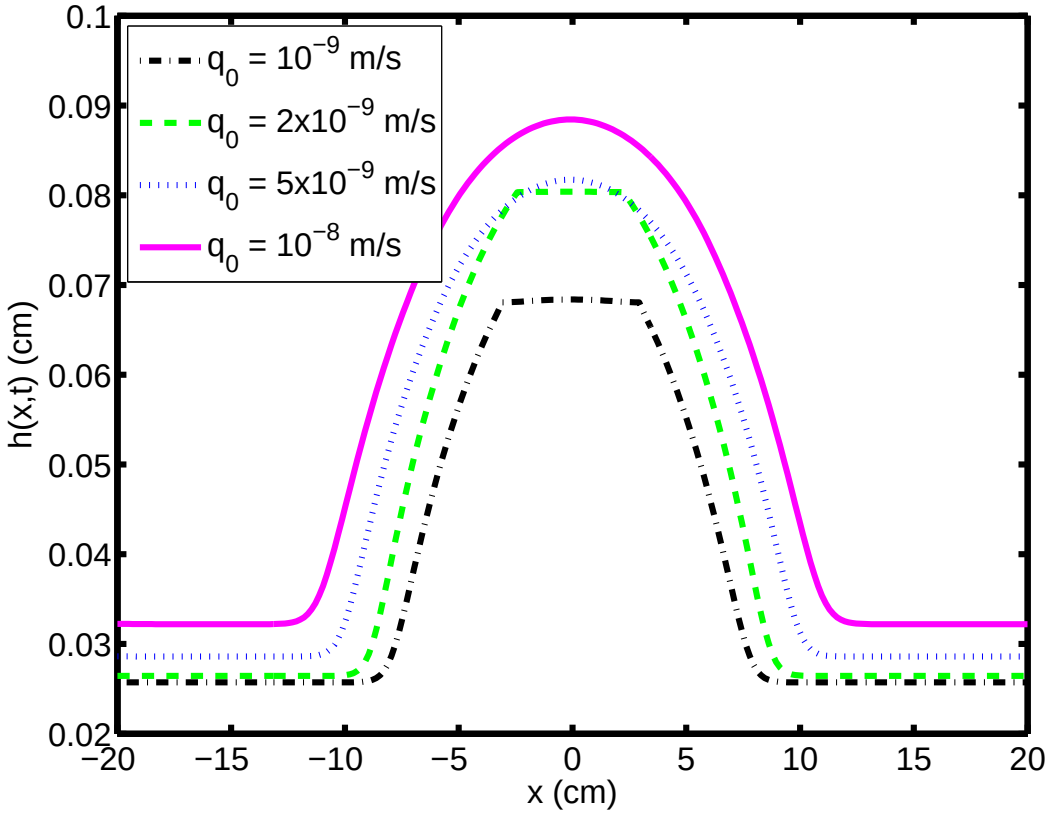

Figure 5.13. ($a_{th} = 10$) Height profile of a prototype film at 2 hours for $q_0 = 10^{-9}\ m/s$, $q_0 = 2 \times 10^{-9}\ m/s$, $q_0 = 5 \times 10^{-9}\ m/s$, and $q_0 = 10^{-8}\ m/s$.

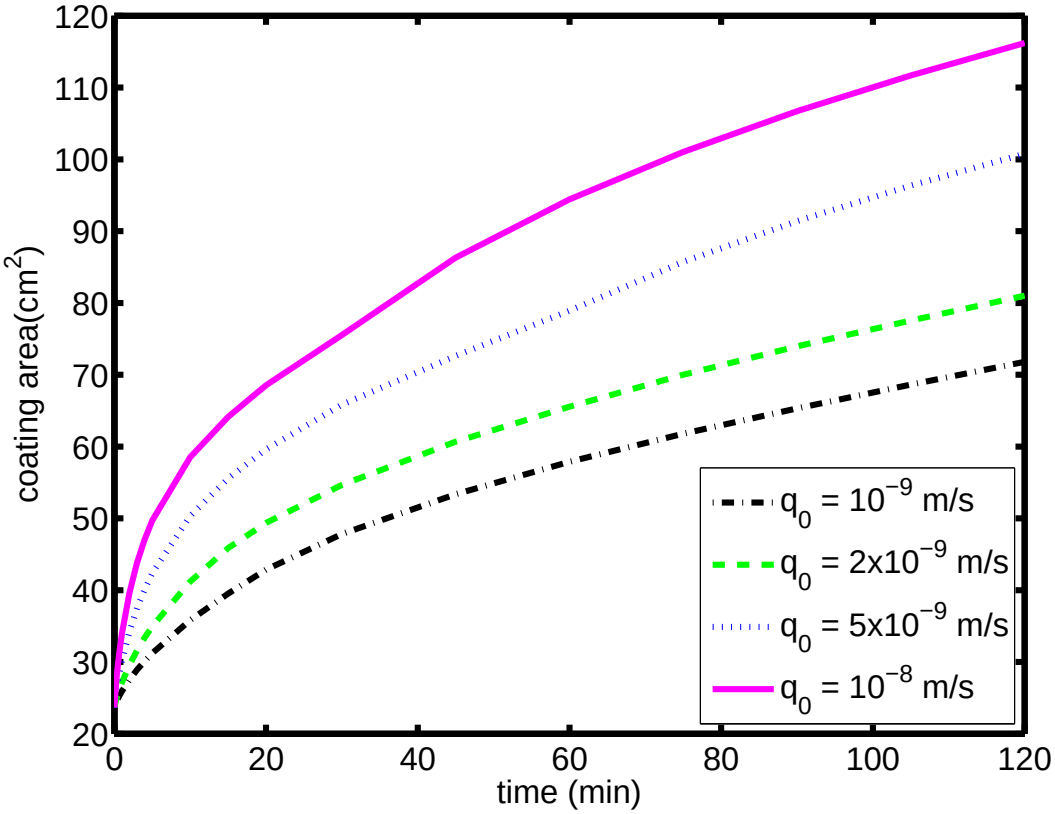

Figure 5.14. ($a_{th} = 10$) Coating area of a prototype film on the surface for $q_0 = 10^{-9}\ m/s$, $q_0 = 2 \times 10^{-9}\ m/s$, $q_0 = 5 \times 10^{-9}\ m/s$, and $q_0 = 10^{-8}\ m/s$.

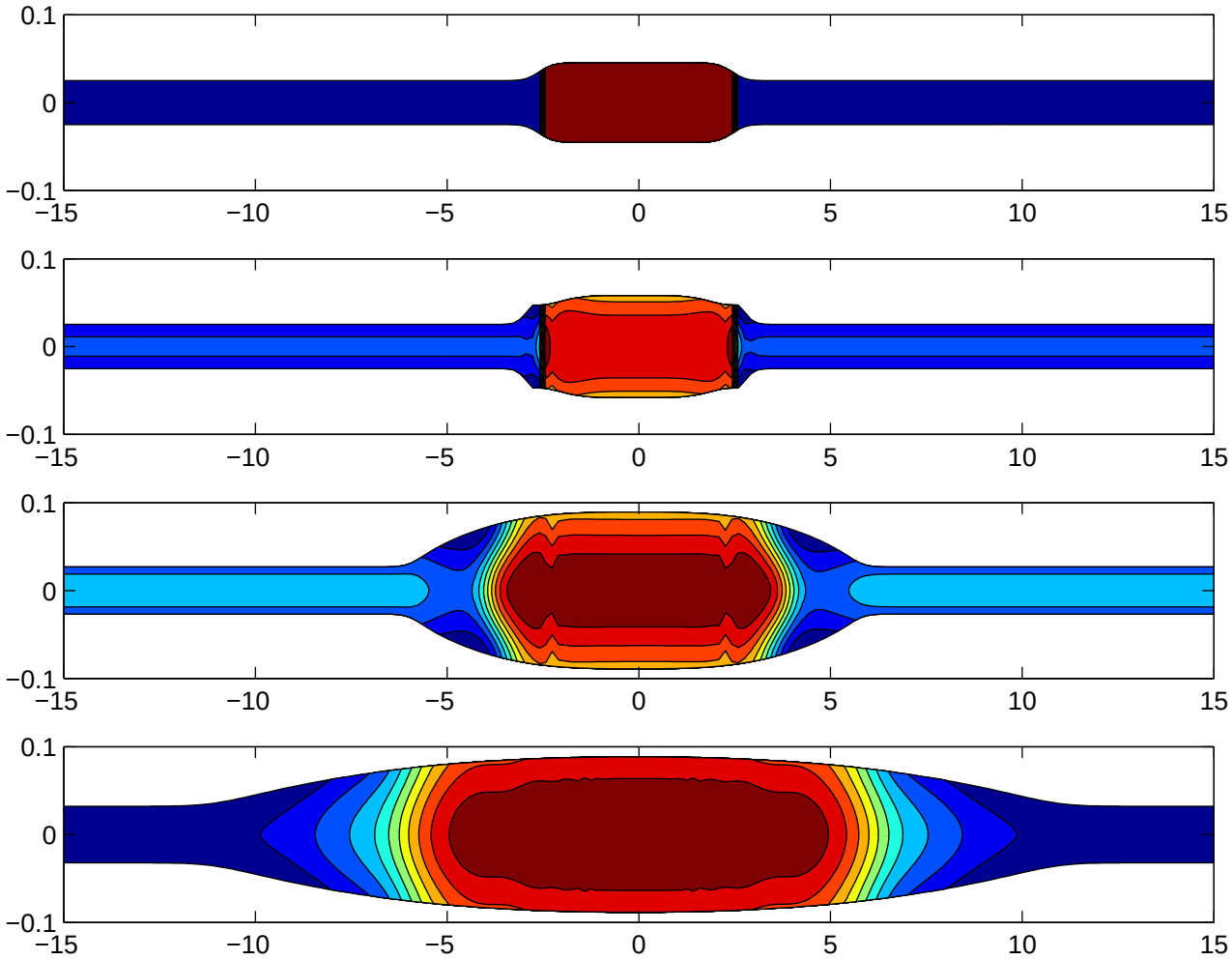

Figure 5.15. ($q_0 = 10^{-8}$ m/s and $a_{th} = 10$) Contour plots for concentration of Tenofovir molecules at $t = 0$, $t = 2$ minutes, $t = 30$ minutes, and $t = 2$ hours.

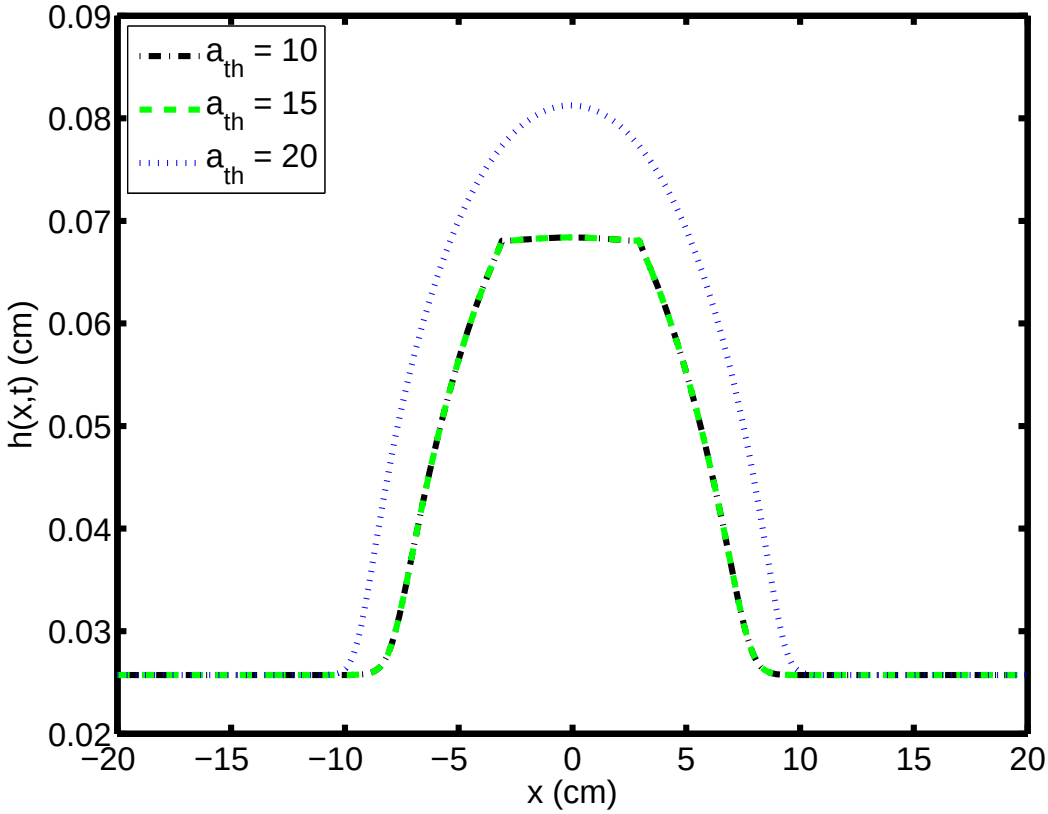

Figure 5.16. ($q_0 = 10^{-10}\ m/s$) Height profile of a prototype film at 2 hours.

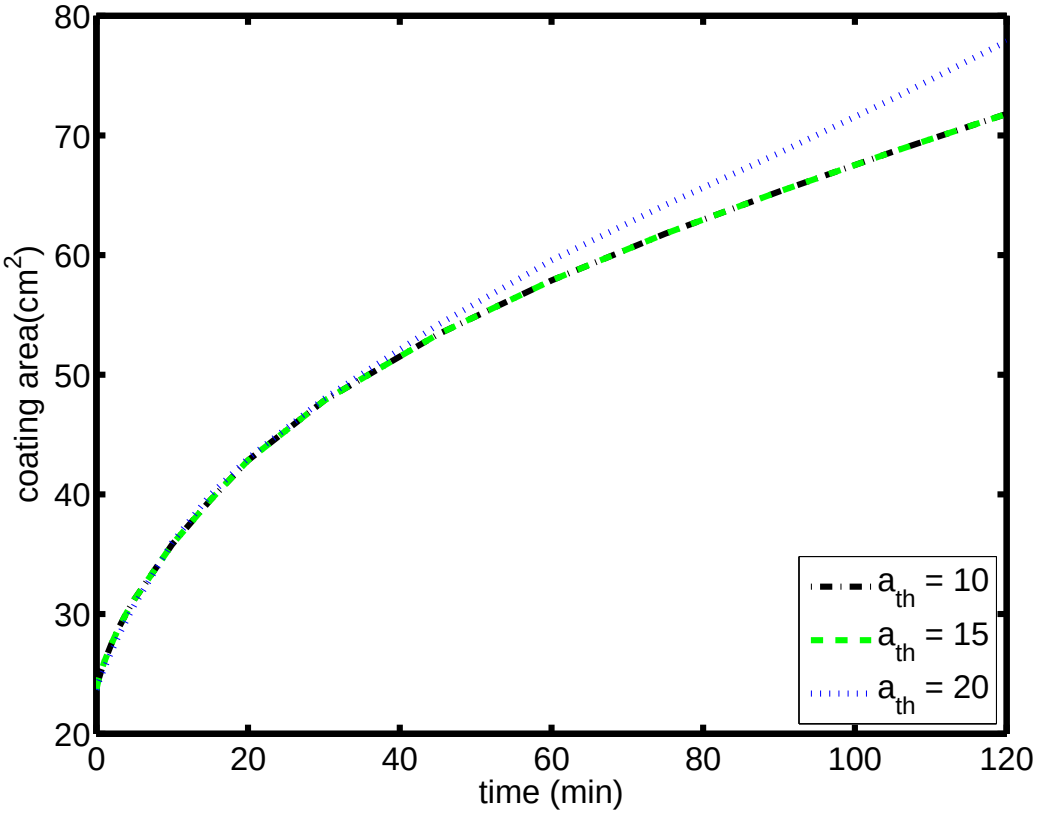

Figure 5.17. ($q_0 = 10^{-10}\ m/s$) Coating area of a prototype film at 2 hours.

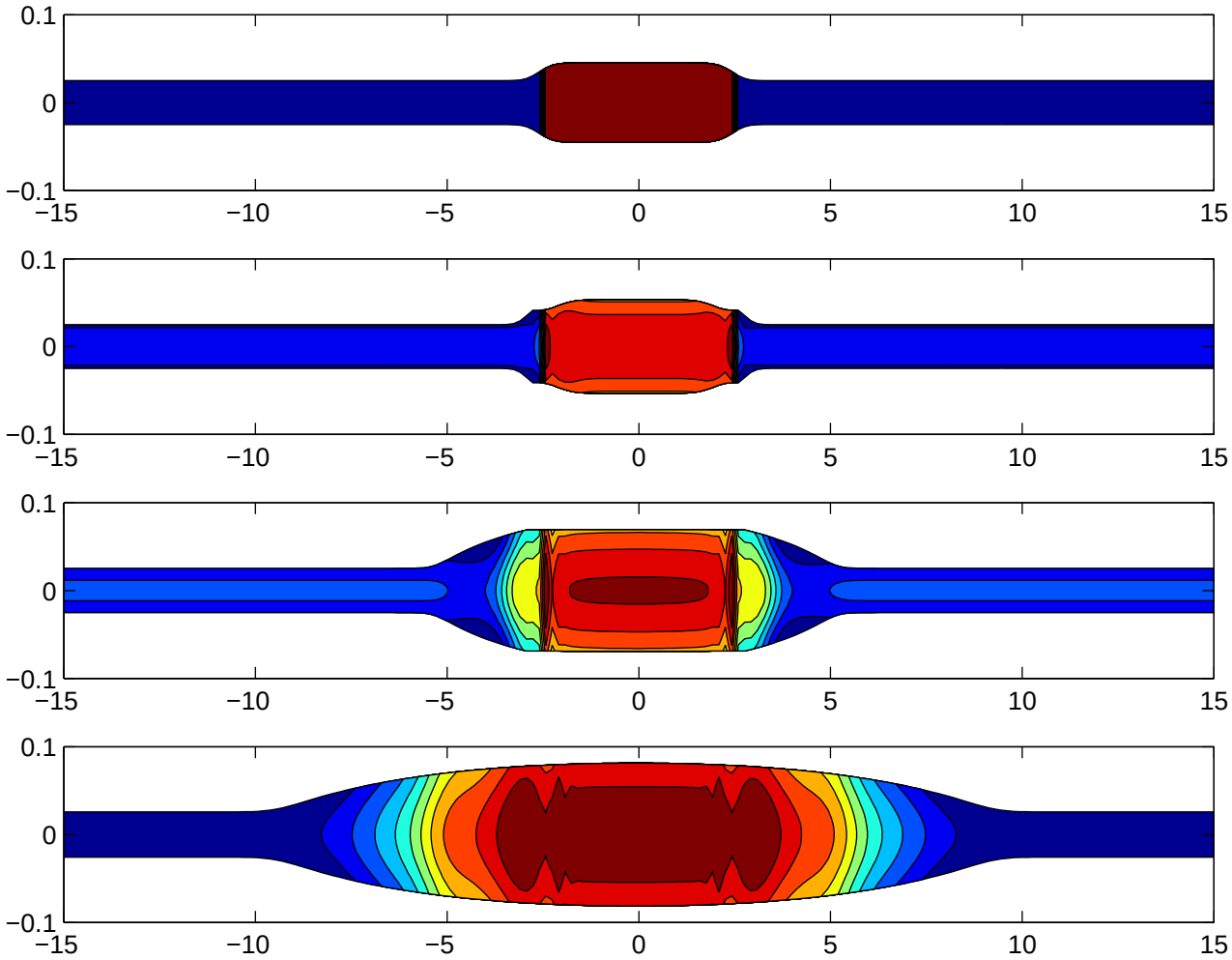

Figure 5.18. ($q_0 = 10^{-9}$ m/s and $a_{th} = 20$) Contour plots for concentration of Tenofovir molecules at $t = 0$, $t = 2$ minutes, $t = 30$ minutes, and $t = 2$ hours.

The film formulations with a range of swelling ratio 3 to 5, i.e. estimated range in real applications, coated less area than that was coated by homogeneously diluted gels.

Then, we developed a model for transient swelling and spreading of a prototype film formulation designed for vaginal microbicide drug delivery. The model took into consideration further swelling of an initially dissolved film, and subsequent distribution of Tenofovir drug molecules throughout the vaginal lumen. The association between swelling of film and rheological properties was obtained experimentally, delineating the way constitutive parameters are modified by swelling and dilution. We proposed two boundary conditions for the absorption of drug molecules (1) transcellular and (2) paracellular. For the latter, we showed that an approximate size of Tenofovir molecule was small enough so that it could move within the intercellular spaces between the vaginal epithelial cells. Then by changing the parameters of the boundary flux, the effects of dilution and swelling were investigated. Results showed that as film was imbibed, varying rheology indicated a rapid coating, enabled the film to spread faster and accelerate the drug molecules, i.e. Tenofovir.

The theory developed here improves our understanding of the biophysics of microbicide film flows *in vivo*, which can lead to improved understanding of drug delivery by those films. In addition, the theory here may find application in other elastohydrodynamic problems of interest.

References

[1] S. Tasoglu, J. J. Peters, S. C. Park, S. Verguet, D. F. Katz, and A. J. Szeri, "The effects of inhomogeneous boundary dilution on the coating flow of an anti-hiv microbicide vehicle," *Phys. Fluids.*, 2011, in review.

[2] Available at: http://www.un.org/waterforlifedecade/background.html. Accessed June, 2011.

[3] Q. A. Karim, S. S. A. Karim, J. A. Frohlich, A. C. Grobler, C. Baxter, L. E. Mansoor, A. B. M. Kharsany, S. Sibeko, K. P. Mlisana, Z. Omar, T. N. Gengiah, S. Maarschalk, N. Arulappan, M. Mlotshwa, L. Morris, and D. Taylor, "Effectiveness and safety of tenofovir gel, an antiretroviral microbicide, for the prevention of hiv infection in women," *Science*, vol. 329, pp. 1168–74, 2010.

[4] San Francisco AIDS Foundation, "How hiv is spread," available at:http://www.sfaf.org/hiv-info/transmission. Accessed March, 2011.

[5] UNAIDS WHO, "2007 aids epidemic update," retrieved 2008-03-12.

[6] M. Zwahlen and M. Egger, "Progression and mortality of untreated hiv-positive individuals living in resource-limited settings: update of literature review and evidence synthesis," in *UNAIDS Obligation HQ/05/422204*, 2006, retrieved 2008-03-19.

[7] B. Korber, M. Muldoon, J. Theiler, F. Gao, R. Gupta, A. Lapedes, B. H. Hahn, S. Wolinsky, and et al., "Timing the ancestor of the hiv-1 pandemic strains," *Science*, vol. 288, p. 178996, 2000.

[8] M. Worobey, M. Gemmel, D. E. Teuwen, and et al., "Direct evidence of extensive diversity of hiv-1 in kinshasa by 1960," *Nature*, vol. 455, pp. 661–4, 2008.

[9] Centers for disease control and prevention,
Available at: http://www.cdc.gov/MMWR/preview/mmwrhtml/00043494.htm. Accessed March, 2011.

[10] National Institute of Allergy and Infection Diseases, "Hiv infection in women," available at: http://www.niaid.nih.gov/topics/HIVAIDS/Understanding/Pages/quickFacts.aspx. Accessed February, 2011.

[11] The Joint United Nations Programme on HIV/AIDS [UNAIDS], "2009 report on the global aids epidemic," available at: http://www.unaids.org/en/media/unaids/contentassets/dataimport/pub/factsheet/2009. Accessed February, 2011.

[12] National Institute of Allergy and Infectious Diseases; NIH, Department of Health and Human Services,
"Workshop summary: Scientific evidence on condom effectiveness for sexually transmitted disease (std) prevention," Virginia, retrieved 2009-01-08.

[13] P. R. Ulin, M. Cayemittes, and R. Gringle, *Bargaining for life: women and the AIDS epidemic in Haiti*, L. D. Long and M. E. Ankrah, Eds. New York: Columbia University Press, 1997.

[14] United Nations Department of Economic and Social Affairs, Population Division, "World contraceptive use," available at:http://www.un.org/esa/population/publications/contraceptive2009/contraceptive2009.htm. Accessed February 2011.

[15] P. Feldblum and L. Peterson, "Fhi phase ii/iii study of c31g in 2 nigerian cities and in ghana," in *Microbicides 2006 Conference*, Cape Town, 2006, Available at: http://www.microbicides2006.com/. Accessed November 2006.

[16] J. Balzarini and L. V. Damme, "Intravaginal and intrarectal microbicides to prevent hiv infection," *CMAJ*, vol. 172, pp. 461–4, 2005.

[17] J. A. Turpin, "Considerations and development of topical microbicides to inhibit the sexual transmission of hiv," *Expert OpinInvestig Drugs*, vol. 11, pp. 1077–97, 2002.

[18] S. J. Scholand, J. A. DeSimone, and R. J. Pomerantz, "Anti-hiv-1 microbicides: chemical condoms designed to limit the scourge of the hiv-1 pandemic," *Curr Pharm Des*, vol. 11, p. 374756, 2005.

[19] J. Kreiss, E. Ngugi, K. Holmes, and et al., "Efficacy ofnonoxynol 9 contraceptive sponge use inpreventing heterosexual acquisition of hiv in nairobi prostitutes," *JAMA*, vol. 268, p. 47782, 1992.

[20] Z. A. Stein, "Hiv prevention: The need for methods women can use," *American Journal of Public Health*, vol. 80, pp. 460–2, 1990.

[21] L. V. Damme, G. Ramjee, M. Alary, and et al., "Effectiveness of col-1492, a nonoxynol-9 vaginal gel, on hiv-1 transmission in female sex workers: a randomised controlled trial," *Lancet*, vol. 360, pp. 971–77, 2002.

[22] R. E. Roddy, L. Zekeng, K. A. Ryan, U. Tamoufe, S. S. Weir, and E. L. Wong, "A controlled trial of nonoxynol 9 film to reduce male-to-female transmission of sexually transmitted diseases," *N. Engl. J. Med.*, vol. 339, pp. 504–10, 1998.

[23] L. Peterson, K. Nanda, B. K. Opoku, and et al., "Savvy (c31g) gel for prevention of hiv infection in women: a phase 3, double-blind,randomized, placebo controlled trial in ghana," *PLoS One*, vol. 2, p. e1312, 2007.

[24] P. Feldblum, A. Adeiga, R. Bakare, and et al., "Savvy vaginal gel (c31g) for prevention of hiv infection: a randomized controlled trial in nigeria," *PLoS One*, vol. 3, p. e1471, 2008.

[25] V. Halpern, F. Ogunsola, O. Obunge, and et al., "Effectiveness of cellulose sulphate vaginal gel for the prevention of hiv infection: results ofa phase iii trial in nigeria," *PLoS One*, vol. 3, p. e3784, 2008.

[26] L. V. Damme, R. Govinden, F. M. F, and et al., "Lack of effectiveness of cellulose sulfategel for the prevention of vaginal hiv transmission," *N. Engl. J. Med.*, vol. 359, p. 46372, 2008.

[27] S. Skoler-Karpoff, G. Ramjee, K. Ahmed, and et al., "Efficacy of carraguard for prevention of hivinfection in women in south africa: a randomised, double-blind, placebo-controlled trial," *Lancet*, vol. 372, pp. 1977–87, 2008.

[28] A. Nunn, S. McCormack, A. Crook, R. Pool, C. Rutterford, and R. Hayes, "Microbicides development programme: design of a phase iii trial to measure the efficacy of the vaginal microbicide pro 2000/5 for hiv prevention," *Trials*, vol. 10, p. 99, 2009.

[29] S. AbdoolKarim, A. Coletti, B. R. B, and et al., "Safety and effectiveness of vaginal microbicides buffer gel and 0.5% pro2000/5 gel for the prevention of hiv infection in women: results of the hptn 035 trial," in *16th CROI*, Montreal,Canada, 2009.

[30] "Mdp: Hiv prevention gel pro 2000 provenineffective," *MDP Press Release*, 2010.

[31] U.S. Food and Drug Administration,
Available at: http://www.fda.gov/ForConsumers/ByAudience/ForPatientAdvocates/. Accessed March, 2011.

[32] P. Ornera, J. Harriesa, D. C. D, and et al., "Challenges to microbicide introduction in south africa," *Soc Sci Med*, vol. 63, p. 96878, 2006.

[33] R. B. Bird, R. C. Armstrong, and O. Hassager, *Dynamics of polymeric liquids, Vol.1 fluid mechanics.* Wiley-Interscience, 1987.

[34] A. J. Szeri, S. C. Park, S. Verguet, A. Weiss, and D. F. Katz, "A model of transluminal flow of an anti-hiv microbicide vehicle: Combined elastic squeezing and gravitational sliding," *Phys. Fluids*, vol. 20, p. 083101, 2008.

[35] H. A. Barnes, "The yield stress - a review or '$\pi\alpha\nu\tau\alpha\ \rho^{\epsilon}\iota$' - everything flows?" *J. Non-Newtonian Fluid Mech.*, vol. 81, pp. 133–78, 1999.

[36] H. A. Barnes and Q. D. Nguyen, "Rotating vane rheometry - a review," *J. Non-Newtonian Fluid Mech.*, vol. 98, pp. 1–14, 2001.

[37] D. Bonn and M. M. Denn, "Yield stress fluids slowly yield to analysis," *Science*, vol. 324, pp. 1401–2, 2009.

[38] Q. D. Nguyen and D. V. Boger, "Measuring the flow properties of yield stress fluids," *Annu. Rev. Fluid Mech.*, vol. 24, pp. 47–88, 1992.

[39] G. L. Leal, *Laminar flow and convective transport processes.* MA: Butterworth-Heinemann, 1992.

[40] W. Deen, *Analysis of transport phenomena.* Oxford University Press, 1998.

[41] J. M. Diamond and W. H. Bossert, "Standing-gradient osmotic flow: A mechanism for coupling of water and solute transport in epithelia," *J. General Physiology*, vol. 50, pp. 2061–83, 1967.

[42] J. Fischbarg, "Fluid transport across leaky epithelia: Central role of the tight junction and supporting role of aquaporins," *Physiol. Rev.*, vol. 90, pp. 1271–90, 2010.

[43] Z. M. Jin and D. Dowson, "Elastohydrodynamic lubrication in biological systems," *Proc. Inst. Mech. Eng., Part J: J. Eng. Tribol.*, vol. 219, pp. 367–380, 2005.

[44] M. J. Lighthill, "Pressure-forcing of tightly fitting pellets along fluid-filled elastic tubes," *J. Fluid Mech.*, vol. 34, pp. 113–43, 1968.

[45] F. J. Holly and T. F. Holly, *in Lacrimal Gland, Tear Film, and Dry Eye Syndromes*, D. A. Sullivan, Ed. New York: Plenum, 1994.

[46] M. B. Jones, G. R. Fulford, C. P. Please, D. L. S. McElwain, and M. J. Collins, "Elastohydrodynamics of the eyelid wiper," *Bull. Math. Biol.*, vol. 70, pp. 323–43, 2008.

[47] A. Gouldstone, R. E. Brown, J. P. Butler, and S. H. Loring, "Elastohydrodynamic separation of pleural surfaces during breathing," *Respir. Physiol. Neurbiol*, vol. 137, pp. 97–106, 2003.

[48] A. Stone, "Microbicides: a new approach to preventing hiv and other sexually transmitted infections," *Nature Reviews Drug Discovery*, vol. 1, pp. 977–85, 2002.

[49] I. McGowan, "Microbicides: A new frontier in hiv prevention," *Biologicals*, vol. 34, pp. 241–55, 2006.

[50] K. Vermani and S. Garg, "The scope and potential of vaginal drug delivery," *Pharm. Sci. Technol. Today*, vol. 3, pp. 359–64, 2000.

[51] P. F. Harrison, Z. Rosenberg, and J. Bowcut, "Topical microbicides for disease prevention: Status and challenges," *Clin. Infect. Dis.*, vol. 36, pp. 1290–4, 2003.

[52] O. J. D'Cruz and F. M. Uckun, "Clinical development of microbicides for the prevention of hiv infection," *Curr. Pharm. Des.*, vol. 10, pp. 315–36, 2004.

[53] S. Verguet, B. Y. Holt, and A. J. Szeri, "Increasing the effectiveness of vaginal microbicides: A biophysical framework to rethink behavioral acceptability," *PLoS ONE*, vol. 5, p. 11, 2010.

[54] D. F. Katz, M. Henderson, D. H. Owen, A. M. Plenys, and D. K. Walmer, "What is needed to advance vaginal formulation technology?" in *Vaginal Microbicide Formulations Workshop.* Philadelphia: Lippencott-Raven, 1998.

[55] S. L. Kieweg, A. R. Geonnotti, and D. F. Katz, "Gravity-induced coating flows of vaginal gel formulations: In vitro experimental analysis," *J. Pharm. Sci.*, vol. 93, pp. 2941–52, 2004.

[56] S. L. Kieweg and D. F. Katz, "Squeezing flows of vaginal gel formulations relevant to microbicide drug delivery," *J. Biomech. Eng.*, vol. 128, pp. 540–53, 2006.

[57] ——, "Interpreting properties of microbicide drug delivery gels: Analyzing deployment due to squeezing," *J. Pharm. Sci.*, vol. 96, pp. 835–50, 2007.

[58] B. E. Lai, Y. Q. Xie, M. Lavine, A. J. Szeri, D. H. Owen, and D. F. Katz, "Dilution of microbicide gels with vaginal fluid and semen simulants: Effects on rheology and coating flow," *J. Pharm. Sci.*, vol. 97, pp. 1030–38, 2008.

[59] B. J. Crosby, M. Mangnus, W. de Groot, R. Daniels, and T. C. B. McLeish, "Characterisation of long chain branching: Dilution-rheology of industrial polyethylenes," *Journal of Rheology*, vol. 46, p. 2, 2002.

[60] J. M. Dealy and R. G. Larson, *Structure and rheology of molten polymers.* Hanser Gardner Pubns, 2006.

[61] D. H. Owen, J. J. Peters, and D. F. Katz, "Rheological properties of contraceptive gels," *Contraception*, vol. 62, pp. 321–26, 2000.

[62] S. Roy, *Barrier Contraceptives: Current Status and Future Prospects.* New York: Wiley, 1994.

[63] M. Schuenke, E. Schulte, L. M. Ross, U. Schumacher, and E. D. Lamperti, *Atlas of anatomy: neck and internal organs.* New York: Thieme, 2010.

[64] D. J. Coyle, "Forward roll coating with deformable rolls: A simple one dimensional elastohydrodynamic model," *Chem. Eng. Sci.*, vol. 43, pp. 2673–84, 1988.

[65] D. H. Owen and D. F. Katz, "A vaginal fluid simulant," *Contraception*, vol. 59, pp. 91–5, 1999.

[66] J. A. Crank, "Theoretical investigation of the influence of molecular relaxation and internal stress on diffusion in polymers," *J. Polym. Sci.*, vol. 11, p. 151, 1953.

[67] K. Podual, F. D. III, and N. A. Peppas, "Modeling of water transport in and release from glucose-sensitive swelling-controlled release systems based on poly (diethylaminoethyl methacrylate-g-ethylene glycol)," *Industrial & engineering chemistry research*, vol. 43, p. 7500, 2004.

[68] S. Verguet, *Transport phenomena in microfluidics and microbicide drug delivery systems.* University of California, Berkeley, 2008.

[69] Y. P. Syrnikov, "Calculation of the self-diffusion coefficient of water," *J. Structural Chem.*, vol. 11, p. 698, 1970.

[70] F. Acarturk and J. R. Robinson, "Vaginal permeability and enzymatic activity studies in normal and ovariectomized rabbits," *Pharmaceutical Research*, vol. 13, p. 5, 1996.

[71] M. Kremer, C. Squier, P. Schlievert, and C. Davis, "Permeability of vaginal mucosa to toxic shock syndrome toxin-1," in *Interscience Conference on Antimicrobial Agents and Chemotherapy. 41st*, Chicago, 2001.

[72] A. Mahalingam, E. Smith, J. Fabian, F. R. Damian, J. J. Peters, M. R. Clark, D. R. Friend, D. F. Katz, and P. F. Kiser, "Design of a semisolid vaginal microbicide gel by relating composition to properties and performance," *Pharmaceutical Research*, vol. 27, pp. 2478–91, 2010.

[73] J. M. Skotheim and L. Mahadevan, "Soft lubrication: The elastohydrodynamics of nonconforming and conforming contacts," *Phys. Fluids.*, p. 092101, 2005.

[74] E. C. Bingham, "An investigation of the laws of plastic flow," *U.S. Bureau of Standards Bulletin*, vol. 13, pp. 309–53, 1916.

[75] D. N. Smyrnaios and J. A. Tsamopoulos, "Squeeze flow of bingham plastics," *J. Non-Newtonian Fluid Mech.*, vol. 100, pp. 165–89, 2001.

[76] G. C. Florides, A. N. Alexandrou, and G. Georgiou, "Flow development in compression of a finite amount of a herchel-bulkley fluid," *J. Non-Newtonian Fluid Mech.*, vol. 143, pp. 38–47, 2007.

[77] K. R. J. Ellwood, G. C. Georgiou, T. C. Papanastasiou, and J. O. Wilkes, "Laminar jets of bingham-plastic liquids," *J. Rheol.*, vol. 34, pp. 787–812, 1990.

[78] T. C. Papanastasiou, "Flows of materials with yield," *J. Rheol.*, vol. 31, pp. 385–404, 1987.

[79] E. J. O'Donovan and R. I. Tanner, "Numerical study of the bingham squeeze film problem," *J. Non-Newtonian Fluid Mech.*, vol. 15, pp. 75–83, 1984.

[80] B. E. Lai, A. R. Geonnotti, M. G. DeSoto, D. C. Montefiori, and D. F. Katz, "Semi-solid gels function as physical barriers to human immunodeficiency virus transport in vitro," *Antiviral Res.*, vol. 88, pp. 143–51, 2010.

[81] J. M. Fitzgerald, "Mechanics of red-cell motion through very narrow capillaries," *Proc. R. Soc. Lond. B.*, vol. 174, pp. 193–227, 1969.

[82] G. G. Lipscomb and M. M. Denn, "Flow of bingham fluids in complex geometries," *J. Non-Newtonian Fluid Mech.*, vol. 14, pp. 337–46, 1984.

[83] S. D. R. Wilson, "Squeezing flow of a bingham material," *J. Non-Newtonian Fluid Mech.*, vol. 47, pp. 211–19, 1993.

[84] S. C. Park, *Fluid mechanics of delivery of a non-Newtonian anti-HIV microbicide.* University of California, Berkeley, 2009.

[85] W. M. Kulicke, O. Arendt, and M. Berger, "Characterization of hydroxypropylmethylcellulose-stabilized emulsions part ii: The flow behaviour," *Colloid. Polym. Sci.*, vol. 276, pp. 1024–31, 1998.

[86] L. C. Rohan, B. J. Moncla, R. P. K. N. Ayudhya, M. Cost, Y. Huang, F. Gai, N. Billitto, J. D. Lynam, K. Pryke, P. Graebing, N. Hopkins, J. F. Rooney, D. Friend, and C. S. Dezzutti, "A mathematical model of electrolyte and fluid transport across corneal endothelium," *PLoS ONE*, vol. 5, p. e9310, 2010.

[87] S. Tasoglu, S. C. Park, J. J. Peters, D. F. Katz, and A. J. Szeri, "The consequences of yield stress on deployment of a non-newtonian anti-hiv microbicide gel," *J. Non-Newtonian Fluid Mech.*, 2011, in press.

[88] R. B. Bird, W. E. Stewart, and E. N. Lightfoot, *Transport Phenomena, Revised 2nd edition.* New York: John Wiley & Sons, 1996.

[89] W. Masters and V. E. Johnson, *Human Sexual Response.* Boston: Little Brown, 1966.

[90] C. Mitchell, K. Paul, K. Agnew, R. Gaussman, R. Coombs, and J. Hitti, "Estimating volume of cervicovaginal secretions in cervicovaginal lavage fluid collected for measurement of genital hiv-1 rna levels in women," *J. Clinical Microbiology*, vol. 49, pp. 735–36, 2011.

[91] J. G. Wijmans, S. Nakao, and C. A. Smolders, "Flux limitation in ultrafiltration: Osmotic pressure model and gel layer model," *J. Membrane Science*, vol. 20, pp. 115–24, 1984.

[92] M. Justin-Temu, F. Damian, R. Kinget, and G. Van Den Mooter, "Intravaginal gels as drug delivery systems," *J. Womens Health*, vol. 13, pp. 834–44, 2004.

[93] K. S. Cole, "Surface forces of the arbacia egg," *J. Cell. and Comp. Physiol.*, vol. 1, p. 1, 1932.

[94] R. P. Rand and A. C. Burton, "Mechanical properties of the red cell membrane i. membrane stiffness and intracellular pressure," *Biophysical Journal*, vol. 4, pp. 115–35, 1964.

[95] J. Fischbarg and F. P. J. Diecke, "A mathematical model of electrolyte and fluid transport across corneal endothelium," *J. Membrane Biol.*, vol. 203, pp. 41–56, 2005.

[96] L. Langbein, C. Grund, C. Kuhn, S. Praetzel, J. Kartenbeck, J. M. Brandner, I. Moll, and W. W. Franke, "Tight junctions and compositionally related junctional structures in mammalian stratified epithelia and cell cultures derived therefrom," *European J. of Cell Biology*, vol. 81, pp. 419–35, 2002.

[97] R. J. Levin, "Actions of spermicidal and virucidal agents on electrogenic ion transfer across human vaginal epithelium in vitro," *Pharmacology and Toxicology*, vol. 81, pp. 219–25, 1997.

[98] S. Duncan and R. J. Levin, "Transuterine, transendocervical and transvaginal potential differences in conscious women measured in situ," *J. Physiol.*, vol. 259, pp. 27–8, 1976.

[99] F. Edwards and R. J. Levin, "The bioelectric parameters of the vagina during the oestrus cycle of the rat," *J. Physiol.*, vol. 248, pp. 307–15, 1975.

[100] J. J. Hajjar and A. M. Mroueh, "Alanine transport across in vitro rabbit vagina," *Contraception*, vol. 19, p. 4, 1979.

[101] R. J. Levin and J. Camfield, "The isolated eyerted vagina a preparation for studying vaginal bioelectric phenomena in vitro," *Life Sciences*, vol. 6, pp. 1871–81, 1967.

[102] J. M. Sanchez, Y. Li, A. Rubashkin, P. Iserovich, Q. Wen, J. W. Ruberti, R. W. Smith, D. Rittenband, K. Kuang, F. P. J. Diecke, and J. Fischbarg, "Evidence for a central role for electro-osmosis in fluid transport by corneal endothelium," *J. Membrane Biol.*, vol. 187, pp. 37–50, 2002.

[103] S. McLaughlin and R. T. Mathias, "Electro-osmosis and the reabsorption of fluid in renal proximal tubules," *J. Gen. Physiol.*, vol. 85, p. 699728, 1985.

[104] C. Coggins, C. J. Elias, R. Atisook, M. T. Bassett, V. Ettiegnene-Traore, P. D. Ghys, L. Jenkins-Woelk, E. Thongkrajai, and N. L. VanDevanter, "Women's preferences regarding the formulation of over-the-counter vaginal spermicides," *AIDS*, vol. 12, pp. 1389–1391, 1998.

[105] S. Garg, K. Vermani, A. Garg, R. A. Anderson, W. B. Rencher, and L. J. D. Zaneveld, "Development and characterization of bioadhesive vaginal films of sodium polystyrene sulfonate (pss), a novel contraceptive antimicrobial agent," *Pharmaceutical Research*, vol. 22, 2005.

[106] A. R. Geonnotti, M. J. Furlow, T. Wu, M. G. DeSoto, M. H. Henderson, P. F. Kiser, and D. F. Katz, "Measuring macrodiffusion coefficients in microbicide hydrogels via postphotoactivation scanning," *Biomacromolecules*, vol. 9, pp. 748–751, 2008.

[107] M. Hackemann, C. Grubb, and K. R. Hill, "The ultrastructure of normal squamous epithelium of the human cervix uteri," *J. Oltrastructure Research*, vol. 22, pp. 443–457, 1968.

[108] A. Rubashkin, P. Iserovich, J. A. Hernandez, and J. Fischbarg, "Epithelial fluid transport: Protruding macromolecules and space charges can bring about electro-osmotic coupling at the tight junctions," *J. Membrane Biol.*, vol. 208, pp. 251–263, 2005.

[109] M. G. Farquhar and G. E. Palade, "Junctional complexes in various epithelia," *J Cell Biol.*, vol. 17, pp. 375–412, 1963.